学　位　論　文

学位論文名

Clonal hematopoiesis with JAK2V617F promotes pulmonary hypertension with ALK1 upregulation in lung neutrophils

(JAK2V617F 変異クローン性造血は肺好中球 ALK1 を介して肺高血圧症を増悪させる)

福島県立医科大学大学院医学研究科
循環病態学　循環器内科学講座
君島　勇輔

Clonal hematopoiesis with JAK2V617F promotes pulmonary hypertension with ALK1 upregulation in lung neutrophils

Yusuke Kimishima, MD

Department of Cardiovascular Medicine, Fukushima Medical University

Abstract

Pulmonary hypertension (PH) is a progressive cardiopulmonary disease characterized by pulmonary arterial remodeling. Clonal somatic mutations including *JAK2*V617F, the most frequent driver mutation among myeloproliferative neoplasms, have recently been identified in healthy individuals without hematological disorders. Here, we reveal that clonal hematopoiesis with JAK2V617F exacerbates PH and pulmonary arterial remodeling in mice. JAK2V617F-expressing neutrophils specifically accumulate in pulmonary arterial regions, accompanied by increases in neutrophil-derived elastase activity and chemokines in chronic hypoxia-exposed JAK2V617F transgenic ($JAK2^{V617F}$) mice, as well as recipient mice transplanted with $JAK2^{V617F}$ bone marrow cells. JAK2V617F progressively upregulates *Acvrl1* (encoding ALK1) during the differentiation from bone marrow stem/progenitor cells peripherally into mature neutrophils of pulmonary arterial regions. JAK2V617F-mediated STAT3 phosphorylation upregulates ALK1-Smad1/5/8 signaling. ALK1/2 inhibition completely prevents the development of PH in $JAK2^{V617F}$ mice. Finally, our prospective clinical study identified *JAK2*V617F-positive clonal hematopoiesis is more common in PH patients than in healthy subjects. These findings indicate that clonal hematopoiesis with JAK2V617F causally leads to PH development associated with ALK1 upregulation.

Introduction

Pulmonary hypertension (PH) is a complex cardiopulmonary disease characterized by increases in pulmonary vascular resistance and pulmonary arterial pressure. Despite recent advances in diagnosis and treatment, PH remains a serious condition, eventually leading to right heart failure with high mortality[1]. A pathological feature of PH is structural remodeling of the small pulmonary arteries, which is associated with intimal thickening, muscularization and the formation of plexiform lesions[2]. Bone marrow (BM)-derived progenitor cells, as well as perivascular inflammatory infiltrates, contribute to the process of pulmonary arterial remodeling[3]. It has been also reported that several hematological disorders, including myeloproliferative neoplasms (MPNs), are often complicated with PH[4]. The incidence of PH has been reported to be higher in MPN patients than in the general population, and high mortality due to cardiovascular diseases has been observed in MPN patients with PH[5, 6]. PH is categorized into five etiological groups according to the WHO clinical classification[7]. Based on the above observations, MPN-associated PH is classified into WHO Group V, which is an important heterogenous group that encompasses unclear multifactorial mechanisms[7].

MPNs including polycythemia vera (PV), essential thrombocythemia (ET), and primary myelofibrosis (MF) are characterized by chronic proliferation of mature myeloid cells,[8] and the myeloproliferative phenotype is driven by somatic mutations in *JAK2*, *CALR*, and *MPL*. Among MPNs, *JAK2*V617F, an activating somatic mutation in *JAK2*, is the most frequently observed driver mutation; it has been observed in over 95% of PV patients as well as 50–60% of ET and primary MF patients[9, 10, 11]. *JAK2*V617F causes cytokine-independent activation of the JAK–STAT pathway, resulting in proliferation of mature myeloid cells[11].

Recent advances in genetic analyses have led to the discovery of clonal hematopoiesis, whose hematopoietic stem/progenitor cells harbor somatic mutations in genes often mutated in myeloid cancers, including MPNs, in healthy individuals without any hematologic disorders[12, 13]. Among clonal hematopoiesis, age-related clonal hematopoiesis implies the presence of any detectable clonal events in hematopoietic cells, and its incidence increases with age. Clonal hematopoiesis of indeterminate potential (CHIP) is defined by somatic mutations with a variant allele frequency (VAF) of at least 2%. Clonal hematopoiesis is quite common, and more than 15% of individuals are affected at age ≥70 years[14]. Whereas the rate of patients who progress from CHIP to myeloid malignancies is estimated to be only 0.5–1%, patients with CHIP exhibit markedly increased cardiovascular diseases such as atherosclerosis[12, 15]. Most frequently mutated genes in clonal hematopoiesis are epigenetic modifiers; *DNMT3A*, *TET2*, and *ASXL1*. *JAK2* is the next most often mutated gene, and the vast majority of these mutants are *JAK2*V617F in clonal hematopoiesis. Murine studies have suggested that CHIP with somatic mutations in epigenetic modifiers, as well as *JAK2*V617F, played causal roles in acceleration of atherosclerosis[16, 17]. MPN patients often show venous and arterial vascular complications[18]. In particular, MPN patients with *JAK2*V617F showed higher incidence of vascular complications compared to those with other driver mutations[18]. However, mechanistic relevance of clonal hematopoiesis with *JAK2*V617F in PH has yet to be elucidated.

Herein, we provide the evidence that clonal hematopoiesis with JAK2V617F plays causal roles in the development of PH with ALK1 upregulation in lung neutrophils.

Results

JAK2V617F expression accelerates pulmonary hypertension in response to chronic hypoxia exposure in mice.

To know the involvement of the JAK-STAT pathway in PH development, adult wild-type (WT) C57BL/6J mice were exposed to chronic hypoxia (10% O_2), which is a well-established method to induce PH in mice[19, 20]. STAT3 phosphorylation levels on whole lung homogenates, not fractionated cells, were significantly increased after exposure to chronic hypoxia for 3 weeks (Supplementary Fig. 1), suggesting that JAK-STAT activation may play a pathophysiological role in chronic hypoxia-induced PH. To clarify the effects of JAK2V617F expression on the pathogenesis of PH, we used $JAK2^{V617F}$ female mice with transgenic expression of *Jak2*V617F[21] after exposure to normoxia or chronic hypoxia. Starting from 2 weeks after chronic hypoxia exposure, we observed noticeable signs of cardio-respiratory distress such as reduced activity, diminished appetite, and piloerection in $JAK2^{V617F}$ mice, but not in WT mice. We determined to analyze the mice at the 2-week point to minimize the secondary alternation for investigation of the molecular mechanisms that cause PH (Fig. 1a). After normoxia exposure, $JAK2^{V617F}$ mice had significantly higher white blood cell and platelet counts, in comparison to WT littermates, indicating an MF-like phenotype in $JAK2^{V617F}$ mice (Fig. 1b), which is consistent with the results of our previous studies[21, 22]. Right ventricular systolic pressure (RVSP) and the ratio of right ventricle weight to left ventricle weight plus septum weight (RV/LV+S) did not differ between WT and $JAK2^{V617F}$ mice after normoxia exposure (Fig. 1c). Although chronic hypoxia significantly elevated hemoglobin values in both WT and $JAK2^{V617F}$ mice, there was no significant difference between them. Notably, we found that RVSP was significantly elevated in $JAK2^{V617F}$

mice compared to WT mice in response to continuous hypoxia (Fig. 1c) in line with the echocardiographic evaluation of pulmonary hemodynamics (Supplementary Fig. 2). Additionally, RV/LV+S in JAK2^{V617F} mice was significantly greater than that in WT mice, indicating more severe RV hypertrophy due to PH in chronic hypoxia-exposed JAK2^{V617F} mice (Fig. 1c). LV fractional shortening or LV+S values were not different among the groups, suggesting that chronic hypoxia was not associated with LV systolic dysfunction or LV hypertrophy in JAK2^{V617F} mice (Supplementary Fig. 2, 3). Of note, we found that even male JAK2^{V617F} mice showed significant increases in RVSP and RV/LV+S compared to male WT mice 2 weeks after chronic hypoxia (Supplementary Fig. 4). Considering the clinical relevance of PH patients that women are more likely to be affected than men[23], we thereafter used female mice in a whole series of the present study unless otherwise indicated.

JAK2^{V617F} mice exhibit pulmonary vascular remodeling accompanied by the increased perivascular neutrophil infiltration in the lungs after chronic hypoxia.

Histological analyses revealed significant increases in medial wall thickness and muscularization of pulmonary vessels in JAK2^{V617F} mice compared to WT mice after exposure to chronic hypoxia (Fig. 1d, e). The numbers of proliferating smooth muscle cells in the pulmonary arteries were significantly increased in JAK2^{V617F} mice compared to WT mice after chronic hypoxia (Supplementary Fig. 5a). These data suggest that the JAK2V617F expression promoted PH with pulmonary arterial structural remodeling in response to chronic hypoxia, rather than spontaneous development of PH under normoxia. We observed increased cellular infiltration surrounding the pulmonary arteries in both normoxia- and chronic hypoxia-exposed JAK2^{V617F} mice in H&E staining

(Supplementary Fig. 5b). Next, we characterized the infiltrating cells by immunohistochemical staining. There were significant increases in $Ly6G^+$ neutrophils specifically in pulmonary arterial regions of $JAK2^{V617F}$ lungs compared to WT lungs (Fig. 1f, g), and more Ly6G-expressing cells within $CD45^+$ cells than $F4/80^+$ macrophages or $CD45R^+$ B cells (Supplementary Fig. 6). Of note, the numbers of $Ly6G^+$ cells in the perivascular and non-perivascular regions of $JAK2^{V617F}$ lungs were further increased after chronic hypoxia exposure compared to those after normoxia exposure (Supplementary Fig. 7). $CD41^+$ megakaryocytes and $TER\text{-}119^+$ erythroblasts were rarely observed in both WT and $JAK2^{V617F}$ lungs (Supplementary Fig. 5b). The activity of elastase, which mainly originates from neutrophils[24], and mRNA expression levels of neutrophil-related chemokines and chemokine receptors, including *Ccl2*, *Cxcl1*, *Ccr1*, *Cxcr2*, as well as cytokines such as *Pdgfrb* and *Tgfb1*, were significantly increased in the lungs of $JAK2^{V617F}$ mice after chronic hypoxia (Fig. 1h, i, Supplementary Fig. 5c). Thus, the infiltrated neutrophils in perivascular regions accompanied by their increased functional activities might play important roles in pulmonary arterial structural remodeling in $JAK2^{V617F}$ mice. We confirmed that in the Sugen-hypoxia model, which is another PH model[25], RVSP and RV/LV+S were significantly elevated in $JAK2^{V617F}$ mice compared to WT mice (Supplementary Fig. 8). There was no statistical significance regarding RVSP and RV/LV+S between aged WT and $JAK2^{V617F}$ mice (8–9 months old) without hypoxia stimulus, but some of the aged $JAK2^{V617F}$ mice displayed comparatively high RVSP and RV/LV+S (Supplementary Fig. 9).

Hematopoietic cell clone with JAK2V617F exacerbates the development of pulmonary hypertension in response to chronic hypoxia in mice.

We next investigated whether a hematopoietic cell clone, rather than lung tissue with JAK2V617F expression, contributes to the development of PH, by means of BM transplantation (BMT)[22]. Donor BM cells from JAK2^{V617F} mice or control WT mice were injected into lethally irradiated recipient WT mice, so that the recipient mice had WT lungs (Fig. 2a). The BMT mice were exposed to chronic hypoxia for 3 weeks. The *Jak2*V617F VAF in blood leukocytes in the recipient mice transplanted with JAK2^{V617F} BM cells (JAK2^{V617F}-BMT) gradually elevated from 4 to 8 weeks after BMT; from 25.5 ± 1.1% to 34.9 ± 6.7% in normoxia-exposed mice, and from 24.5 ± 0.8% to 51.1 ± 5.4% in chronic hypoxia-exposed mice (Fig. 2b), suggesting the nearly complete engraftment of hematopoietic cells with heterozygous *Jak2*V617F. However, blood cell counts in JAK2^{V617F}-BMT mice did not exhibit significant increases compared to those in the recipient mice transplanted with WT BM cells (WT-BMT) after normoxia exposure (Fig. 2c), differently from those in individual JAK2^{V617F} mice (Fig. 1b). This finding was consistent with the previously established evidence that recipient mice transplanted with hematopoietic stem/progenitor cells carrying JAK2V617F often fail to show MPN-like phenotypes[26]. Although RVSP and RV/LV+S did not differ between WT-BMT and JAK2^{V617F}-BMT mice after normoxia exposure, JAK2^{V617F}-BMT mice showed significant increases in both RVSP and RV/LV+S compared to WT-BMT mice in response to exposure to chronic hypoxia for 3 weeks (Fig. 2d), which is consistent with the echocardiography used to assess pulmonary hemodynamics (Supplementary Fig. 10). LV+S values did not differ among the groups (Supplementary Fig. 11). Medial wall thickness, percentage of muscularized vessels and numbers of proliferating smooth muscle cells of pulmonary arteries were significantly increased in JAK2^{V617F}-BMT mice compared to WT-BMT mice after hypoxia exposure (Fig. 2e, f, Supplementary Fig. 12a).

These findings strongly indicate that a hematopoietic cell clone with JAK2V617F could accelerate PH with pulmonary arterial remodeling in WT lung tissues in response to chronic hypoxia, even without phenotypic MPNs, mimicking PH due to clonal hematopoiesis, such as CHIP. The numbers of $Ly6G^+$ neutrophils in pulmonary arterial regions were significantly increased in $JAK2^{V617F}$-BMT mice compared to WT-BMT mice either after normoxia or chronic hypoxia exposure, and the numbers of $Ly6G^+$ cells in both perivascular and non-perivascular regions in chronic hypoxia-exposed $JAK2^{V617F}$-BMT mice were further increased compared to those in normoxia-exposed $JAK2^{V617F}$-BMT mice (Fig. 2g, h, Supplementary Fig. 13, 14). $Ly6G^+$ cells significantly contributed to $CD45^+$ cells rather than $F4/80^+$ or $CD45R^+$ cells in hypoxia-exposed $JAK2^{V617F}$-BMT lungs (Supplementary Fig. 13). The numbers of $CD41^+$ or $TER\text{-}119^+$ cells were not different between WT and $JAK2^{V617F}$-BMT mice (Supplementary Fig. 12b). Notably, elastase activity, neutrophil-related chemokines and chemokine receptors, and cytokines were significantly elevated in the lungs of $JAK2^{V617F}$-BMT mice in response to chronic hypoxia compared to the other groups (Fig. 2i, j, Supplementary Fig. 12c). Taken together, these data suggest that the neutrophils specifically infiltrating in pulmonary arterial regions induced by clonal hematopoiesis with JAK2V617F are involved in the development of PH.

Characterization of bone marrow-derived hematopoietic cells with JAK2V617F in the lungs by using GFP-transgene.

To visualize and further characterize BM-derived hematopoietic cells carrying JAK2V617F in pulmonary arterial remodeling, we generated double transgenic mice ($JAK2^{V617F}$/CAG-EGFP mice) by crossing $JAK2^{V617F}$ mice with CAG-EGFP mice[27]. We

transplanted BM cells from JAK2^{V617F}/CAG-EGFP mice or control WT/CAG-EGFP littermates into lethally irradiated WT mice. After BMT followed by exposure to chronic hypoxia for 3 weeks, immunostaining showed that the GFP$^+$ cells were substantially accumulated in pulmonary arterial regions in BMT recipients transplanted with BM cells from JAK2^{V617F}/CAG-EGFP mice (JAK2^{V617F}-GFP-BMT), whereas recipients transplanted with BM cells from WT/CAG-EGFP mice (WT-GFP-BMT) showed fewer GFP$^+$ cells in the lungs (Fig. 3a, b). There was no co-localization between GFP and α-smooth muscle actin (αSMA) in the lungs of either WT-GFP-BMT or JAK2^{V617F}-GFP-BMT mice. In JAK2^{V617F}-GFP-BMT mice, nearly half of the GFP$^+$ cells expressed Ly6G in pulmonary arterial regions, and Ly6G$^+$ cells predominantly contributed to BM-derived cells rather than F4/80$^+$ or CD45R$^+$ cells (Fig. 3c, d, Supplementary Fig. 15). The percentage of these Ly6G-expressing GFP$^+$ cells was significantly higher than that in WT-GFP-BMT mice, while all Ly6G$^+$ cells expressed GFP in both WT-GFP-BMT and JAK2^{V617F}-GFP-BMT mice (Fig. 3e). These data indicate that the accumulated Ly6G$^+$ neutrophils carrying JAK2V617F are originated from BM to pulmonary arterial regions.

Small clones with JAK2V617F lead to PH development.

We next performed a competitive transplantation using different ratios of a mixture of WT-GFP or JAK2^{V617F}-GFP BM cells and WT without GFP BM cells (Fig. 4a, Supplementary Fig. 16a). In the control non-competitive group, flow cytometry showed that chimerism assessed by GFP$^+$ cells within CD45$^+$ cells in the blood was significantly elevated at 8 weeks compared to that at 4 weeks in 100% WT-GFP-BMT and 100% JAK2^{V617F}-GFP-BMT mice (Supplementary Fig. 16b). To determine the minimum threshold of PH aggravation in JAK2^{V617F}-GFP-BMT mice, we categorized the recipient

mice according to the chimerism level 8-weeks after BMT. Interestingly, when we analyzed the recipients limited to the chimerism of 1–19% as well as 20–49% and 50–100%, the JAK2^{V617F}-GFP-BMT mice showed significant increases in RVSP and RV/LV+S compared to the WT-GFP-BMT mice (Fig. 4b, Supplementary Fig. 16c–e). Moreover, the JAK2^{V617F}-GFP-BMT mice with lower chimerism of <1% tended to display increases in RVSP and RV/LV+S compared to the WT-GFP-BMT mice (Supplementary Fig. 16f). These data suggest that even small clones with *Jak2*V617F are associated with PH development.

JAK2V617F is associated with selective migration of neutrophils into the lungs and maturation for the myeloid lineage from hematopoietic precursors in the lungs.

We isolated cell fraction from the lungs and the blood in WT-GFP-BMT and JAK2^{V617F}-GFP-BMT mice with 1–19% chimerism at 8 weeks after BMT. The percentages of GFP$^+$ cells within Ly6G$^+$ neutrophils in JAK2^{V617F}-GFP-BMT mice were significantly higher in the lungs than in the blood, while those in WT-GFP-BMT mice were not different between the lungs and the blood (Fig. 4c, d). These findings suggest that JAK2^{V617F} neutrophils have an intrinsic capability of increased migration into the lungs, and this migration is enhanced in response to hypoxia. Accordingly, *ex vivo* analysis using chemotaxis assay revealed that JAK2^{V617F}-Ly6G$^+$ cells in the blood displayed a higher capability of neutrophil migration than WT-Ly6G$^+$ cells (Fig. 4e). To investigate the involvement of hematopoietic progenitors in JAK2^{V617F} lungs, CD117 (c-kit)$^+$ cells were sorted from the lungs and subjected to a colony-forming assay. There were substantial increases in the colony-forming ability of JAK2V617F-expressing progenitor cells, especially toward the myeloid lineage (Fig. 4f, Supplementary Fig. 17). These data

indicate that the accumulated $Ly6G^+$ neutrophils carrying JAK2V617F are migrated from BM to pulmonary arterial regions, and potentially proliferated and maturated from the precursors in the lungs.

Alternation of gene profiling during neutrophil differentiation with JAK2V617F.

To elucidate the underlying mechanisms of how BM-derived neutrophils carrying JAK2V617F were causally related to PH development, we performed gene expression profiling of the neutrophils at several stages of differentiation by RNA sequencing in sorted $Ly6G^+$ cells from BM, peripheral blood (PB) and lungs of $JAK2^{V617F}$ mice in comparison to WT mice. The purity of the lung $Ly6G^+$ cell enrichment was confirmed by immunofluorescence (Supplementary Fig. 18). To compare these data with the cells at the hematopoietic stem/progenitor cell level, we used the available RNA sequencing results of $lineage^-Sca1^+Kit^+$ (LSK) cells in BM from our previous study[22]. We found that 451, 849, 1142, and 1022 genes were upregulated, and 580, 841, 1123, and 1006 genes were downregulated in LSK cells and $Ly6G^+$ cells of the BM, PB and lungs, respectively, in $JAK2^{V617F}$ mice compared to WT mice (Fig. 5a, Supplementary Data 1). Differentially expressed genes in $JAK2^{V617F}$ mice were more frequently overlapped among the BM, PB and lung $Ly6G^+$ cells than between the LSK cells and BM $Ly6G^+$ cells. Next, we subjected these RNA sequencing results to the pathway analysis (Fig. 5b). Hierarchical clustering analysis showed that the gene profiling was branched from the LSK cells, and diverged into BM myeloid cells and neutrophils in the lungs and PB, suggesting that the neutrophils were spread peripherally. Some of the canonical pathways were commonly up- and down-regulated at each stage. There were also pathways that were enhanced in accordance with differentiation and that were specifically enhanced in the final stage before peripherally.

312 Thus, the gene expression profiles were differently altered from the LSK cells to lung
313 neutrophils in JAK2^{V617F} mice.
314
315 **Ly6G^{+} cells carrying JAK2V617F progressively increased *Acvrl1* gene expression**
316 **during the process of differentiation into peripheral pulmonary arterial regions of**
317 **the lungs.**
318 A gene set enrichment analysis revealed that the canonical IL6-JAK-STAT3 pathway was
319 upregulated at each stage of neutrophil differentiation in JAK2^{V617F} mice compared to
320 WT mice (Fig. 5c), with some alterations of differentially expressed individual genes
321 (Fig. 5d). Interestingly, *Activin A receptor like type 1* (*Acvrl1*), which encodes ALK1 and
322 is known as a type I transmembrane serine/threonine kinase receptor, is associated with
323 the pathogenesis of PH[7, 28] and has been found to be the most upregulated gene in the
324 canonical IL6-JAK-STAT3-pathway in Ly6G^{+} neutrophils of the lungs and PB of
325 JAK2^{V617F} mice (Fig. 5d). *Acvrl1* was slightly upregulated in the BM Ly6G^{+} myeloid cells
326 and LSK cells of JAK2^{V617F} mice (Fig. 5d). Furthermore, the genes associated with
327 neutrophil functions such as protein secretion, degranulation, and granulation were
328 exclusively enriched in the periphery, especially in the lung Ly6G^{+} neutrophils with
329 JAK2V617F (Fig. 5e–g).
330
331 ***Acvrl1* mRNA expressions and phosphorylation of Smad1/5/8 and Stat3 in the lungs**
332 **of JAK2^{V617F} mice in response to chronic hypoxia.**
333 *Acvrl1* mRNA expression levels in the lung homogenates of JAK2^{V617F} mice were higher
334 than those of WT mice after exposure to normoxia (Fig. 6a). In response to chronic
335 hypoxia, *Acvrl1* levels were increased in both WT and JAK2^{V617F} lungs, but the levels in

336 JAK2^{V617F} lungs were greater than those in WT lungs. *Acvrl1* mRNA levels in sorted
337 Ly6G^{+} neutrophils were significantly elevated in JAK2^{V617F} lungs compared to WT lungs
338 after both normoxia and hypoxia, but not in CD31^{+} endothelial cells, suggesting that the
339 changes in *Acvrl1* in the lungs resulted from different expression levels of *Acvrl1* in
340 Ly6G^{+} neutrophils, although *Acvrl*1 expression levels were higher in CD31^{+} cells than in
341 Ly6G^{+} cells (Fig. 6a, Supplementary Fig. 19a). Similarly, phosphorylation levels of
342 Smad1/5/8, which is down-stream of ALK1, were significantly elevated in JAK2^{V617F}
343 lungs compared to WT lungs after chronic hypoxia (Fig. 6b). There was a significant
344 difference between the 10-fold increase in *Acvrl1* mRNA levels versus the 2-fold increase
345 in phosphorylated Smad1/5/8 levels in chronic hypoxia-exposed JAK2^{V617F} lungs,
346 indicating that the relationship of *Acvrl1* mRNA expression and the phosphorylation of
347 Smad1/5/8 was not completely linear, and Smad1/5/8 phosphorylation may be regulated
348 by multiple pathways. *Acvr1* mRNA encoding the ALK2 in the lung homogenates was
349 significantly increased after chronic hypoxia in both WT and JAK2^{V617F} mice, but there
350 were no differences between the groups after normoxia or hypoxia. However, *Acvr1*
351 mRNA in Ly6G^{+} cells was decreased in both WT and JAK2^{V617F} mice after hypoxia, and
352 the changes in *Acvr1* levels were observed in the opposite direction to those seen in *Acvrl1*
353 (Supplementary Fig. 19b). There were no differences in *Bmpr2* mRNA between WT and
354 JAK2^{V617F} mice in the lung homogenates, Ly6G^{+}, or CD31^{+} cells (Supplementary Fig.
355 19c). STAT3 phosphorylation levels were significantly increased in JAK2^{V617F} lungs
356 compared to WT lungs after normoxia exposure; however, after exposure to chronic
357 hypoxia, these levels in JAK2^{V617F} lungs were even more upregulated compared to the
358 other groups (Fig. 6c). HIF1α expression levels in the lungs were increased in both WT
359 and JAK2^{V617F} mice after chronic hypoxia, but there was no difference between the

groups (Supplementary Fig. 20). Immunoprecipitation analysis showed that STAT3 protein weakly interacted with HIF1α in JAK2^{V617F} lungs at normoxia, and chronic hypoxia increased the bindings (Supplementary Fig. 21). The conditioned medium from hypoxia-exposed JAK2^{V617F} neutrophils pretreated with a HIF1α inhibitor partly attenuated the increases in the proliferation of pulmonary arterial smooth muscle cells (Supplementary Fig. 22). Thus, JAK-STAT3 signaling in the lungs was constitutively activated in JAK2^{V617F} mice at baseline, whereas both the JAK-STAT3 and ALK1-Smad1/5/8 pathways were further upregulated in JAK2^{V617F} lungs in response to chronic hypoxia, which may be associated with HIF1α. These data suggest that ALK1-Smad1/5/8 in the lungs is associated with PH development due to clonal hematopoiesis with JAK2V617F.

_JAK2_V617F transcriptionally upregulates _ACVRL1_ by STAT3-binding.

To investigate the regulatory mechanisms of *ACVRL1* by *JAK2*V617F, heterozygous *JAK2*V617F knock-in (*JAK2*$^{V617F/+}$) HCT116 cell lines were analyzed. Smad1/5/8 was phosphorylated by stimulation of BMP9, a high affinity in ALK1 ligand, in HCT116 cells (Supplementary Fig. 23). Phosphorylation levels of STAT3 in *JAK2*$^{V617F/+}$ cells were significantly elevated compared to those in *JAK2*$^{+/+}$ cells (Fig. 7a). *JAK2*$^{V617F/+}$ cells exhibited significant increases in the expression levels of *ACVRL1* mRNA as well as ALK1 protein and phosphorylation levels of Smad1/5/8 compared to *JAK2*$^{+/+}$ cells (Fig. 7b, c, Supplementary Fig. 24), but not in *ACVR1* (ALK2) expressions (Supplementary Fig. 25). To assess the effects of *JAK2*V617F on the transcriptional activity of *ACVRL1*, an *in silico* analysis was performed, which identified putative STAT3 binding sites in the *ACVRL1* promoter region in both humans and mice (Fig. 7d). The chromatin

immunoprecipitation (ChIP) coupled with qPCR showed that the bindings of STAT3 and the putative *ACVRL1* promoter regions were significantly increased in *JAK2*$^{V617F/+}$ HCT116 cells compared to *JAK2*$^{+/+}$ HCT116 cells (Fig. 7e). Next, we performed the luciferase reporter assay using the luciferase construct containing the human *ACVRL1* putative promoter sequence from -1035 bp to +210 bp of the transcriptional start site[29]. The promoter activity of *ACVRL1* in *JAK2*$^{V617F/+}$ cells was significantly increased compared to those of *JAK2*$^{+/+}$ cells (Fig. 7f). Ruxolitinib, a specific JAK1/2 inhibitor, decreased the *ACVRL1* promoter activity in a dose-dependent manner in *JAK2*$^{V617F/+}$ HCT116 cells (Fig. 7g). In addition, the administration of stattic, an inhibitor of STAT3, attenuated the *ACVRL1* promoter activity (Fig. 7h). Taken together, *JAK2*V617F increased *ACVRL1* transcriptional activity via STAT3-binding, resulting in phosphorylation of Smad1/5/8 in HCT116 cells.

Inhibition of ALK1/2 prevents chronic hypoxia-induced pulmonary hypertension in JAK2^{V617F} mice.

We investigated whether the inhibition of ALK1 could ameliorate chronic hypoxia-induced PH in JAK2^{V617F} mice (Fig. 8a). K02288, a chemical inhibitor of ALK1/2[30,31] clearly decreased the phosphorylation levels of Smad1/5/8 in chronic hypoxia-exposed JAK2^{V617F} lungs as well as *JAK2*$^{V617F/+}$ HCT116 cells (Supplementary Fig. 26). Administration of K02288 did not affect blood cell counts in JAK2^{V617F} mice (Fig. 8b). Remarkably, K02288 treatment significantly decreased RVSP and RV/LV+S in JAK2^{V617F} mice compared to DMSO-treated JAK2^{V617F} mice after exposure to chronic hypoxia (Fig. 8c, Supplementary Fig. 27). In contrast, K02288 administration did not significantly change the levels of RVSP or RV hypertrophy in chronic hypoxia-exposed

WT mice. There were significant decreases in medial wall thickness and muscularization, as well as in the numbers of proliferating smooth muscle cells in pulmonary arteries of K02288-treated JAK2^{V617F} mice compared to DMSO-treated JAK2^{V617F} mice (Fig. 8d, e, Supplementary Fig. 28). The numbers of Ly6G^{+} neutrophils in perivascular regions were decreased in K02288-treated JAK2^{V617F} lungs compared to DMSO-treated JAK2^{V617F} lungs (Fig. 8f, g). In addition, K02288 treatment significantly decreased elastase activity in JAK2^{V617F} lungs (Fig. 8h). Of note, we found that the treatment of LDN-212854, another ALK1/2 inhibitor,[31] significantly decreased RVSP and RV/LV+S in chronic hypoxia-exposed JAK2^{V617F} mice, similar to K02288 (Supplementary Fig. 29, 30). K02288 or LDN-212854 did not affect the levels of RVSP and RV/LV+S in WT or JAK2^{V617F} mice after normoxia (Supplementary Fig. 31). A higher dose of K02288 did not attenuate the PH levels of hypoxia-exposed WT mice (Supplementary Fig. 32). Collectively, these results suggest that the ALK1/2 pathway is involved in chronic hypoxia-induced PH in JAK2^{V617F} mice.

Prevalence of *JAK2*V617F-clonal hematopoiesis in PH patients.

To clarify the clinical relevance of clonal hematopoiesis with *JAK2*V617F in PH, we prospectively recruited PH patients, and examined the prevalence of clonal hematopoiesis with *JAK2*V617F in 70 PH patients by allele specific quantitative PCR analysis[32]. Strikingly, we found that 7.1% of the PH patients (n = 5) showed *JAK2*V617F somatic mutation in peripheral leukocytes, which was significantly higher than that of the age- and sex-matched control subjects (Fig. 9a, Supplementary Table 1). Among these five PH patients with *JAK2*V617F, three patients, who were categorized into WHO Group IV (chronic thromboembolic pulmonary hypertension), were regarded as CHIP with a

*JAK2*V617F VAF of ≥ 2% (Fig. 9b, Supplementary Table 2). The *JAK2*V617F VAF was < 2% in the remaining two patients, who were classified into WHO Group I (pulmonary arterial hypertension). These two patients were in their 50s and 30s; younger than the average age of patients with age-related clonal hematopoiesis. Of note, none of the *JAK2*V617F-positive PH patients met the criteria of hematological disorders including MPNs[33]. There were no significant differences in clinical characteristics, laboratory data including blood cell counts, echocardiographic parameters, or hemodynamics between the PH patients with and without the *JAK2*V617F mutation (Fig. 9c, d, Supplementary Table 3). These data indicate that clonal hematopoiesis with *JAK2*V617F is related to the onset and development of PH in the carriers of this mutant, regardless of blood cell counts or PH severity.

Discussion

The present study demonstrates that clonal hematopoiesis with JAK2V617F accelerated PH in both the absence and presence of phenotypic MPNs in mice. Neutrophils-derived vascular remodeling was involved in JAK2V617F-mediated PH development. JAK2V617F progressively upregulated *Acvrl1* expression from BM stem/progenitor cells into neutrophils in pulmonary arterial regions in the lungs. JAK2V617F further increased ALK1-Smad1/5/8 signaling accompanied with increases in neutrophil-derived elastase activity and multiple chemokines, resulting in pulmonary arterial remodeling after chronic hypoxia. Correspondingly, *JAK2*V617F-positive clonal hematopoiesis was more common in the PH patients than in the healthy subjects, despite no signs of hematological disorders.

In the current study, we employed two experimental mouse models mimicking hematological clinical scenarios. Namely, in one model, $JAK2^{V617F}$ mice which displayed an MPN-like phenotype were used, and in the other, recipient mice transplanted with $JAK2^{V617F}$ BM cells were used to model clonal hematopoiesis without hematologic phenotypes. Both $JAK2^{V617F}$ mice and $JAK2^{V617F}$-BMT mice similarly showed that the number of neutrophils was prominently increased specifically in pulmonary arterial regions, accompanied by vascular remodeling after chronic hypoxia, suggesting that JAK2 activation in neutrophils play a central role in PH. It is likely that the $JAK2^{V617F}$ neutrophils largely migrated into pulmonary arterial regions from BM. JAK2V617F may increase the adhesion and rolling of neutrophils partly due to increases in formyl peptide receptor (FPR)[17], as our RNA sequencing data demonstrated that both *Fpr1* and *Fpr2* were higher in the $Ly6G^{+}$ lung neutrophils of $JAK2^{V617F}$ mice (3.1- and 3.8-fold, respectively) than in those of WT mice. Moreover, it is possible that the $JAK2^{V617F}$

467 hematopoietic precursor cells in the lungs can display the capacity to lodge and complete
468 maturation there. PH patients with or without MPNs have increased circulating $CD34^+$
469 hematopoietic stem/progenitor cells[34]. Engraftment of hematopoietic progenitors from
470 PH patients who did not display any hematological disorder into xenografts showed
471 increases in the growth of myeloid colonies and the expression of myeloid transcription
472 factors, resulting in pulmonary vascular remodeling and right heart hypertrophy[35],
473 suggesting that the intrinsic capability of hematopoietic progenitors is associated with
474 PH. In line with our $JAK2^{V617F}$-BMT model that did not show elevation of white blood
475 cells or platelets, the activation of JAK-STAT in myeloid cells may lead to PH phenotypes
476 even without elevation of leukocyte or platelet counts. The rheological effects of
477 leukocytes and thrombocytes on PH need to be clarified. $JAK2^{V617F}$ mice developed a PH
478 pathology in response to chronic hypoxia, but did not develop PH in normoxia, indicating
479 that JAK2V617F alone is not sufficient to induce PH, and that a trigger such as chronic
480 hypoxia is required for PH phenotypes in $JAK2^{V617F}$ mice. In contrast, patients with
481 MPNs can develop PH in the setting of normoxia. However, not all MPN patients develop
482 PH. As MPNs occurs later in life[36], an additional genetic and/or environmental hit in
483 addition to JAK2V617F may be needed for the onset and development of PH in
484 predisposed subjects.

485 Enhanced neutrophil-derived elastase activity is involved in the response of pulmonary
486 arterial smooth muscle cells, resulting in excessive muscularity of the vessels[3, 24, 37].
487 Neutrophils produce a wide range of substances that could contribute to exaggerated
488 contractility and proliferation of vascular cells, leading to vascular remodeling in the
489 lungs[38]. While the infiltration of neutrophils was increased by hematopoietic JAK2V617F
490 expression even after normoxia exposure, the increased $JAK2^{V617F}$ neutrophils did not

induce pulmonary vascular remodeling or elevate RVSP. RNA sequencing indicated that the differentiated JAK2^{V617F} neutrophils in the lungs and PB, but not in BM myeloid cells or LSK cells, were activated in terms of protein secretion, degranulation and granulation after normoxia exposure. However, elastase activity or neutrophil-derived chemokines were not elevated in JAK2^{V617F} lungs after normoxia exposure. These findings raise the possibility that biological mechanisms such as elastase activity by neutrophils, leading to pulmonary vascular remodeling, might be compensated, unless there is an additional factor, such as chronic hypoxia. Increased physical interactions of HIF1α and STAT3[39] in response to hypoxia might trigger PH phenotypes in JAK2^{V617F} mice, but further mechanisms and investigation by other PH models such as the monocrotaline-pyrrole need to be clarified.

The binding of STAT3 to *ACVRL1* promoter regions induced by *JAK2*V617F upregulated *ACVRL1* gene expression at the transcriptional level, in addition to the previously reported finding of transcriptional regulation of *ACVRL1*[29]. It is known that *ACVRL1* is one of the genes affected by germline mutations identified in patients with pulmonary arterial hypertension[28]. Germline mutations of *ACVRL1* also cause hereditary hemorrhagic telangiectasia, a dominant autosomal vascular dysplasia, and PH is recognized as a severe complication of this disease[40, 41]. It has been reported that *ACVRL1* mutations in hereditary hemorrhagic telangiectasia led to a loss of function[42,43]. Most of *ACVRL1* mutations found in pulmonary arterial hypertension are the same mutations described in HHT which result in a loss of function. The loss-of-function mutations in *ACVRL1* are important causes of heritable pulmonary arterial hypertension.[44] Consistently, heterozygous ALK1 knockout mice developed PH in adulthood[45]. In contrast, the inhibition of BMP9 partly protected chronic hypoxia-induced PH in the adult

515 mice and systemic administration of ALK1 inhibitor, a ligand trap targeting ALK1,
516 prevented the monocrotaline and Sugen hypoxia-induced PH in the adult rats[46],
517 suggesting that systemic blockade of the BMP9/ALK1 pathways is beneficial for PH in
518 the adult rodents. In the present study, we showed that ALK1/2 inhibitor administration
519 prevented the progression of chronic hypoxia-induced PH in JAK2^{V617F} mice, indicating
520 that JAK2V617F-related ALK1 upregulation in myeloid cells had detrimental effects in
521 PH. Although the molecular roles of ALK1 have been investigated particularly in
522 endothelial cells, ALK1 expressions in myeloid cells may have a different impact on PH
523 from the lung endothelial cells. As the functional relevance of ALK1 in PH is not fully
524 understood, a conditional knockout model of hematopoietic cells is needed to clarify the
525 role of ALK1 on PH in the hematopoietic system.

526 It has recently been reported that clonal hematopoiesis was especially associated with
527 atherosclerotic cardiovascular diseases[12,15]. Among the somatic mutations related to
528 clonal hematopoiesis, individuals with *JAK2*V617F showed a higher risk of coronary
529 heart disease compared to those without CHIP and those with mutations other than
530 *JAK2*V617F[15]. We showed here the association between clonal hematopoiesis and PH.
531 Importantly, five out of the 70 PH patients (7.1%) were carriers of *JAK2*V617F-positive
532 clonal hematopoiesis, three of whom fulfilled the criteria of CHIP, with a *JAK2*V617F
533 VAF exceeding 2%. The remaining two patients were in their 30s and 50s, younger than
534 the average age of patients with age-related clonal hematopoiesis. Our murine study
535 demonstrated that even small clones with *JAK2*V617F led to PH development. Given that
536 *JAK2*V617F VAF as low as 0.1–2% was associated with the elevation of blood cell
537 counts, manifestations of MPNs, thrombotic events, and survival in both *JAK2*V617F-
538 positive general populations without MPNs and patients with MPNs,[47,48,49,50] the presence

539 of *JAK2*V617F, even with low VAF, may have a clinically biological impact. Further
540 study into the relationship between *JAK2*V617F VAF levels and PH prevalence is
541 required.

542 Currently, no treatment has yet been established to prevent or directly modify clonal
543 hematopoiesis-associated cardiovascular diseases. The JAK1/2 inhibitor ruxolitinib is
544 now routinely used in patients with MF and PV for improvements of splenomegaly and
545 disease-related symptoms[51, 52]. For MPN patients with PH complications, ruxolitinib has
546 been shown efficacy to ameliorate PH only in a small number of patients[53,54] or has
547 actually exacerbated PH in some cases[55]. There are concerns, such as hematologic
548 toxicities, dysfunction of lymphocytes, and reactivation of viral infections, regarding the
549 use of ruxolitinib for patients with clonal hematopoiesis without any hematologic
550 disorders. The only possible treatment to eliminate clones with somatic mutations,
551 including *JAK2*V617F, is hematopoietic stem cell transplantation, which is however often
552 associated with serious comorbidity and treatment-related mortality. Moreover, it has
553 recently been reported that PH is associated with poor outcome of hematopoietic stem
554 cell transplantation in patients with MPNs[56]. Therefore, transplantation may not be a
555 suitable strategy for PH patients with MPNs or clonal hematopoiesis, unless the patient
556 is in a severe hematologic condition, such as acute leukemia.

557 Although medical therapies for PH, such as prostanoids and endothelin receptor
558 antagonists, have been greatly improved, PH remains a progressive and fatal disease[1].
559 Precision medicine may be a novel approach that identifies *JAK2*V617F-positive PH
560 patients regardless of the etiologies of PH. In the present study, we did not find any
561 significant differences in clinical characteristics, including blood cell counts or
562 hemodynamics, between the *JAK2*V617F-positive and -negative PH patients. In turn,

these findings suggest that examination of *JAK2*V617F may be a potential strategy, which may help in the diagnosis and treatment of *JAK2*V617F-positive PH patients. Furthermore, three patients with *JAK2*V617F were categorized into Group IV, implying that JAK2V617F promotes venous thrombosis resulting in pulmonary embolisms[57]; however, our murine data showed that pulmonary arterial structural remodeling was accelerated in the presence of hematopoietic JAK2V617F with no distinct features of venous thrombosis in the lungs. Notably, ALK1/2 inhibitors completely prevented chronic hypoxia-induced PH in JAK2V617F-mediated clonal hematopoiesis, without causing hematologic toxicity. Inhibition of ALK1/2 may be effective especially in the JAK2V617F lung neutrophils. Although we cannot exclude the potential effects of ALK2 on PH, ALK1 is a promising therapeutic target for PH patients with clonal hematopoiesis induced by *JAK2*V617F.

A limitation of this study was that overexpression levels of the transgenic mice expressing murine JAK2V617F might non-specifically affect the varieties of individual phenotypes; therefore, we also used BMT models. In human studies, inherited genetic backgrounds or other CHIP-related mutations could not be determined in the PH patients in a small sample size. Future work is needed to validate our findings in larger cohorts.

In conclusion, we unveiled that a hematopoietic cell clone with JAK2V617F was involved in the development of PH with neutrophil-derived vascular remodeling with ALK1 upregulation. Our study provides an approach for precision medicine that identifies *JAK2*V617F in PH patients, and suggests ALK1 as a possible candidate of therapeutic target.

Methods

Animals

JAK2^{V617F} mice of transgenic-*Jak2*V617F with a C57BL/6J background were obtained as described previously[21, 22]. Female JAK2^{V617F} mice aged between 8 and 10 weeks (body weight range, 18–24 g) were used in the present study. WT littermates were used as controls. CAG-EGFP reporter mice with a C57BL/6J background were purchased from Japan SLC. JAK2^{V617F} mice were crossed with CAG-EGFP mice to generate JAK2^{V617F}/CAG-EGFP double transgenic mice (JAK2^{V617F}-GFP)[27], and WT littermates were used as controls (WT-GFP). We used female mice unless otherwise indicated. Mice were housed with food and water ad libitum during 12-hour light/12-hour dark cycles (light, 7:00–19:00; dark, 19:00–7:00), and ambient temperature (21.5 °C) and humidity (55 ± 10%) were monitored.

Peripheral blood analysis

Blood was collected from the tail vein and blood cell counts were determined using Sysmex pocH-100i (Sysmex).

Exposure to chronic hypoxia

The mice were exposed to normoxia (21% O_2) or hypoxia (10% O_2) for 2 or 3 weeks in a ventilated chamber[20]. The hypoxic environment was kept in a mixture of air and nitrogen (Teijin Ltd.). The chamber was kept closed, and was only opened to supply food and water as well as for cleaning twice a week. In a Sugen-hypoxia model, the mice received a single weekly injection of a VEGF inhibitor, SU-5416 (HY-10374, Med Chem Express), at 20 mg/kg followed by 2 weeks of hypoxia (10% O_2).

610

611 **Echocardiography**

612 Transthoracic echocardiography was performed using Vevo 2100 High-Resolution In
613 Vivo Imaging System (Visual Sonics Inc.) with a 40-MHz imaging transducer. Mice were
614 lightly anesthetized by titrating isoflurane (0.5–1.5%) to achieve a heart rate of around
615 400/min. RV fractional area change, RV diastolic dimension, PA acceleration time, PA
616 ejection time, RV anterior wall diameter, tricuspid annular plane systolic excursion,
617 cardiac output, and LV fractional shortening were determined[58].

618

619 **Hemodynamics and assessment for right ventricular hypertrophy**

620 After chronic exposure to normoxia or hypoxia, the mice were anesthetized by
621 intraperitoneal injection of 2,2,2-tribromo-ethanol (0.25 mg/g per body weight)[20]. A 1.2F
622 micromanometer catheter (Transonic Scisense Inc.) was inserted from the right jugular
623 vein, and RVSP was continuously measured. The RVSP was blindly analyzed by
624 LabScribe3 software (IWORX) and averaged over 10 sequential beats. To evaluate RV
625 hypertrophy, the RV was dissected from the LV, including the septum, and RV/LV+S
626 was calculated.

627

628 **Histological analysis**

629 Lung samples were fixed in 4% paraformaldehyde solution for paraffin embedding.
630 Frozen lung tissues were embedded in the O.C.T. compound (Tissue-Tek). The paraffin-
631 embedded sections were stained with H&E or Elastica-Masson (EM), or they were used
632 for immunostaining. In the EM-stained sections, the wall area between the internal and
633 external lamina of the pulmonary arteries with a diameter between 50 and 100 μm was

measured and expressed as the percentage of medial wall thickness divided by the vessel area using ImageJ software (National Institutes of Health)[58]. In the sections stained with αSMA (M0851, Dako), the pulmonary vessels with a diameter of less than 50 μm were classified into three groups; the vessels with αSMA-positives throughout the entire circumference of the vessel cross-section was defined as "fully" muscularized, the vessels with αSMA-positives with 5–99% around the vessel was defined as "partially" muscularized, and the vessels with αSMA-positives with < 5% around the vessel was classified as "non" muscularized.[58] Based on the anatomical characteristics, pulmonary arteries, distributed along the bronchi and displayed an eccentric morphology with thick and elastic walls, are distinguishable from pulmonary veins. The percentage of muscularized pulmonary vessels was determined by dividing the sum of the partially and fully muscular vessels by the total number of vessels[58]. For immunofluorescence staining, the paraffin-embedded tissue sections were incubated with primary antibodies against Ly6G (1:100, ab25377, Abcam), CD45 (1:100, 70257, Cell Signaling Technology; sc-53665, Santa Cruz Biotechnology Inc.), F4/80 (1:100, 70076, Cell Signaling Technology), CD45R (1:100, 103201, Biolegend), Ki67 (1:100, ab15580, Abcam), αSMA (1:100, M0851, Dako; 19245, Cell Signaling Technology), or GFP (1:100, NBP2-22111, Novus Biologicals). This was followed by incubation with the appropriate secondary antibodies, including Alexa Fluor 488 (1:1000, ab150105, Abcam), Alexa Fluor 594 (1:1000, R37119, A-21211; Thermo Fisher Scientific), and Alexa Fluor 647 (1:1000, ab150159, Abcam), then mounted with DAPI-containing mounting media (Fluoro Gel II, Electron Microscopy Sciences). Immunohistochemical staining of the paraffin-embedded or O.C.T.-embedded sections was performed with the following primary antibodies; CD41 (1:100, ab63983, Abcam) or TER-119 (1:100, 116201,

BioLegend) followed by anti-rabbit or anti-rat IgG antibody labeled with peroxidase (14341F, 414311F, Nichirei Bioscience) with DAB peroxidase substrate system (Dojin Co., Ltd.) and counterstaining with hematoxylin. For quantification of perivascular cellular infiltration, more than 100 cells were counted around the distal pulmonary arteries, with a diameter of 50–100 μm in each mouse[59]. All images were acquired by a microscope (BZ-X700, Keyence Co.) using Keyence BZ II Viewer software (Keyence Co.).

Western blot analysis

Snap frozen mouse lung samples or cultured cells were initially homogenized in lysis buffer (Cell Lysis Buffer, Cell Signaling Technology) containing protease inhibitor cocktail (BD Biosciences)[60]. Protein concentration was determined using a Pierce BCA Protein Assay Kit (Thermo Fisher Scientific). Aliquots of proteins were subjected to SDS-polyacrylamide gel electrophoresis, transferred onto polyvinylidene difluoride membranes (Merck Millipore), and probed with the following primary antibodies; HIF1α (1:1000, 36169, Cell Signaling Technology), Phospho-STAT3 (1:1000, 9145, Cell Signaling Technology), STAT3 (1:1000, 4904, Cell Signaling Technology), Phospho-Smad1/Smad5/Smad8 (1:1000, AB3848-I, Merck Millipore), Smad1 (1:1000, 9743, Cell Signaling Technology), ALK1 (1:1000, 14745-1-AP, Proteintech), ALK2 (1:1000, MAB637, R&D Systems) and GAPDH (1:1000, 60004-1-Ig, Proteintech) followed by appropriate goat anti-rabbit or mouse horseradish peroxidase-conjugated secondary antibodies (1:10000, sc-2357, sc-516102, Santa Cruz Biotechnology Inc.). Immunoreactive bands were visualized by an Amersham ECL system (Amersham Pharmacia Biotech UK Ltd.), and signals were detected with an ImageQuant LAS-4000

digital imaging system (GE Healthcare). Or fluorescent immunoreactive bands were detected by an Odyssey CLX imaging system (LI-COR Biosciences) when the appropriate IRDye 680 or IRDye 800 secondary antibodies (1:20000, 925-68070, 925-68071, 925-32210, 925-32210, LI-COR Biosciences) were used. Optical densities of individual bands were analyzed using ImageJ software or Image Studio software (LI-COR Biosciences).

Reverse transcription quantitative polymerase chain reaction (RT-qPCR)

Total RNA was extracted from mouse lungs, sorted cells or cultured cells using Trizol reagent according to the manufacture's protocol (Thermo Fisher Scientific). The RNA from the lung samples was further purified using RNeasy Fibrous Tissue Mini Kit (Qiagen Inc.). cDNA was synthesized using ReverTra Ace qPCR RT Master Mix (Toyobo Co., Ltd.). Quantitative PCR was performed to determine the mRNA expression of *Ccl2*, *Cxcl1*, *Ccr1*, *Cxcr2*, *Pdgfrb*, *Tgfb1*, *Acvrl1, Acvr1,* and *Bmpr2* using THUNDERBIRD SYBR qPCR Mix (Toyobo Co., Ltd.) in a CFX Connect real-time PCR System (Bio-Rad) with Bio-Rad CFX Manager 3.1 software (Bio-Rad). A standard curve method on serially diluted templates was applied for the lung samples, and a delta CT method was used for the cell samples. All data were normalized to *18s rRNA* and expressed as a fold increase of the control group. Primer sequences are described in Supplementary Table 4.

Elastase assay

Elastase activity in the lung tissue was evaluated using the EnzChek Elastase Assay Kit (Molecular Probes)[24, 61]. Briefly, the frozen lung samples (20 mg) were homogenized and

mixed with the extraction buffer containing NaAc and Na azide, and then rotated overnight at 4°C. After centrifuge, the pellet was reextracted by adding $(NH_4)_2SO_4$ buffer. After overnight precipitation, the centrifuged pellet was resuspended in 50 mM TrisHCl assay buffer (pH 8.0) to reactivate the elastase. Elastase activity was then measured by adding bovine DQ-Elastin as a fluorogenic substrate in duplicate wells.

Bone marrow transplantation (BMT)

Recipient female C57BL/6J mice aged between 8 and 10 weeks (Charles River Japan, Inc.) were lethally irradiated with a total dose of 9.0 Gy 24 h before BMT[22]. Whole BM cells were harvested from donor femurs and tibiae. The cells were washed with PBS and 5.0×10^6 of BM cells were injected in the recipient mice via the tail vein. Peripheral blood parameters and chimerism were analyzed at 4 weeks after transplantation and at the termination of the experiments. DNA was isolated using the QuickGene DNA whole blood kit (KURABO) and quantitative PCR was performed using THUNDERBIRD SYBR qPCR Mix with the following primers; forward primer for donor and recipients, 5'-CTTTCTTCGAAGCAGCAAGCATGA-3', reverse primer for recipients; 5'-CTGGCTTTACTTACTCTCCTCTCCACAGAC-3' reverse primer for donors; 5'-AACCAGAATGTTCTCCTCTCCACAGAA-3'. Delta Ct (Ct_{donor}– Ct_{total}) was calculated to estimate *Jak2*V617F VAF in $JAK2^{V617F}$-BMT mice.

Magnetic-activated cell sorting (MACS)

Myeloid cells and neutrophils from the BM, PB and lungs were isolated by using MACS MS columns (Miltenyi Biotec GmbH) with Ly6G MicroBeads according to the manufacturer's protocols. To form a cell suspension from the lungs, the tissues were

minced and digested in 2 mg/mL collagenase type II (Worthington Biochemical) for 30 min. Then the tissues were passed through an 18-gauge needle and a 70 μm cell strainer. The purity of the neutrophils was > 98% as determined by May-Giemsa staining, and the specificity was confirmed with positive immunostaining by anti-Ly6G (ab25377, Abcam) and anti-Myeloperoxidase (ab9535, Abcam) antibodies and with negative immunostaining by an anti-CD31 antibody (102401, BioLegend). The hematopoietic stem progenitor cells from the lungs were isolated using CD117 MicroBeads. The endothelial cells from the lungs were isolated by CD31 MicroBeads. All MicroBeads were purchased from Miltenyi Biotec GmbH.

Flow cytometry

Leukocytes were isolated from the peripheral blood and the lungs. The single cell suspensions from the lung tissues were prepared by the same methods described in MACS. After lysing red blood cells using an ammonium chloride-containing buffer, cells were stained with the relevant antibodies (CD45.2, 109814, BioLegend; Ly6G, 560599, BD Biosciences), assessed by flow cytometry using a FACSCanto II (BD Biosciences) and analyzed by FlowJo (version 10.2, Tree Star Inc.).[22] HCT116 cells were collected and incubated with an anti-ALK1 antibody (14745-1-AP, Proteintech) followed by R-PE-conjugated donkey anti-rabbit secondary antibody (711-116-152, Jackson ImmunoResearch). The gating strategies are provided in Supplementary Fig. 33.

Transwell chemotaxis assays

Chemotaxis in neutrophils from mouse blood was assessed using CytoSelect 96-well (3 μm, Fluorometric Format) according to the manufacturer's protocol.

754

755 **Colony assay**

756 The MACS-isolated lung CD117^{+} cells were cultured in 1 mL of MethoCult M3434
757 (Stemcell Technologies) on a 35-mm plate. After 7 days, types of colonies and colony
758 numbers were determined based on manufacturer's instructions. Images were captured
759 by BZ-X700 microscope.

760

761 **RNA sequencing**

762 RNA from MACS-isolated Ly6G^{+} cells from the BM, PB and lungs was purified using
763 an RNeasy Plus Micro Kit (Qiagen) according to the manufacturer's protocol. RNA
764 concentrations and integrities were evaluated using the TapeStation (Agilent). Total RNA
765 was subjected to reverse transcription and amplification with the SMARTer Ultra Low
766 Input RNA Kit for Sequencing (Clontech). After sonication using ultrasonicator
767 (Covaris), the libraries for RNA sequencing were generated from fragmented DNA with
768 10 cycles of amplification using a NEB Next Ultra DNA Library Prep Kit (New England
769 BioLabs). After the libraries were quantified using the TapeStation (Agilent), the samples
770 were subjected to sequencing with Hiseq2500 (Illumina) and 61 cycles of the sequencing
771 reactions were performed. TopHat2 (version 2.0.13; with default parameters) and
772 Bowtie2 (version 2.1.0) were used for alignment to the reference mouse genome (mm10
773 from the University of California, Santa Cruz Genome Browser;
774 http://genome.ucsc.edu/). Levels of gene expression were quantified using Cuffdiff
775 (Cufflinks version 2.2.1; with default parameters). We also used the data from our
776 previous study's RNA sequencing of flow cytometry-sorted LSK cells.[22]

777

Analyses of pathways and gene set enrichment

Affected pathways or gene set enrichment were compared among $Ly6G^+$ cells from the lungs, PB, and BM, and LSK cells from our previous study[22] using the comparison analysis in IPA™ (Ingenuity Pathways Analysis, Qiagen) or Gene Set Enrichment Analysis (GSEA, Broad Institute), respectively, according to the RPKM+1 value for each gene determined by RNA sequencing.

Immunoprecipitation

Samples of $JAK2^{V617F}$ mouse lung tissue were lysed with lysis buffer (75 mmol/L NaCl, 50 mmol/L Tris-HCl, 0.5% Nonidet P-40, pH 8.0) with a protease inhibitor cocktail. Protein was subjected to immunoprecipitation using protein A-coupled magnetic beads (Thermo Fisher Scientific) and an anti-HIF1α antibody (36169, Cell Signaling Technology) for 1 h at room temperature. Rabbit IgG was used as control.

Preparation of primary pulmonary arterial smooth muscle cells (PASMCs) and assessment of proliferation using neutrophil-derived conditioned medium

Mouse PASMCs were isolated from WT mice with a C57BL/6J background by enzymatic dissociation of the minced lung with collagenase type II (Worthington)[58] and cultured in DMEM (Wako) containing 20% fetal bovine serum. The PASMCs were seeded in 96-well plates or on coverslips in 24-well plates. Conditioned medium from neutrophils in hypoxia incubator chamber (10% O_2, ASTEC) 3 h after incubation was collected. The neutrophils were pretreated with Echinomycin (Sigma) prior to hypoxia for 1 h. Then, the PASMCs were incubated with the conditioned medium for 48 h and then subjected to CellTiter 96 AQueous One Solution Cell Proliferation Assay (Promega)

802 and immunofluorescent analysis with anti-Ki67 (NB600-1252, Novus Biologicals) and
803 αSMA (19245, Cell Signaling Technology) antibodies.
804
805 **Cell culture**
806 *JAK2*$^{V617F/+}$ knock-in HCT116 cells as well as wild-type *JAK2*$^{+/+}$ HCT116 cells were
807 purchased from Horizon Discovery Ltd. The cells were cultured in RPMI 1640 (Sigma)
808 containing 2 mM L-glutamine and 25 mM sodium bicarbonate supplemented with 10%
809 FBS, 100 mg/mL of streptomycin and 100 IU/mL of penicillin at 37 °C in the presence
810 of 5% CO_2. Recombinant human BMP9 was purchased from Biolegend, Inc. Cells were
811 transfected with scrambled negative control siRNA (1022076, Qiagen) or ACVRL1-
812 specific siRNA (VHS41063, 129001, Thermo Fisher Scientific) using Lipofectamine
813 RNAiMAX (Thermo Fisher Scientific) according to manufacturer's instructions.
814
815 **Prediction of STAT binding sites on *ACVRL1* promotor**
816 To search for putative STAT binding sites on *ACVRL1* promotor, the *in silico* analysis
817 was performed using the online databases JASPAR and TFBIND/TRANSFAC[62].
818
819 **ChIP-qPCR**
820 ChIP assays were performed using SimpleChIP enzymatic chromatin IP kit with magnetic
821 beads (9003, Cell Signaling Technology). The crosslinked chromatin was digested with
822 micrococcal nuclease followed by sonication to break into 150–900 bp fragments.
823 Immunoprecipitation was performed using anti-STAT3 (4904, Cell Signaling
824 Technology) or Rabbit IgG. The enriched fragments were purified and analyzed by qPCR.
825 The signal relative to input was evaluated using the formula as follows; percent input =

826 $2\% \times 2^{(\text{CT 2\% input sample} - \text{CT IP sample})}$, where CT indicates threshold cycle of qPCR reaction;
827 IP, immunoprecipitation. The qPCR primers used are listed in Supplementary Table 5.
828
829 **Construction of DNA plasmid and dual luciferase assay**
830 The putative human *ACVRL1* promoter sequence (GeneBank: NC_000012.12, position
831 51906383 to 51907627) was amplified by the forward primer; 5'-
832 GGGGGTACCATAACCAGGAGGCTAGG-3' and the reverse primer; 5'-
833 TTTAAGCTTCGCGGCCGCAGTTG-3'. The obtained fragment was then subcloned
834 into pGL3-basic vector (Promega) at the KpnI and HindIII sites [29]. The construct was
835 verified by restriction digestion and DNA sequencing. The pGL3-basic vector containing
836 the putative *ACVRL1* promoter region and pNL1.1.TK [Nluc/TK] as a control vector were
837 co-transfected by using ScreenFect A Plus (Wako) according to the manufacturer's
838 protocol. The promoter activity of *ACVRL1* was determined by using Dual-Glo
839 Luciferase Assay System (Promega). The cells were incubated with ruxolitinib (Novartis
840 Pharmaceuticals) or stattic (Cayman Chemical) for 24 h prior to the luciferase assay. Each
841 experiment was performed in duplicate.
842
843 **Administration of ALK1/2 inhibitors**
844 The ALK1/2 inhibitor, K02288 (12 or 24 mg/kg body weight, Selleck Chemicals) or
845 LDN-212854 (9 mg/kg body weight, Selleck Chemicals), dissolved in DMSO was
846 administered to mice via an intraperitoneal injection a week for 2 weeks. DMSO was used
847 as a control.
848
849 **Human blood samples and clinical data**

We prospectively analyzed the blood samples taken from patients with PH (n = 70) and control subjects (n = 83) between April 2018 and April 2020 at Fukushima Medical University Hospital. PH was diagnosed according to the 2015 European Respiratory Society guidelines[1] by independent cardiologists. For the control group, we recruited healthy volunteers or patients with no history of PH or no history of cardiopulmonary diseases. The blood samples were collected in a polypropylene tube containing EDTA-2Na (TERUMO). Genomic DNA was extracted from 200 μL whole blood by using a QuickGene DNA whole blood kit. The *JAK2*V617F VAF was determined by an allelic discrimination PCR assay using THUNDERBIRD Probe qPCR Mix (TOYOBO) in a QuantStudio 3 real-time PCR system (Thermo Fisher Scientific). We used the primers, probe and protocols described in Assay 5 in previous literature (Supplementary Table 6)[32]. The *JAK2*V617F VAF was calculated by Delta Ct ($Ct_{JAK2V617F}$ - $Ct_{wild\text{-}type}$) and expressed as the percentage of *JAK2*V617F divided by total *JAK2* (*JAK2*V617F / *JAK2*V617F + *JAK2*wild-type)[63]. Clinical information, including hospital laboratory data, echocardiographic analysis and hemodynamic assessment by right heart catheterization, was collected with our standard clinical practice[64, 65].

Ethical statement

All animal studies were reviewed and approved by the Fukushima Medical University Animal Research Committee (approval number; 2019084). The protocols were compliant with relevant ethical regulations, and all experiments were performed in accordance with the guidelines provided in the Guide for the Use and Care of Laboratory Animals from the Institute for Laboratory Animal Research. All efforts were made to minimize the suffering of the animals. The protocols for human participants were approved by the

institutional ethics committee of Fukushima Medical University Hospital (approval number; 29348). Written informed consent was given by all subjects. This study complied with all relevant regulations regarding the use of human study participants and was conducted in accordance to the criteria set by the 1975 Declaration of Helsinki.

Statistical analysis

Comparisons of values between two groups were performed by the unpaired or paired Student's t-test, or Mann-Whitney U-test. When more than two groups were evaluated, one-way ANOVA or two-way ANOVA was performed followed by multiple comparisons with the Tukey test. Categorical variables were compared using Fisher's exact test or Chi-square test. Statistical analyses were performed using the Statistical Package for Social Sciences version 26 (SPSS Inc) or GraphPadPrism version 8.1.2 (GraphPad Software). A value of $P < 0.05$ was considered statistically significant.

Data availability

The RNA sequencing data generated in this study have been deposited in the DNA Data Bank of Japan database under accession code DDBJ PRJDB9389 [https://ddbj.nig.ac.jp/DRASearch/study?acc=DRP007018]. The putative STAT binding sites were assessed using JASPAR [http://jaspar.genereg.net/] and TFBIND/TRANSFAC [https://tfbind.hgc.jp/] databases. Source data are provided with this paper. Any remaining raw data will be available from the corresponding author upon reasonable request.

References

1. Galie N*, et al.* 2015 ESC/ERS Guidelines for the diagnosis and treatment of pulmonary hypertension: The Joint Task Force for the Diagnosis and Treatment of Pulmonary Hypertension of the European Society of Cardiology (ESC) and the European Respiratory Society (ERS): Endorsed by: Association for European Paediatric and Congenital Cardiology (AEPC), International Society for Heart and Lung Transplantation (ISHLT). *Eur Heart J* **37**, 67-119 (2016).

2. Tuder RM, Marecki JC, Richter A, Fijalkowska I, Flores S. Pathology of pulmonary hypertension. *Clin Chest Med* **28**, 23-42, vii (2007).

3. Rabinovitch M, Guignabert C, Humbert M, Nicolls MR. Inflammation and immunity in the pathogenesis of pulmonary arterial hypertension. *Circ Res* **115**, 165-175 (2014).

4. Machado RF, Farber HW. Pulmonary hypertension associated with chronic hemolytic anemia and other blood disorders. *Clin Chest Med* **34**, 739-752 (2013).

5. Dingli D, Utz JP, Krowka MJ, Oberg AL, Tefferi A. Unexplained pulmonary hypertension in chronic myeloproliferative disorders. *Chest* **120**, 801-808 (2001).

6. Venton G*, et al.* Pulmonary hypertension in patients with myeloproliferative neoplasms: A large cohort of 183 patients. *Eur J Intern Med* **68**, 71-75 (2019).

7. Simonneau G*, et al.* Updated clinical classification of pulmonary hypertension. *J Am Coll Cardiol* **62**, D34-41 (2013).

8. Levine RL, Gilliland DG. Myeloproliferative disorders. *Blood* **112**, 2190-2198 (2008).

9. Vainchenker W, Kralovics R. Genetic basis and molecular pathophysiology of classical myeloproliferative neoplasms. *Blood* **129**, 667-679 (2017).

10. Campbell PJ, Green AR. The myeloproliferative disorders. *N Engl J Med* **355**, 2452-2466 (2006).

11. James C*, et al.* A unique clonal JAK2 mutation leading to constitutive signalling causes polycythaemia vera. *Nature* **434**, 1144-1148 (2005).

12. Jaiswal S*, et al.* Age-related clonal hematopoiesis associated with adverse outcomes. *N Engl J Med* **371**, 2488-2498 (2014).

13. Genovese G*, et al.* Clonal hematopoiesis and blood-cancer risk inferred from blood DNA sequence. *N Engl J Med* **371**, 2477-2487 (2014).

14. Bejar R. CHIP, ICUS, CCUS and other four-letter words. *Leukemia* **31**, 1869-1871 (2017).

15. Jaiswal S*, et al.* Clonal Hematopoiesis and Risk of Atherosclerotic Cardiovascular Disease. *N Engl J Med* **377**, 111-121 (2017).

16. Fuster JJ*, et al.* Clonal hematopoiesis associated with TET2 deficiency accelerates atherosclerosis development in mice. *Science* **355**, 842-847 (2017).

17. Wang W*, et al.* Macrophage Inflammation, Erythrophagocytosis, and Accelerated Atherosclerosis in Jak2 (V617F) Mice. *Circ Res* **123**, e35-e47 (2018).

18. Barbui T*, et al.* Development and validation of an International Prognostic Score of thrombosis in World Health Organization-essential thrombocythemia (IPSET-thrombosis). *Blood* **120**, 5128-5133; quiz 5252 (2012).

19. Gomez-Arroyo J*, et al.* A brief overview of mouse models of pulmonary arterial hypertension: problems and prospects. *Am J Physiol Lung Cell Mol Physiol* **302**, L977-991 (2012).

20. Sugimoto K, Yokokawa T, Misaka T, Nakazato K, Ishida T, Takeishi Y. Senescence Marker Protein 30 Deficiency Exacerbates Pulmonary Hypertension in Hypoxia-Exposed Mice. *Int Heart J* **60**, 1430-1434 (2019).

21. Shide K*, et al.* Development of ET, primary myelofibrosis and PV in mice expressing JAK2 V617F. *Leukemia* **22**, 87-95 (2008).

22. Ueda K, *et al.* Hmga2 collaborates with JAK2V617F in the development of myeloproliferative neoplasms. *Blood Adv* **1**, 1001-1015 (2017).

23. Farber HW, *et al.* Five-Year outcomes of patients enrolled in the REVEAL Registry. *Chest* **148**, 1043-1054 (2015).

24. Cowan KN, Heilbut A, Humpl T, Lam C, Ito S, Rabinovitch M. Complete reversal of fatal pulmonary hypertension in rats by a serine elastase inhibitor. *Nat Med* **6**, 698-702 (2000).

25. Ciuclan L, *et al.* A novel murine model of severe pulmonary arterial hypertension. *Am J Respir Crit Care Med* **184**, 1171-1182 (2011).

26. Lundberg P, *et al.* Myeloproliferative neoplasms can be initiated from a single hematopoietic stem cell expressing JAK2-V617F. *J Exp Med* **211**, 2213-2230 (2014).

27. Okabe M, Ikawa M, Kominami K, Nakanishi T, Nishimune Y. 'Green mice' as a source of ubiquitous green cells. *FEBS Lett* **407**, 313-319 (1997).

28. Soubrier F, *et al.* Genetics and genomics of pulmonary arterial hypertension. *J Am Coll Cardiol* **62**, D13-21 (2013).

29. Garrido-Martin EM*, et al.* Characterization of the human Activin-A receptor type II-like kinase 1 (ACVRL1) promoter and its regulation by Sp1. *BMC Mol Biol* **11**, 51 (2010).

30. Sanvitale CE*, et al.* A new class of small molecule inhibitor of BMP signaling. *PLoS One* **8**, e62721 (2013).

31. Mohedas AH, Xing X, Armstrong KA, Bullock AN, Cuny GD, Yu PB. Development of an ALK2-biased BMP type I receptor kinase inhibitor. *ACS Chem Biol* **8**, 1291-1302 (2013).

32. Jovanovic JV*, et al.* Establishing optimal quantitative-polymerase chain reaction assays for routine diagnosis and tracking of minimal residual disease in JAK2-V617F-associated myeloproliferative neoplasms: a joint European LeukemiaNet/MPN&MPNr-EuroNet (COST action BM0902) study. *Leukemia* **27**, 2032-2039 (2013).

33. Arber DA*, et al.* The 2016 revision to the World Health Organization classification of myeloid neoplasms and acute leukemia. *Blood* **127**, 2391-2405 (2016).

34. Farha S*, et al.* Hypoxia-inducible factors in human pulmonary arterial hypertension: a link to the intrinsic myeloid abnormalities. *Blood* **117**, 3485-3493 (2011).

35. Asosingh K*, et al.* Pulmonary vascular disease in mice xenografted with human BM progenitors from patients with pulmonary arterial hypertension. *Blood* **120**, 1218-1227 (2012).

36. Srour SA*, et al.* Incidence and patient survival of myeloproliferative neoplasms and myelodysplastic/myeloproliferative neoplasms in the United States, 2001-12. *Br J Haematol* **174**, 382-396 (2016).

37. Zaidi SH, You XM, Ciura S, Husain M, Rabinovitch M. Overexpression of the serine elastase inhibitor elafin protects transgenic mice from hypoxic pulmonary hypertension. *Circulation* **105**, 516-521 (2002).

38. Taylor S, Dirir O, Zamanian RT, Rabinovitch M, Thompson AAR. The Role of Neutrophils and Neutrophil Elastase in Pulmonary Arterial Hypertension. *Front Med (Lausanne)* **5**, 217 (2018).

39. Pawlus MR, Wang L, Hu CJ. STAT3 and HIF1alpha cooperatively activate HIF1 target genes in MDA-MB-231 and RCC4 cells. *Oncogene* **33**, 1670-1679 (2014).

40. McDonald J, Wooderchak-Donahue W, VanSant Webb C, Whitehead K, Stevenson DA, Bayrak-Toydemir P. Hereditary hemorrhagic telangiectasia: genetics and molecular diagnostics in a new era. *Front Genet* **6**, 1 (2015).

41. Yokokawa T*, et al.* A Case of Pulmonary Hypertension and Hereditary

Hemorrhagic Telangiectasia Related to an ACVRL1 Mutation. *Intern Med*, (2019).

42. Ricard N*, et al.* Functional analysis of the BMP9 response of ALK1 mutants from HHT2 patients: a diagnostic tool for novel ACVRL1 mutations. *Blood* **116**, 1604-1612 (2010).

43. Alaa El Din F*, et al.* Functional and splicing defect analysis of 23 ACVRL1 mutations in a cohort of patients affected by Hereditary Hemorrhagic Telangiectasia. *PLoS One* **10**, e0132111 (2015).

44. Trembath RC, et al. Clinical and molecular genetic features of pulmonary hypertension in patients with hereditary hemorrhagic telangiectasia. N Engl J Med **345**, 325-334 (2001).

45. Jerkic M*, et al.* Pulmonary hypertension in adult Alk1 heterozygous mice due to oxidative stress. *Cardiovasc Res* **92**, 375-384 (2011).

46. Tu L*, et al.* Selective BMP-9 Inhibition Partially Protects Against Experimental Pulmonary Hypertension. *Circ Res* **124**, 846-855 (2019).

47. Nielsen C, Bojesen SE, Nordestgaard BG, Kofoed KF, Birgens HS. JAK2V617F somatic mutation in the general population: myeloproliferative neoplasm development and progression rate. *Haematologica* **99**, 1448-1455 (2014).

48. Perricone M*, et al.* The relevance of a low JAK2V617F allele burden in clinical practice: a monocentric study. *Oncotarget* **8**, 37239-37249 (2017).

49. Cordua S, Kjaer L, Skov V, Pallisgaard N, Hasselbalch HC, Ellervik C. Prevalence and phenotypes of JAK2 V617F and calreticulin mutations in a Danish general population. *Blood* **134**, 469-479 (2019).

50. Limvorapitak W, Parker J, Hughesman C, McNeil K, Foltz L, Karsan A. No Differences in Outcomes Between JAK2 V617F-Positive Patients with Variant Allele Fraction < 2% Versus 2-10%: A 6-Year Province-wide Retrospective Analysis. *Clin Lymphoma Myeloma Leuk* **20**, e569-e578 (2020).

51. Harrison C*, et al.* JAK inhibition with ruxolitinib versus best available therapy for myelofibrosis. *N Engl J Med* **366**, 787-798 (2012).

52. Vannucchi AM*, et al.* Ruxolitinib versus standard therapy for the treatment of polycythemia vera. *N Engl J Med* **372**, 426-435 (2015).

53. Tabarroki A*, et al.* Ruxolitinib leads to improvement of pulmonary hypertension in patients with myelofibrosis. *Leukemia* **28**, 1486-1493 (2014).

54. Miyawaki H*, et al.* Long-term Effects of the Janus Kinase 1/2 Inhibitor Ruxolitinib on Pulmonary Hypertension and the Cardiac Function in a Patient

with Myelofibrosis. *Intern Med* **59**, 229-233 (2020).

55. Low AT, Howard L, Harrison C, Tulloh RM. Pulmonary arterial hypertension exacerbated by ruxolitinib. *Haematologica* **100**, e244-245 (2015).

56. Gupta R*, et al.* Pulmonary hypertension is associated with increased nonrelapse mortality after allogeneic hematopoietic cell transplantation for myelofibrosis. *Bone Marrow Transplant*, (2019).

57. Edelmann B*, et al.* JAK2-V617F promotes venous thrombosis through beta1/beta2 integrin activation. *J Clin Invest* **128**, 4359-4371 (2018).

58. Kikuchi N*, et al.* Selenoprotein P Promotes the Development of Pulmonary Arterial Hypertension. *Circulation* **138**, 600-623 (2018).

59. Chen G*, et al.* Inhibition of CRTH2-mediated Th2 activation attenuates pulmonary hypertension in mice. *J Exp Med* **215**, 2175-2195 (2018).

60. Misaka T*, et al.* Deficiency of senescence marker protein 30 exacerbates angiotensin II-induced cardiac remodelling. *Cardiovasc Res* **99**, 461-470 (2013).

61. Spiekerkoetter E*, et al.* Reactivation of gammaHV68 induces neointimal lesions in pulmonary arteries of S100A4/Mts1-overexpressing mice in association with degradation of elastin. *Am J Physiol Lung Cell Mol Physiol* **294**, L276-289 (2008).

62. Wasserman WW, Sandelin A. Applied bioinformatics for the identification of regulatory elements. *Nat Rev Genet* **5**, 276-287 (2004).

63. Levine RL*, et al.* X-inactivation-based clonality analysis and quantitative JAK2V617F assessment reveal a strong association between clonality and JAK2V617F in PV but not ET/MMM, and identifies a subset of JAK2V617F-negative ET and MMM patients with clonal hematopoiesis. *Blood* **107**, 4139-4141 (2006).

64. Takahashi T*, et al.* Associations between diabetes mellitus and pulmonary hypertension in chronic respiratory disease patients. *PLoS One* **13**, e0205008 (2018).

65. Misaka T*, et al.* Plasma levels of melatonin in dilated cardiomyopathy. *J Pineal Res* **66**, e12564 (2019).

Acknowledgments

The authors thank Ms Tomiko Miura and Ms Shoko Sato in the Department of Cardiovascular Medicine, Fukushima Medical University, and Ms Chisato Kubo in the Office for Gender Equality Support, Fukushima Medical University, for their technical assistance. This work was supported by JSPS KAKENHI grant JP19K17609 to YK and JP19K08523 to YT, and research grant from the Uehara Memorial Foundation 201890006 to KI.

Author contributions

YK and TM designed the research, performed the experiments, analyzed the results, and wrote the manuscript. TY, KW, KU, K. Sugimoto, and KM performed the experiments and analyzed the results. MO, SK and AI performed and analyzed the RNA sequencing, supervised the research, and wrote the manuscript. KN and TI supervised the study. K. Shide and K. Shimoda provided $JAK2^{V617F}$ mice and interpreted the results. KI designed the research, analyzed the data, and wrote the manuscript. YT designed and supervised the research and approved the final version of the manuscript.

Competing interests

TM's department is supported by Fukuda Denshi Co., Ltd., Japan. TY and KS's department is supported by Actelion Pharmaceuticals Japan, Ltd., Japan. Ruxolitinib was provided by Novartis Pharmaceuticals to KI. These companies were not associated with the contents of this study. All other authors declare no competing interests.

Figure legends

Figure 1. JAK2^{V617F} mice accelerate pulmonary hypertension accompanied by perivascular neutrophil infiltration in response to chronic hypoxia.

Figure 2. Clonal hematopoiesis with JAK2V617F exacerbates pulmonary hypertension and infiltration of perivascular neutrophils in bone marrow transplanted recipients with wild-type lungs in response to chronic hypoxia.

Figure 3. Characterization of bone marrow-derived JAK2V617F hematopoietic cells in the lungs by the use of GFP-transgene.

Figure 4. Small clones with JAK2V617F lead to PH development, associated with selective migration of neutrophils into the lungs and maturation from the lung hematopoietic precursors for the myeloid lineage.

Figure 5. Gene expression profiles of neutrophils with JAK2V617F at several differential stages.

Figure 6. *Acvrl1* mRNA expressions and phosphorylation of Smad1/5/8 and STAT3 in the lungs of JAK2^{V617F} mice in response to chronic hypoxia.

Figure 7. *JAK2*V617F transcriptionally upregulates *ACVRL1* by STAT3-binding.

Figure 8. Inhibition of ALK1/2 improves chronic hypoxia-induced pulmonary hypertension in JAK2^{V617F} mice.

Figure 9. Prevalence of *JAK2*V617F-positive clonal hematopoiesis in PH patients.

Supplementary Figure 1. Changes in phosphorylation levels of STAT3 on whole lung homogenates during chronic hypoxia in the wild-type (WT) mice.

Supplementary Figure 2. Echocardiographic analysis in JAK2V617F mice after exposure to chronic hypoxia.

Supplementary Figure 3. Left ventricular weight in JAK2V617F mice after exposure to chronic hypoxia.

Supplementary Figure 4. Male JAK2V617F mice also develop pulmonary hypertension in response to exposure to chronic hypoxia.

Supplementary Figure 5. Histological images and mRNA expression of the lung in JAK2V617F mice after exposure to chronic hypoxia.

Supplementary Figure 6. Characterization of the infiltrated leukocytes in the pulmonary arterial regions in JAK2V617F mice after exposure to chronic hypoxia.

Supplementary Figure 7. Chronic hypoxia increased Ly6G+ neutrophils in perivascular regions as well as non-perivascular regions of the lungs in JAK2V617F mice.

Supplementary Figure 8. Pulmonary hypertension is accelerated in JAK2V617F mice in a Sugen-hypoxia model.

Supplementary Figure 9. Characterization of aged JAK2V617F mice in the setting of normoxia.

Supplementary Figure 10. Echocardiographic analyses in JAK2V617F-BMT mice after exposure to chronic hypoxia.

Supplementary Figure 11. Left ventricular weight in JAK2V617F-BMT mice after exposure to chronic hypoxia.

Supplementary Figure 12. Histological images and mRNA expression of the lungs in JAK2V617F-BMT mice after exposure to chronic hypoxia.

Supplementary Figure 13. Characterization of the infiltrated leukocytes in the pulmonary arterial regions in JAK2V617F-BMT mice after exposure to chronic hypoxia.

Supplementary Figure 14. Chronic hypoxia increased Ly6G+ neutrophils in perivascular regions as well as non-perivascular regions of the lungs in JAK2V617F-BMT mice.

Supplementary Figure 15. Characterization of bone marrow-derived JAK2V617F hematopoietic cells in the lungs by the use of GFP-transgene.

Supplementary Figure 16. A competitive transplantation model using JAK2V617F-GFP bone marrow cells.

Supplementary Figure 17. Colony-forming assay to estimate the presence of hematopoietic progenitor cells in the JAK2V617F lungs for the myeloid lineage.

Supplementary Figure 18. Immunofluorescence of sorted cells from the mouse lung.

Supplementary Figure 19. Acvrl1, Acvr1, and Bmpr2 mRNA expressions in the lung homogenates or sorted cells from the lungs after exposure to chronic hypoxia.

Supplementary Figure 20. HIF1α expression in the lungs of JAK2V617F mice in response to exposure to chronic hypoxia.

Supplementary Figure 21. Binding of HIF1α and STAT3 in the lungs.

Supplementary Figure 22. Inhibition of HIF1α in JAK2V617F-expressing neutrophils reduced the mouse pulmonary artery smooth muscle cell (PASMC) proliferation.

Supplementary Figure 23. Smad1/5/8 phosphorylation in response to BMP9 stimulation in HCT116 cells to express an active ALK1 receptor.

Supplementary Figure 24. ALK1 expression in JAK2V617F/+ HCT116 cells by flow cytometry.

Supplementary Figure 25. ACVR1 (ALK2) expressions in JAK2V617F/+ HCT116 cells.

Supplementary Figure 26. Effects of K02288, an ALK1/2 inhibitor, on the phosphorylation of Smad1/5/8 in the mouse lung and HCT116 cells.

Supplementary Figure 27. Left ventricular weight in K02288-treated JAK2V617F mice after exposure to chronic hypoxia.

Supplementary Figure 28. K02288, an ALK1/2 inhibitor, attenuates chronic hypoxia-induced proliferation of pulmonary arterial smooth muscle cells in JAK2V617F mice.

Supplementary Figure 29. Effects of LDN-212854, an ALK1/2 inhibitor, on the phosphorylation of Smad1/5/8 in the mouse lungs and HCT116 cells.

Supplementary Figure 30. LDN-212854, an ALK1/2 inhibitor, improves chronic hypoxia-induced pulmonary hypertension in JAK2V617F mice.

Supplementary Figure 31. No effects of ALK1/2 inhibitors of K02288 or LDN-212854 on pulmonary hypertension in WT mice and JAK2V617F mice under normoxia.

Supplementary Figure 32. Effects of a high dose of K02288, an ALK1/2 inhibitor, on pulmonary hypertension in WT mice after chronic hypoxia.

Supplementary Figure 33. Gating strategy used in the present study.

Figure 1.

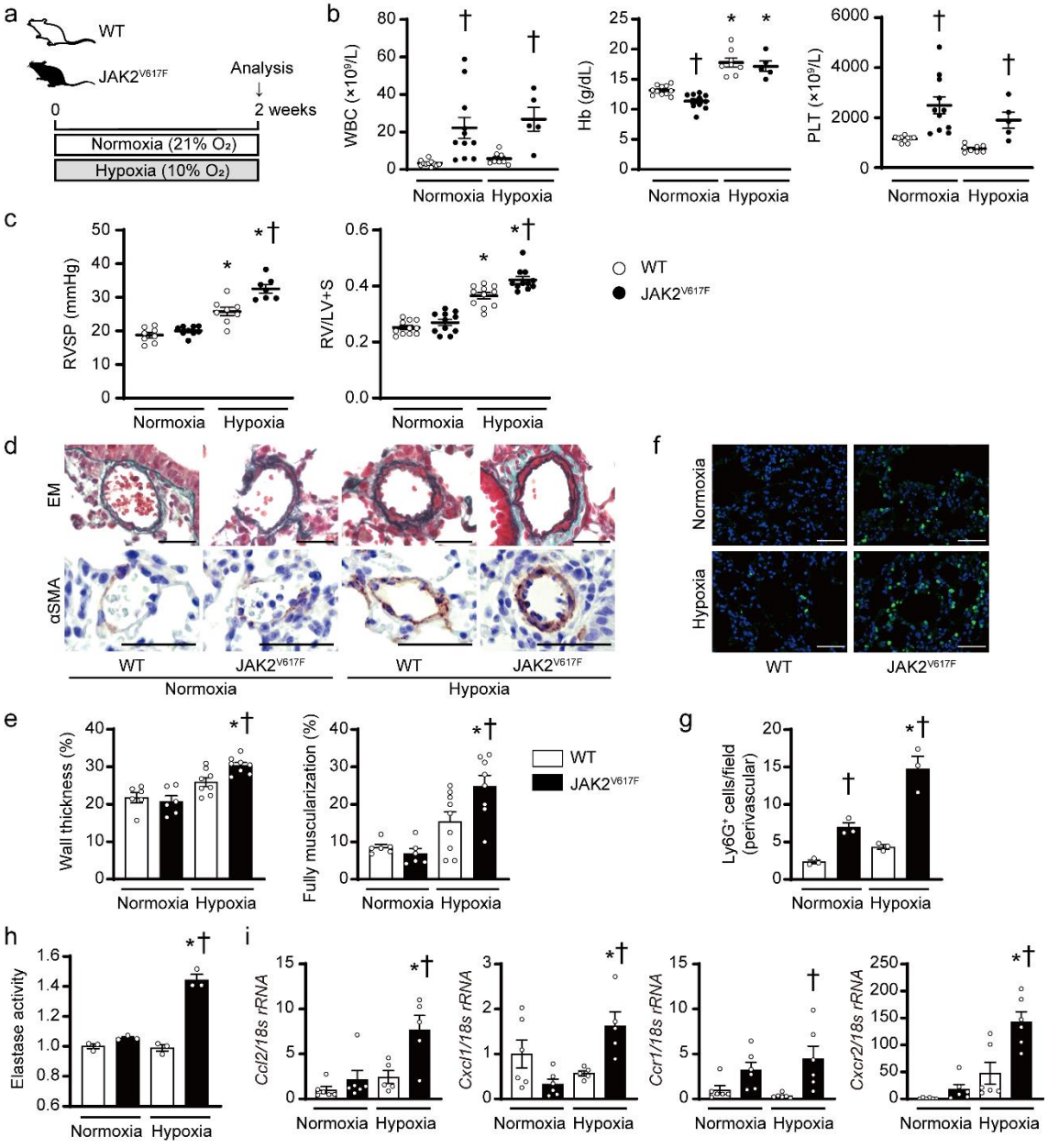

a Experimental design. Wild-type (WT) mice and mice with transgenic expression of *Jak2*V617F ($JAK2^{V617F}$) exposed to normoxia (21% O_2) or hypoxia (10% O_2) for 2 weeks were analyzed. **b** Peripheral blood cell counts in WT mice or $JAK2^{V617F}$ mice under normoxia or hypoxia for 2 weeks (n = 11, 11, 8, 5, $^{\dagger}P = 0.0036$ [left], 0.0185 [right] for WBC, n = 11, 11, 8, 5, $^{*}P < 0.0001$ [left], < 0.0001 [right], $^{\dagger}P = 0.0335$ for Hb, n = 10,

11, 8, 5, $^{\dagger}P = 0.0008$ [left], 0.0396 [right] for PLT). **c** Right ventricular systolic pressure (RVSP, n = 8, 9, 8, 7, $^{*}P < 0.0001$ [left], < 0.0001 [right], $^{\dagger}P = 0.0002$) and right ventricular hypertrophy determined by the ratio of right ventricle (RV) weight to left ventricle weight plus septum weight (RV/LV+S, n = 11 in each group, $^{*}P < 0.0001$ [left], < 0.0001 [right], $^{\dagger}P = 0.0027$). **d** Representative images of Elastica-Masson (EM)-stained sections and sections immunostained with anti-α–smooth muscle actin (αSMA) antibody from WT mice and $JAK2^{V617F}$ mice. Scale bars, 25 μm. **e** Quantitative analysis of medial wall thickness in EM-stained sections (left, n = 6, 6, 8, 8, $^{*}P < 0.0001$, $^{\dagger}P = 0.0413$) and the percentage of muscularized distal pulmonary vessels in αSMA-immunostained sections (right, n = 6, 6, 9, 8, $^{*}P = 0.0001$, $^{\dagger}P = 0.0263$). **f** Representative immunofluorescence images of lung sections stained with anti-Ly6G (green) antibody and DAPI (blue). Scale bars, 50 μm. **g** Quantitative analysis of Ly6G-positive cells in perivascular regions (n = 3 in each group, $^{*}P = 0.0015$, $^{\dagger}P = 0.0318$ [left], 0.0002 [right]). **h** Elastase activity in the lungs from WT and $JAK2^{V617F}$ mice. The average value from normoxia-exposed WT mice was set to 1 (n = 3 in each group, $^{*}P < 0.0001$, $^{\dagger}P < 0.0001$). **i** Relative mRNA expression levels of *Ccl2*, *Cxcl1*, *Ccr1*, and *Cxcr2* in the lungs. The *18s rRNA* was used for normalization. The average value from normoxia-exposed WT mice was set to 1 (n = 6, 6, 5, 5, $^{*}P = 0.0049$, $^{\dagger}P = 0.0105$ for *Ccl2*, n = 6, 6, 5, 5, $^{*}P = 0.0044$, $^{\dagger}P = 0.0284$ for *Cxcl1*, n = 6, 6, 6, 6, $^{\dagger}P = 0.0139$ for *Ccr1*, n = 6, 6, 6, 6, $^{*}P < 0.0001$, $^{\dagger}P = 0.0008$ for *Cxcr2*). All data are presented as mean ± SEM. $^{*}P < 0.05$ versus the corresponding normoxia-exposed group and $^{\dagger}P < 0.05$ versus the corresponding WT mice by the one-way ANOVA with Tukey post-hoc analysis. WBC, white blood cell count; Hb, hemoglobin concentration; PLT, platelet count.

Figure 2.

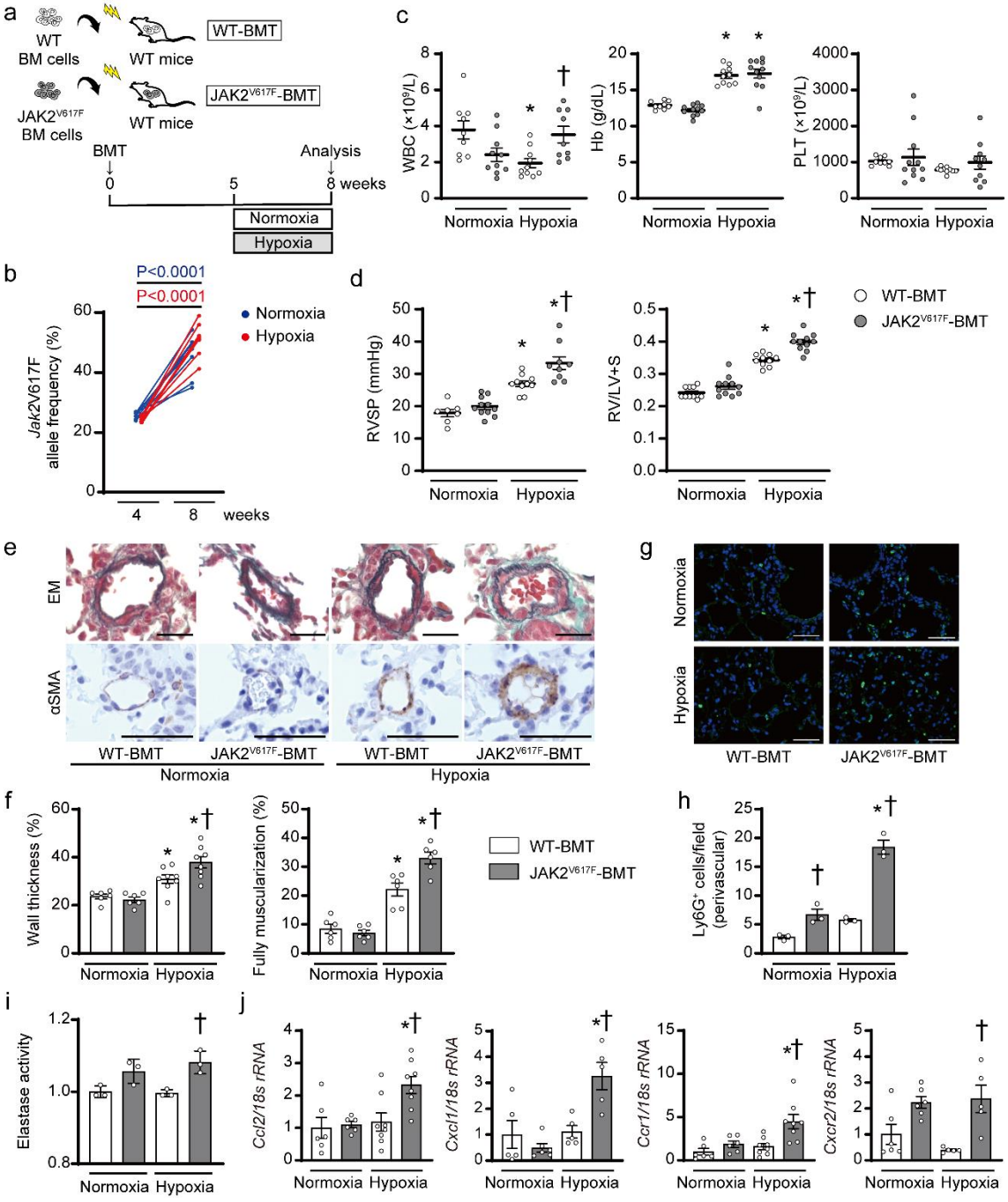

a Schematic diagram of the experimental design. Bone marrow (BM) cells from WT or JAK2^{V617F} mice were injected into lethally irradiated recipient WT mice with the same C57BL/6J background. Five weeks after BM transplantation (BMT), the recipient mice transplanted with JAK2^{V617F} BM cells (JAK2^{V617F}-BMT) or WT BM cells (WT-BMT)

were exposed to normoxia or hypoxia for 3 weeks. **b** *Jak2*V617F allele frequencies (%) in peripheral blood of each JAK2^{V617F}-BMT mouse at 4 and 8 weeks after BMT at normoxia (blue circles, n = 8) or chronic hypoxia exposure (red circles, n = 8). Statistical comparison was performed by the paired Student's t-test (two-sided). **c** Peripheral blood cell counts in WT-BMT or JAK2^{V617F}-BMT mice after exposure to normoxia or hypoxia (n = 9, 10, 10, 9, *P = 0.0121, †P = 0.0388 for WBC, n = 9, 11, 10, 11, *P < 0.0001 [left], < 0.0001 [right] for Hb, n = 9, 11, 10, 10 for PLT). **d** RVSP and RV hypertrophy determined by RV/LV+S in WT-BMT or JAK2^{V617F}-BMT mice after exposure to normoxia or hypoxia (n = 7, 11, 10, 9, *P = 0.0002 [left], < 0.0001 [right], †P = 0.0054 for RVSP, n = 10, 11, 10, 11, *P < 0.0001 [left], < 0.0001 [right], †P < 0.0001 for RV/LV+S). **e** Representative images of EM-stained sections and sections immunostained with anti-αSMA antibody from WT-BMT and JAK2^{V617F}-BMT mice. Scale bars, 25 μm. **f** Quantitative analysis of medial wall thickness in EM-stained sections (left, n = 6, 6, 8, 8, *P = 0.0465 [left], < 0.0001 [right], †P = 0.0346) and the percentage of muscularized distal pulmonary vessels in αSMA-immunostained sections (right, n = 6 in each group, *P = 0.0001 [left], < 0.0001 [right], †P = 0.0016). **g** Representative immunofluorescence images of lung sections stained with anti-Ly6G (green) antibody and DAPI (blue). Scale bars, 50 μm. **h** Quantitative analysis of Ly6G-positive cells in the perivascular regions (n = 3 in each group, *P < 0.0001, †P = 0.0387 [left], < 0.0001 [right]). **i** Elastase activity in the lungs from WT -BMT and JAK2^{V617F}-BMT mice. The average value of normoxia-exposed WT-BMT mice was set to 1 (n = 3 in each group, †P = 0.0128). **j** Relative mRNA expression levels of *Ccl2*, *Cxcl1*, *Ccr1* and *Cxcr2* in the lungs. The *18s rRNA* was used for normalization. The average value from the normoxia-exposed WT-BMT mice was set to 1 (n = 6, 6, 8, 8, *P = 0.0171, †P = 0.0159 for *Ccl2*, n= 5, 6, 5, 5 *P = 0.0004, †P =

0.0065 for *Cxcl1*, 6, 6, 8, 8, *P = 0.0171, †P = 0.0040 for *Ccr1*, n = 6, 6, 5, 5, †P =0.0056 for *Cxcr2*). The data are presented as mean ± SEM. *P < 0.05 versus the corresponding normoxia-group and †P < 0.05 versus the corresponding WT-BMT mice by the one-way ANOVA with Tukey post-hoc analysis. WT-BMT, recipient WT mice transplanted with BM cells of WT mice; JAK2^{V617F}-BMT, recipient WT mice transplanted with BM cells of JAK2^{V617F} mice. WBC, white blood cell count; Hb, hemoglobin concentration; PLT, platelet count.

Figure 3.

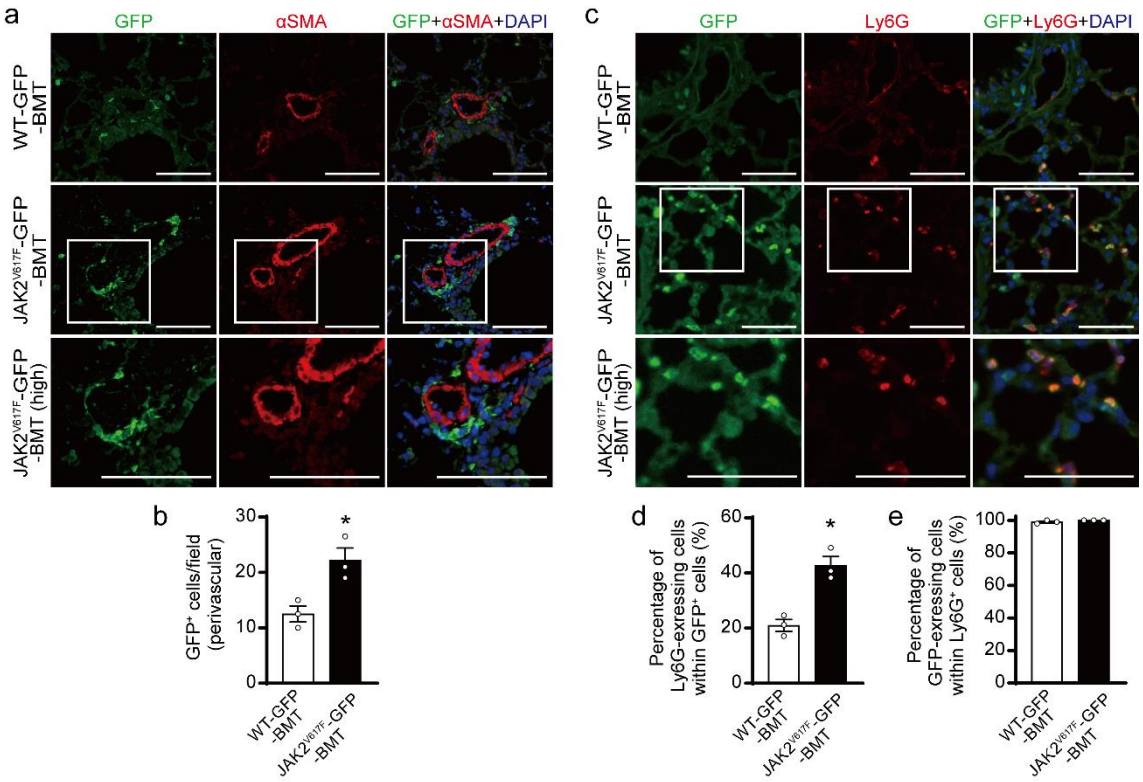

a Lethally irradiated WT mice were transplanted with bone marrow (BM) cells from control WT/CAG-EGFP (WT-GFP) or JAK2^{V617F}/CAG-EGFP (JAK2^{V617F}-GFP) double transgenic mice. Five weeks after BM transplantation (BMT), the recipient mice were subjected to chronic hypoxia for 3 weeks, and then the lungs were fixed and stained with the indicated antibodies. Representative immunofluorescence images of lung sections stained with anti-GFP (green) and anti-αSMA (red) antibodies and DAPI (blue) in WT-GFP-BMT or JAK2^{V617F}-GFP-BMT mice. The boxed areas from JAK2^{V617F}-GFP-BMT mice at higher magnifications (high) are shown in the bottom panels. Scale bars, 100 μm. **b** Quantitative analysis of Ly6G^{+} cells in the perivascular regions (n = 3 in each group, *P = 0.0223). **c** Representative immunofluorescence images of lung sections stained with anti-GFP (green) and anti-Ly6G (red) antibodies, as well as DAPI (blue) in WT-GFP-BMT or JAK2^{V617F}-GFP-BMT mice. The boxed areas from JAK2^{V617F}-GFP-BMT mice

at higher magnifications are shown in the bottom panels (high). Scale bars, 100 μm. **d, e** Quantitative analysis of Ly6G-exressing cells in GFP^+ cells (**d**, n = 3 in each group, $^*P = 0.0052$) and GFP-expressing cells in $Ly6G^+$ cells (**e**, n = 3 in each group). More than 100 GFP^+ cells and $Ly6G^+$ cells were counted in each section and expressed as the percentage of the cells. All data are presented as mean ± SEM. WT-GFP-BMT, recipient WT mice transplanted with WT-GFP BM cells; $JAK2^{V617F}$-GFP-BMT, recipient WT mice transplanted with $JAK2^{V617F}$-GFP BM cells. $^*P < 0.05$ versus WT-GFP recipients by the unpaired t-test (two-sided).

Figure 4.

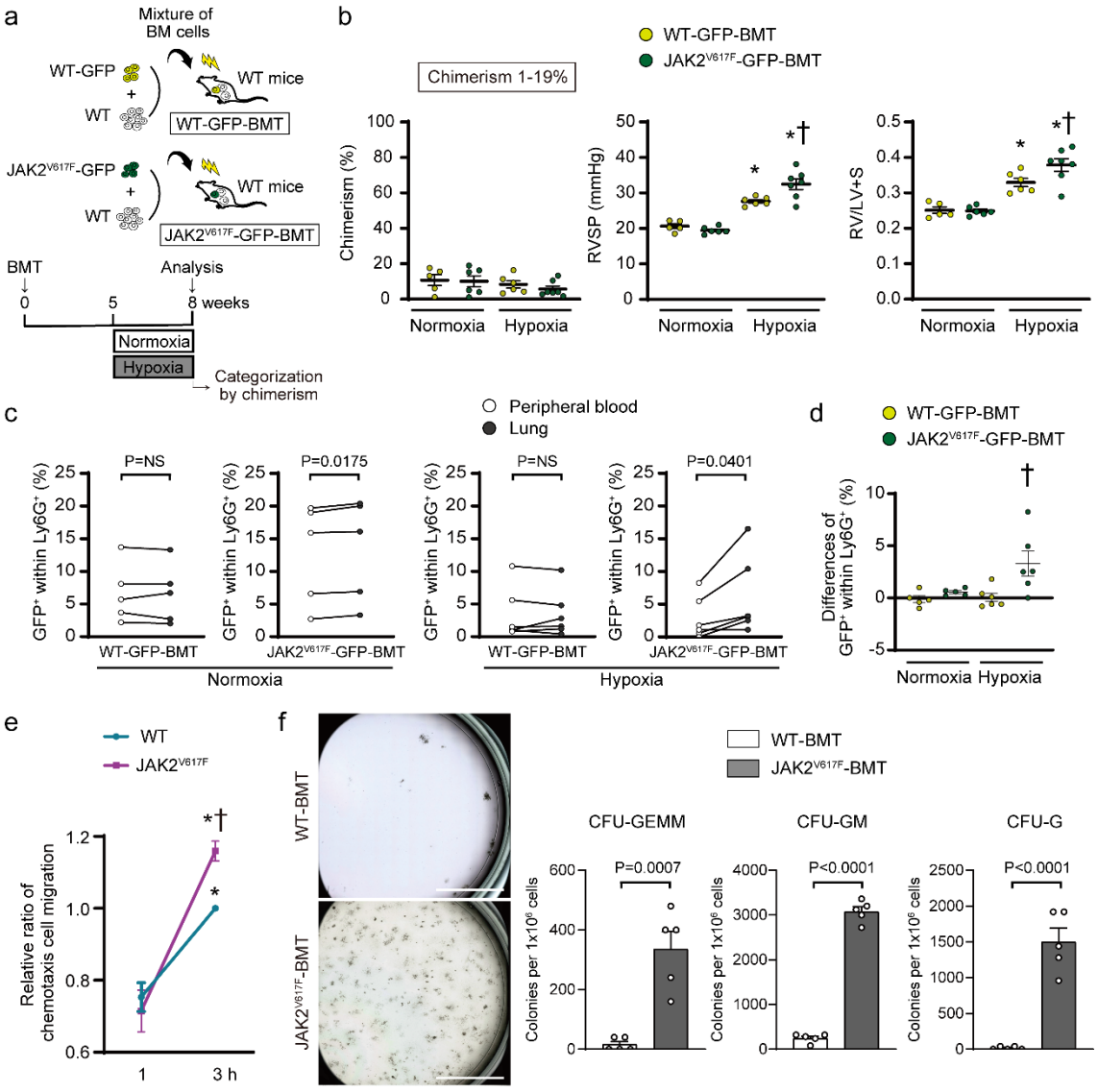

a Schematic depiction of the competitive transplantation. The different ratios of WT-GFP or JAK2^{V617F}-GFP and WT without GFP competitor were transplanted into the lethally irradiated recipient WT mice. **b** The recipients with donor chimerism of 1–19% at 8 weeks after bone marrow transplantation (BMT), determined by the percentages of GFP^{+} cells within CD45^{+} cells by flow cytometry, were enrolled for statistical comparison (n = 5, 6, 6, 7). The other categories of the donor chimerism are presented in Supplementary Figure 16. RVSP and RV/LV+S are shown (n = 5, 6, 6, 7, *P = 0.0008 [left], < 0.0001 [right], †P

= 0.0113 for RVSP, n = 5, 6, 6, 7 $^{*}P = 0.0029$ [left], < 0.0001 [right], $^{\dagger}P = 0.0049$ for RV/LV+S). $^{*}P < 0.05$ versus the corresponding normoxia-group and $^{\dagger}P < 0.05$ versus the corresponding WT-GFP-BMT mice by the one-way ANOVA with Tukey post-hoc analysis. **c, d** JAK2V617F neutrophils showed an intrinsic increased migration capability into the lungs. The percentages of GFP^{+} cells within $CD45^{+}$ cells in the peripheral blood and the lungs were analyzed at 8 weeks in the BMT mice with 1–19% chimerism by flow cytometry (**c**, n = 5, 5, 6, 6). The comparison was performed by the paired Student's t-test (two-sided). NS, not significant. The differences of GFP^{+} cells within $CD45^{+}$ cells between the lungs and the peripheral blood are shown (**d**, n = 5, 5, 6, 6). $^{\dagger}P = 0.0173$ versus the corresponding WT-GFP-BMT mice by the one-way ANOVA with Tukey post-hoc analysis. **e** Chemotaxis migration assay. The sorted $Ly6G^{+}$ neutrophils from the blood in WT or $JAK2^{V617F}$ mice were placed on the top of Transwell in triplicate and were allowed to migrate for 1 or 3 h. Data are expressed as a relative ratio to WT-3 h from six independent experiments and presented as mean ± SEM. $^{*}P < 0.01$ versus corresponding 1 h ($^{*}P = 0.0009$ for WT, <0.0001 for $JAK2^{V617F}$) and $^{\dagger}P = 0.0342$ versus WT-3 h by the two-way ANOVA with Tukey post-hoc analysis. **f** Colony-forming assay of the hematopoietic progenitors in the lungs. CD117 (c-kit)$^{+}$ cells sorted from the lungs of WT-BMT and $JAK2^{V617F}$-BMT mice were grown in the methylcellulose-based medium for 7 days. Representative images of the 35 mm plates are shown in the left panels. Scale bars, 10 mm. Right, quantification of numbers of the colonies derived from colony-forming unit (CFU)-granulocyte, -erythroid, -macrophage, -megakaryocyte (CFU-GEMM), CFU-granulocyte, -monocyte (CFU-GM), CFU-granulocyte (CFU-G). The comparison was performed by the two-sided unpaired Student's t-test (n = 5 in each group). All data are presented as mean ± SEM.

Figure 5.

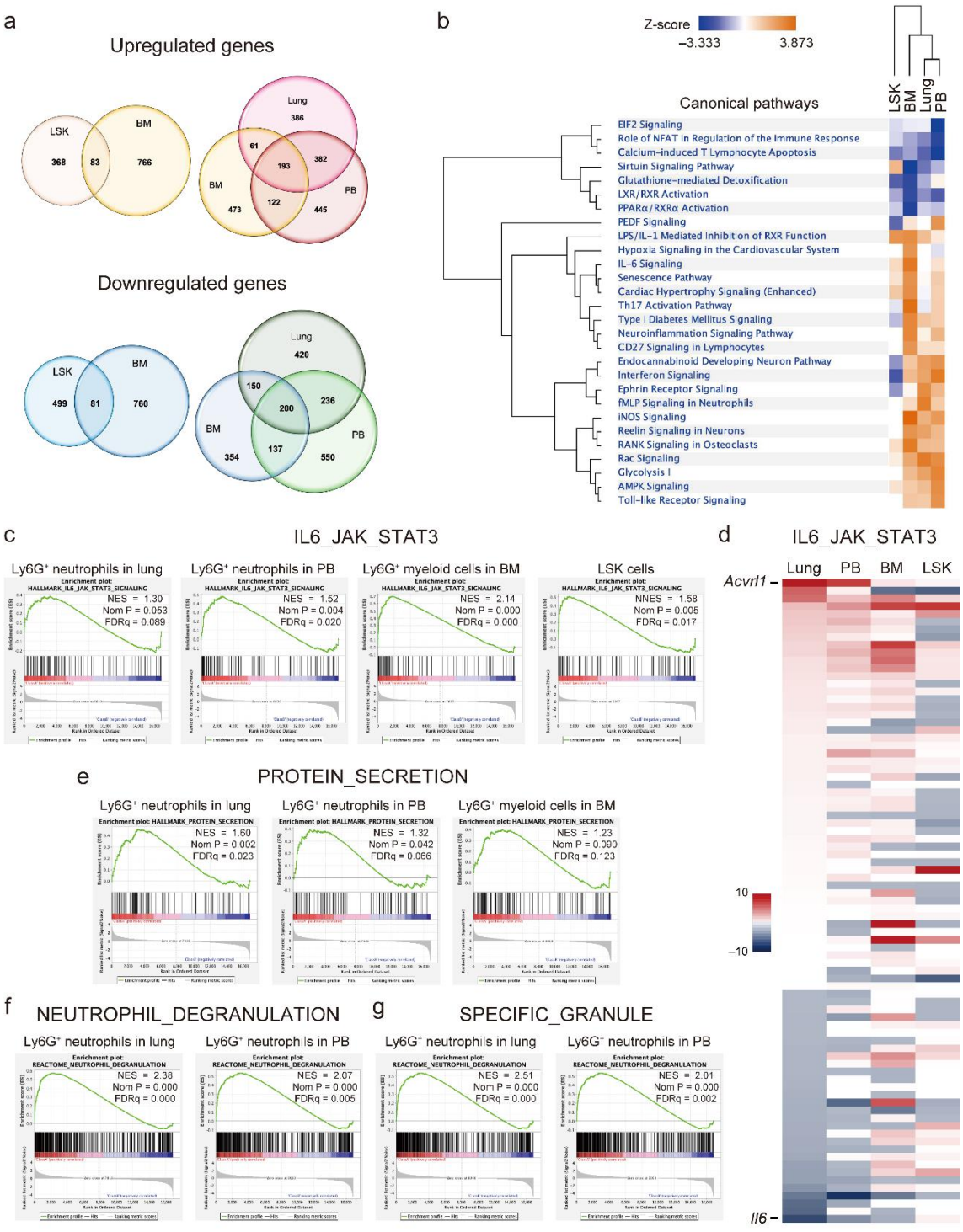

a Venn diagrams show the numbers of upregulated and downregulated genes (> 1.5-fold) in Ly6G$^+$ neutrophils in lungs and peripheral blood (PB), and Ly6G$^+$ myeloid cells in BM, and lineage$^-$Sca1$^+$Kit$^+$ (LSK) cells isolated from JAK2^{V617F} mice (n = 3) compared to

those from WT mice (n = 5) by RNA sequencing. **b** Strongly affected pathways (|z| > 2.58) at least one cell type according to the gene expression of $Ly6G^{+}$ neutrophils and LSK cells from $JAK2^{V617F}$ mice relative to those from WT mice. Hierarchical clustering of pathways and cell types are also shown. **c–g** A gene set enrichment analysis (GSEA) of RNA sequencing. Among Hallmark analyses, the IL6-JAK-STAT3 pathway was consistently enriched in $JAK2^{V617F}$ myeloid cells at each differential stage (**c**), but the expression profiles of the individual genes were different between the stem/progenitor and periphery levels (**d**). The expression level of *Acvrl1* was the highest in the lung and PB neutrophils, while slightly upregulated in the BM myeloid cells and LSK cells in this pathway. **e–g** Gene sets of PROTEIN-SECRETION (**e**), NEUTROPHIL-DEGRANULATION (**f**), and SPECIFIC-GRANULE (**g**) were enriched in mature $Ly6G^{+}$ neutrophils.

Figure 6.

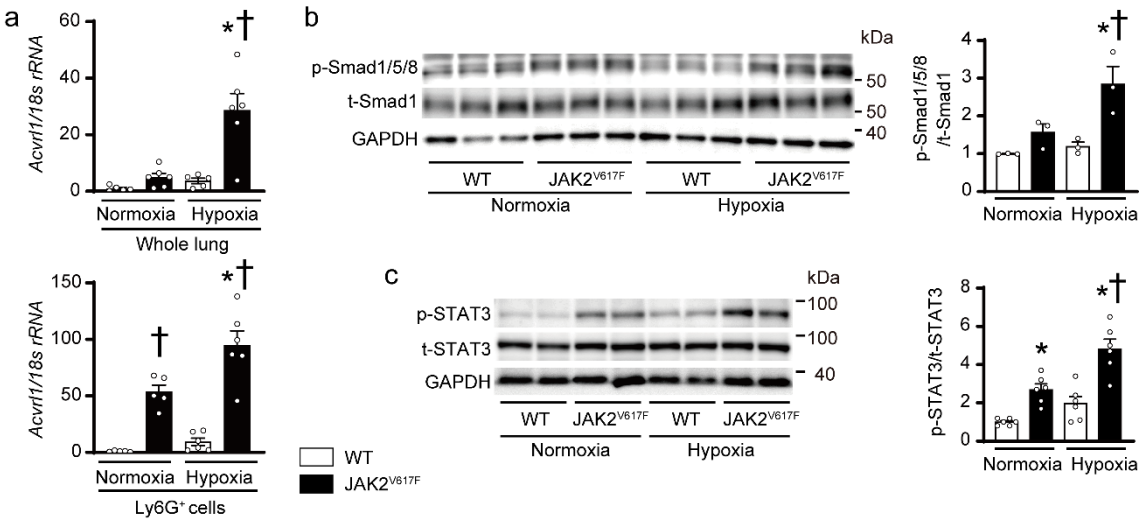

a mRNA expression of *Acvrl1* in whole lung extracts (top) or the sorted Ly6G$^+$ cells from the lungs (bottom) of WT mice and JAK2^{V617F} mice exposed to normoxia or hypoxia. The data were normalized to *18s rRNA* levels (n = 5, 6, 5, 6, *P = 0.0004, †P = 0.0004 for whole lung extracts, n = 5, 5, 6, 6, *P = 0.0069, †P = 0.0012 [left], < 0.0001 [right] for sorted Ly6G$^+$ cells). **b, c** Western blot analysis on the SMAD (**b**) and STAT (**c**) pathways in the lungs. Lung extracts from WT mice or JAK2^{V617F} mice were immunoblotted with the indicated antibodies. The ratios of phosphorylated Smad1/5/8 (p-Smad1/5/8) to total Smad1 (t-Smad1) and phosphorylated-STAT3 (p-STAT3) to total STAT3 (t-STAT3) are shown in the bar graphs. The average value for normoxia-WT mice was set to 1 (**b**, n = 3 in each group, *P = 0.0382, †P = 0.0100; **c**, n = 6 in each group, *P = 0.0125 [left], 0.0019 [right], †P < 0.0001). GAPDH was used as the loading control. All data are presented as mean ± SEM. *P < 0.05 versus the corresponding normoxia-group and †P < 0.05 versus the corresponding WT mice by the one-way ANOVA with Tukey post-hoc analysis.

Figure 7.

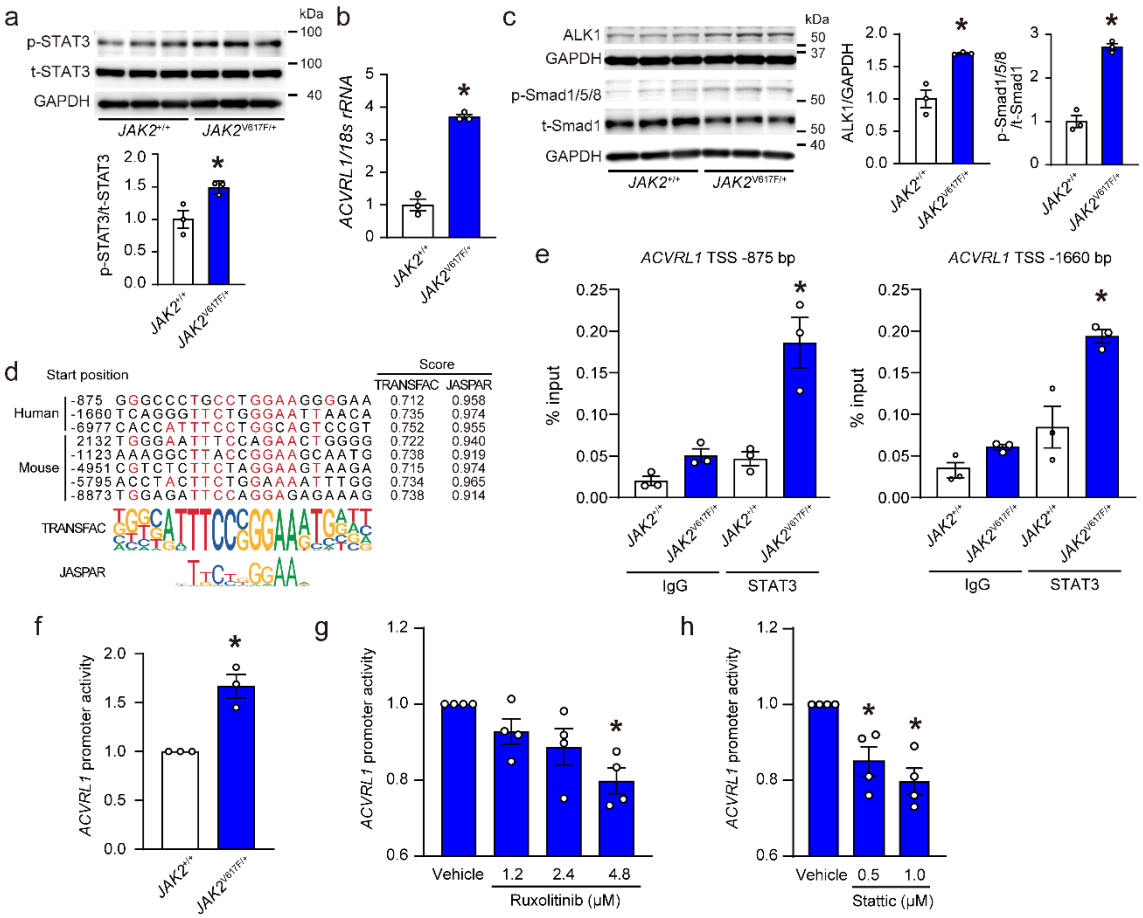

a Western blot analysis of STAT3 in *JAK2*$^{V617F/+}$ knock-in HCT116 cells. p-STAT3 and t-STAT3 indicate phosphorylated and total STAT3, respectively. p-STAT3 to t-STAT3 ratios are shown in the bar graph (n = 3, *P = 0.0296). The average value of *JAK2*$^{+/+}$ HCT116 cells was set to 1. **b** mRNA expression in *ACVRL1* in *JAK2*$^{V617F/+}$ cells. The data were normalized to *18s rRNA* levels. The average value of *JAK2*$^{+/+}$ cells was set to 1 (n = 3, *P = 0.0001). **c** Western blot analysis of the ALK1-SMAD pathway. The graphs show the densitometric analysis for ALK1, p-Smad1/5/8 and t-Smad1 (n = 3 in each, *P = 0.0070, 0.0004, respectively). p-Smad1/5/8 and t-Smad1 indicate phosphorylated Smad1/5/8 and total Smad1, respectively. GAPDH was used as the loading control. **d** Sequence alignments of putative STAT3 binding sites of *Acvrl1* in human (hg19) and mouse (m10).

Numbers are given according to the genomic sequence from transcriptional start site (TSS). The sequences of the STAT3 binding motifs are highlighted in red. Sequence logos for the motifs analyzed by TRANSFAC and JASPAR databases are displayed. **e** ChIP-qPCR analysis for STAT3 binding to the putative *ACVRL1* promoter. Chromatin was extracted from *JAK2*$^{+/+}$ and *JAK2*$^{V617F/+}$ HCT116 cells, and then precipitated with an anti-STAT3 antibody or IgG (negative control). The genomic DNA fragments of *ACVRL1* promoter were evaluated for enrichment by qPCR using the specific primers to the *Acvrl1* promoter given from TSS. Data are expressed as the respective DNA inputs (n = 3 independent experiments, *P = 0.0015, 0.0026, respectively). **f** Dual luciferase reporter assays for the *ACVRL1* gene promoter. The pGL3-basic vector containing the putative *ACVRL1* promoter region (TSS -875 bp) and pNL1.1.TK [Nluc/TK] as a control vector were co-transfected in *JAK2*$^{V617F/+}$ HCT116 cells. Twenty-four h after transfection, cell lysates were collected, and relative luciferase activity was determined by the ratio of firefly luciferase to Nano luciferase activity (n = 3 independent experiments, *P = 0.0051). **g, h** Inhibition of JAK1/2 or STAT3 reduced the elevated *ACVRL1* promoter activity in *JAK2*$^{V617F/+}$ cells. Twenty-four h after transfection, the *JAK2*$^{V617F/+}$ HCT116 cells were incubated with a specific JAK1/2 inhibitor, ruxolitinib or a specific STAT3 inhibitor, stattic, at the indicated concentration for a further 24 h, and then luciferase activity was measured (n = 4 independent experiments, **g**, *P = 0.0059; **h**, n =4, *P = 0.0164 [left], 0.0027 [right]). All data are presented as mean ± SEM. *P < 0.05 versus *JAK2*$^{+/+}$ cells or vehicle by the unpaired Student's t-test (two-sided) or the one-way ANOVA with Tukey post-hoc analysis.

Figure 8.

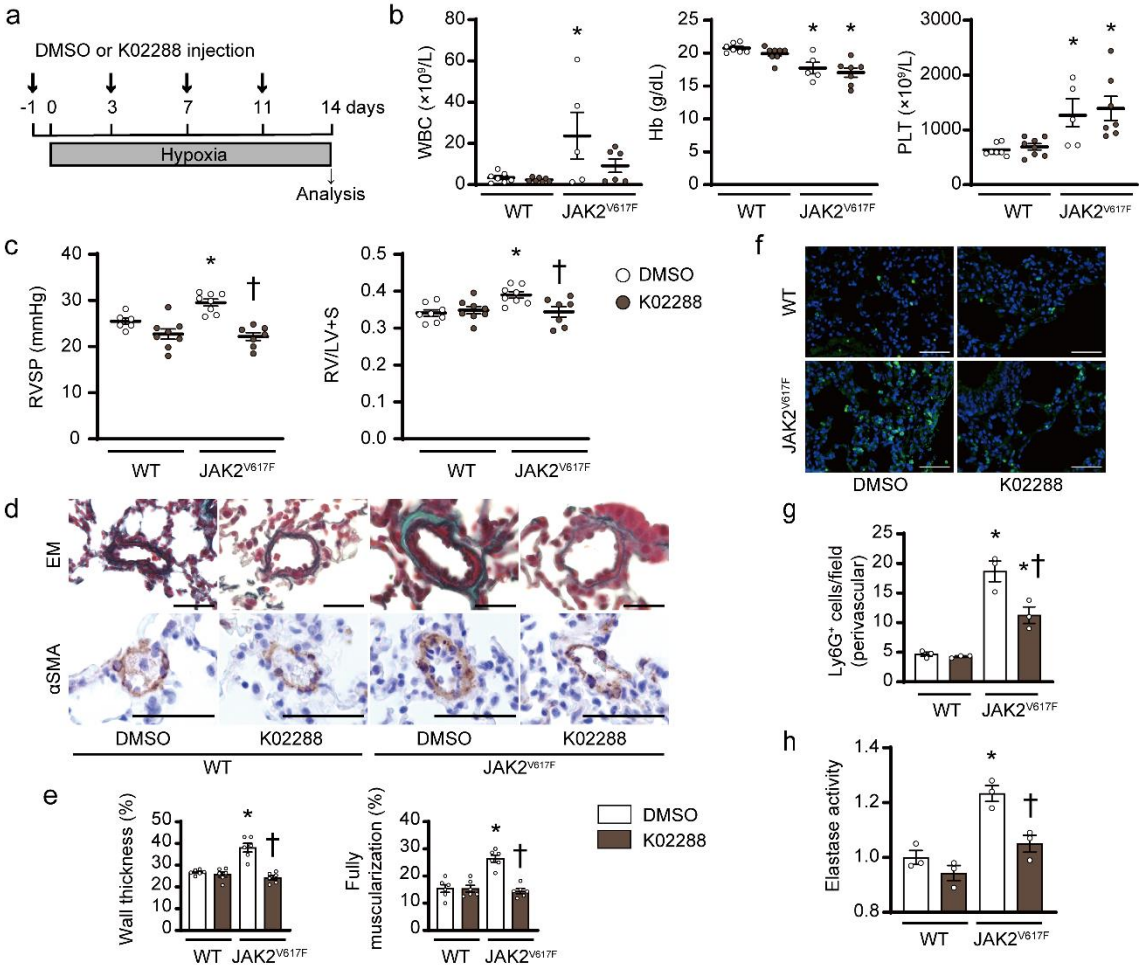

a Schematic protocol. Vehicle (DMSO) or an ALK1/2 inhibitor, K02288 was administered via an intraperitoneal injection of 12 mg/kg body weight during 2-week chronic hypoxia-exposure, as indicated. **b** Peripheral blood cell counts in DMSO- or K02288-treated WT mice and JAK2^{V617F} mice after exposure to chronic hypoxia for 2 weeks (n = 7, 7, 5, 6, *P = 0.0381 for WBC, n =7, 8, 5, 7, *P = 0.0074 [left], 0.0037 [right] for Hb, n = 7, 8, 5, 7, *P = 0.0401 [left], 0.0120 [right] for PLT). **c** RVSP and RV hypertrophy determined by RV/LV+S in DMSO- or K02288-treated WT mice and JAK2^{V617F} mice (n = 6, 8, 8, 7, *P = 0.0238 for RVSP, n = 8, 8, 8, 7, *P = 0.0112, †P = 0.0240 for RV/LV+S). **d** Representative images of EM-stained sections and sections

immunostained with anti-αSMA antibody from DMSO- or K02288-treated WT mice and JAK2^{V617F} mice. Scale bar, 25 μm. **e** Quantitative analysis of medial wall thickness in EM-stained sections (left, n = 6 in each group, *P < 0.0001, †P < 0.0001) and the percentage of muscularized distal pulmonary vessels in αSMA-immunostained sections (right, n = 6 in each group, *P < 0.0001, †P < 0.0001). **f** Representative immunofluorescence images of lung sections stained with anti-Ly6G (green) antibody and DAPI (blue). Scale bars, 50 μm. **g** Quantitative analysis of the numbers of Ly6G^{+} cells in the perivascular regions (n = 3 in each group, *P = 0.0001 [left], 0.0103 [right], †P = 0.0074). **h** Elastase activity in the lung extracts from DMSO- or K02288-treated WT mice and JAK2^{V617F} mice. The average value for DMSO-treated WT mice was set to 1 (n = 3 in each group, *P = 0.0017, †P = 0.0075). All data are presented as mean ± SEM. *P < 0.05 versus the corresponding WT mice and †P < 0.05 versus DMSO-treated JAK2^{V617F} mice by the one-way ANOVA with Tukey post-hoc analysis. WBC; white blood cell count, Hb; hemoglobin concentration; PLT, platelet count.

Figure 9.

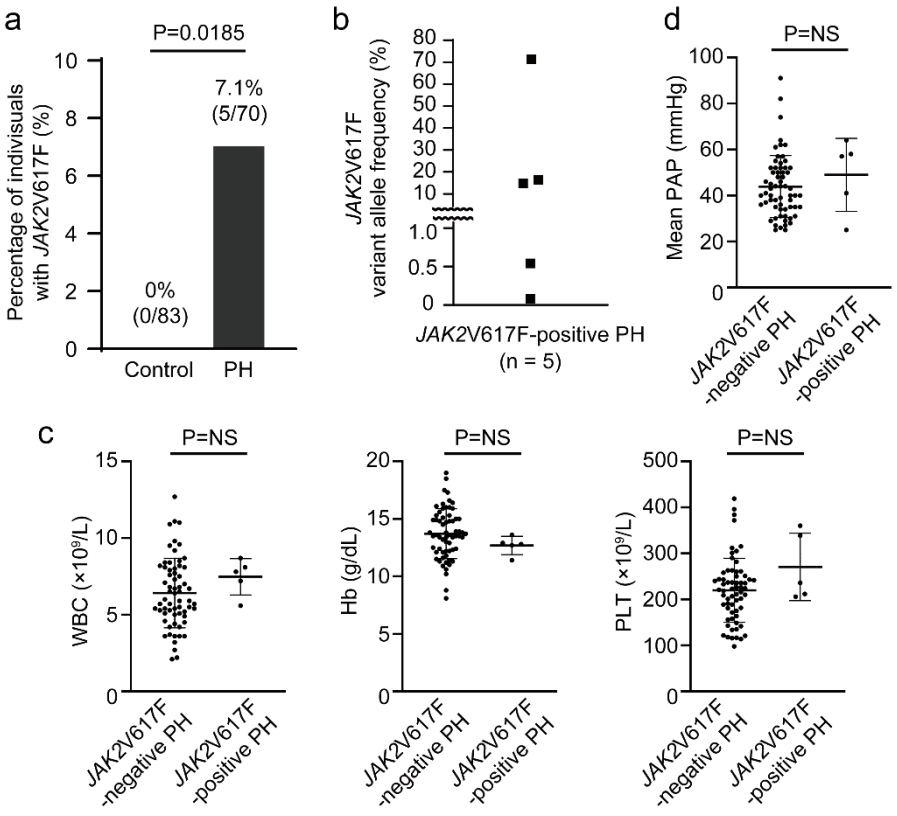

a *JAK2*V617F-positive clonal hematopoiesis was more common in PH patients. The comparison between PH patients (n = 70) and age- and sex-matched control subjects (n = 83) was made by Fisher's exact test (two-sided). **b** *JAK2*V617F variant allele frequency. **c, d,** Peripheral blood cell counts, and mean PAP (pulmonary arterial pressure) evaluated by right heart catheterization between *JAK2*V617F-negative and *JAK2*V617F-positive PH patients (n = 64, 5 for WBC, Hb, PLT and n = 63, 5 for mean PAP). **d**. Data are presented as mean ± SD. Comparisons of values between the two groups were performed by the unpaired Student's t-test (two-sided). WBC, white blood cell count; Hb, hemoglobin concentration; PLT, platelet count; NS, not significant.

Supplementary Figure 1.

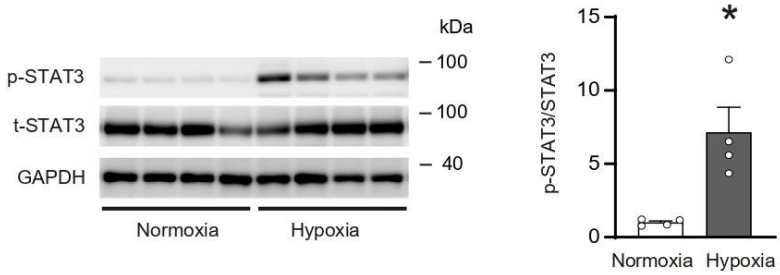

Lung homogenates obtained from the adult WT mice with a C57BL/6J background after normoxia (21% O2) or chronic hypoxia (10% O2) for 3 weeks were analyzed by immunoblotting with anti-phosphorylated-STAT3 and STAT3 antibodies. p-STAT3 and t-STAT3 indicate phosphorylated and total STAT3, respectively. p-STAT3 to t-STAT3 ratios are shown in the bar graph (n = 4 in each group). Data are presented as mean ± SEM. *P = 0.0116 versus the normoxia group by the unpaired Student's t-test (two-sided).

Supplementary Figure 2.

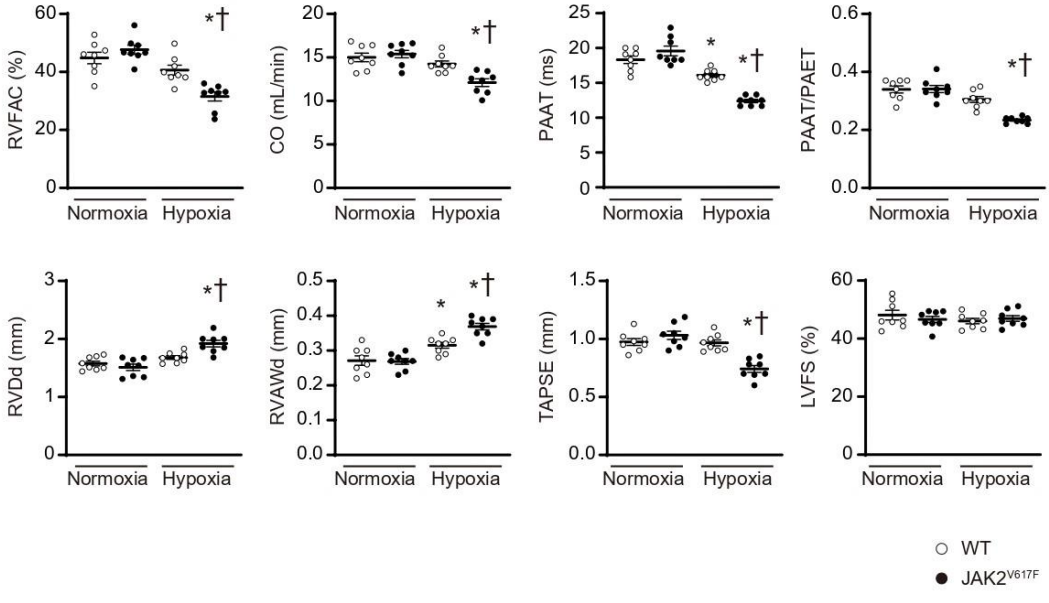

Echocardiography was performed to evaluate pulmonary hemodynamics and cardiac function 2 weeks after normoxia or chronic hypoxia (n = 8 in each group). All data are

presented as mean ± SEM. *P < 0.05 versus the corresponding normoxia-exposed group and †P < 0.05 versus the corresponding WT mice by one-way ANOVA with Tukey post-hoc analysis. *P < 0.0001, †P = 0.0039 for RVFAC, *P < 0.0001, †P = 0.0078 for CO, *P = 0.0134 [left], < 0.0001 [right], †P < 0.0001 for PAAT, *P < 0.0001, †P = 0.0002 for PAAT/PAET, *P < 0.0001, †P = 0.0052 for RVDd, *P = 0.0235 [left], < 0.0001 [right], †P = 0.0042 for RVAWd, *P < 0.0001, †P < 0.0001 for TAPSE. RVFAC, right ventricular fractional area change; CO, cardiac output; PAAT, pulmonary artery acceleration time; PAET, pulmonary artery ejection time; RVDd, right ventricular diastolic diameter, RVAWd, right ventricular anterior wall diameter; TAPSE, tricuspid annular plane systolic excursion; LVFS, left ventricular fractional shortening; WT, wild-type mice; JAK2V617F, JAK2V617F-expressing transgenic mice.

Supplementary Figure 3.

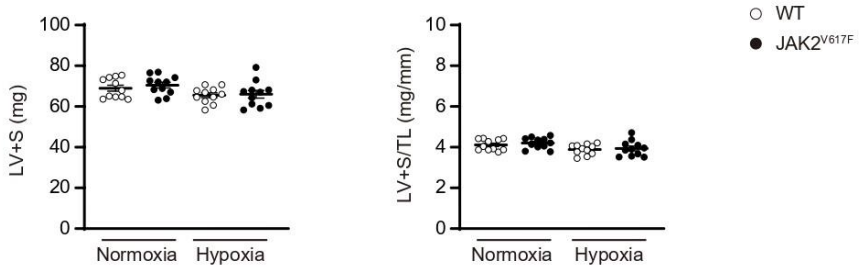

Left ventricular (LV) weight including septum (S) was measured after exposure to normoxia or chronic hypoxia for 2 weeks (n = 11 in each group). LV+S was normalized by tibia length (TL). All data are presented as mean ± SEM. The statistical comparison was performed by the one-way ANOVA. WT, wild-type mice; JAK2V617F, JAK2V617F-expressing transgenic mice. Source data are provided as a Source Data file.

Supplementary Figure 4.

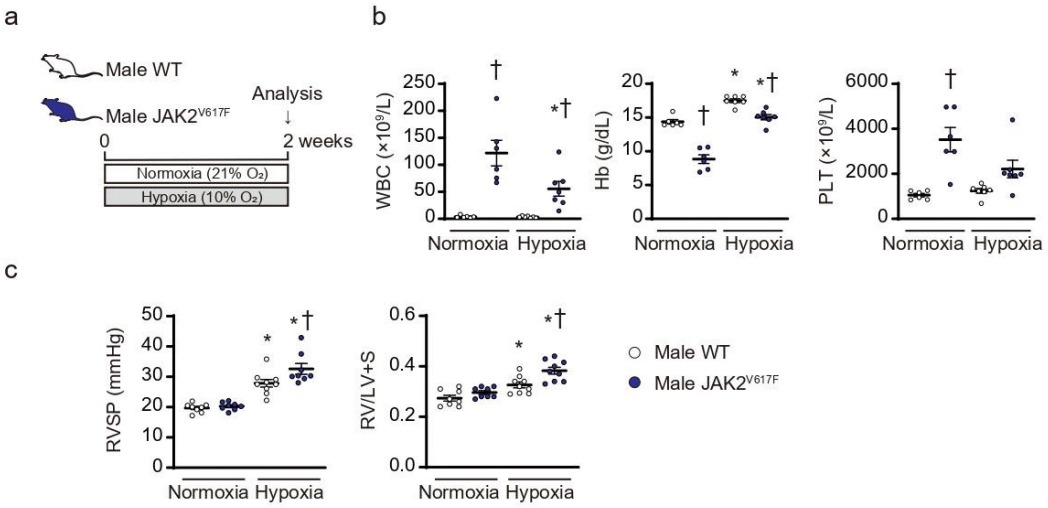

(a) Experimental design. Male wild-type (WT) mice and male JAK2V617F mice aged between 8 and 10 weeks were exposed to normoxia (21% O2) or hypoxia (10% O2) for 2 weeks. (b) Peripheral blood cell counts in WT mice or JAK2V617F mice after normoxia or hypoxia for 2 weeks (n = 6, 6, 7, 7, *P = 0.0088, †P < 0.0001 [left], 0.0360 [right] for WBC, n = 6, 6, 7, 7, *P = 0.0002 [left], < 0.0001 [right], †P < 0.0001 [left], 0.0015 [right] for Hb, n = 6, 6, 7, 7, †P = 0.0003 for PLT). (c) Right ventricular systolic pressure (RVSP) and right ventricular hypertrophy determined by the ratio of right ventricle (RV) weight to left ventricle weight plus septum weight (RV/LV+S) (n = 8, 8, 9, 8, *P < 0.0001 [left], < 0.0001 [right], †P = 0.0302 for RVSP, n = 8, 8, 9, 8, *P =0.0171 [left], < 0.0001 [right], †P = 0.00052 for RV/LV+S). All data are presented as mean ± SEM. *P < 0.05 versus the corresponding normoxia-exposed group and †P < 0.05 versus the corresponding WT mice by the one-way ANOVA with Tukey post-hoc analysis. WBC, white blood cell count; Hb, hemoglobin concentration; PLT, platelet count. WT, wild-type mice; JAK2V617F, JAK2V617F-expressing transgenic mice.

Supplementary Figure 5.

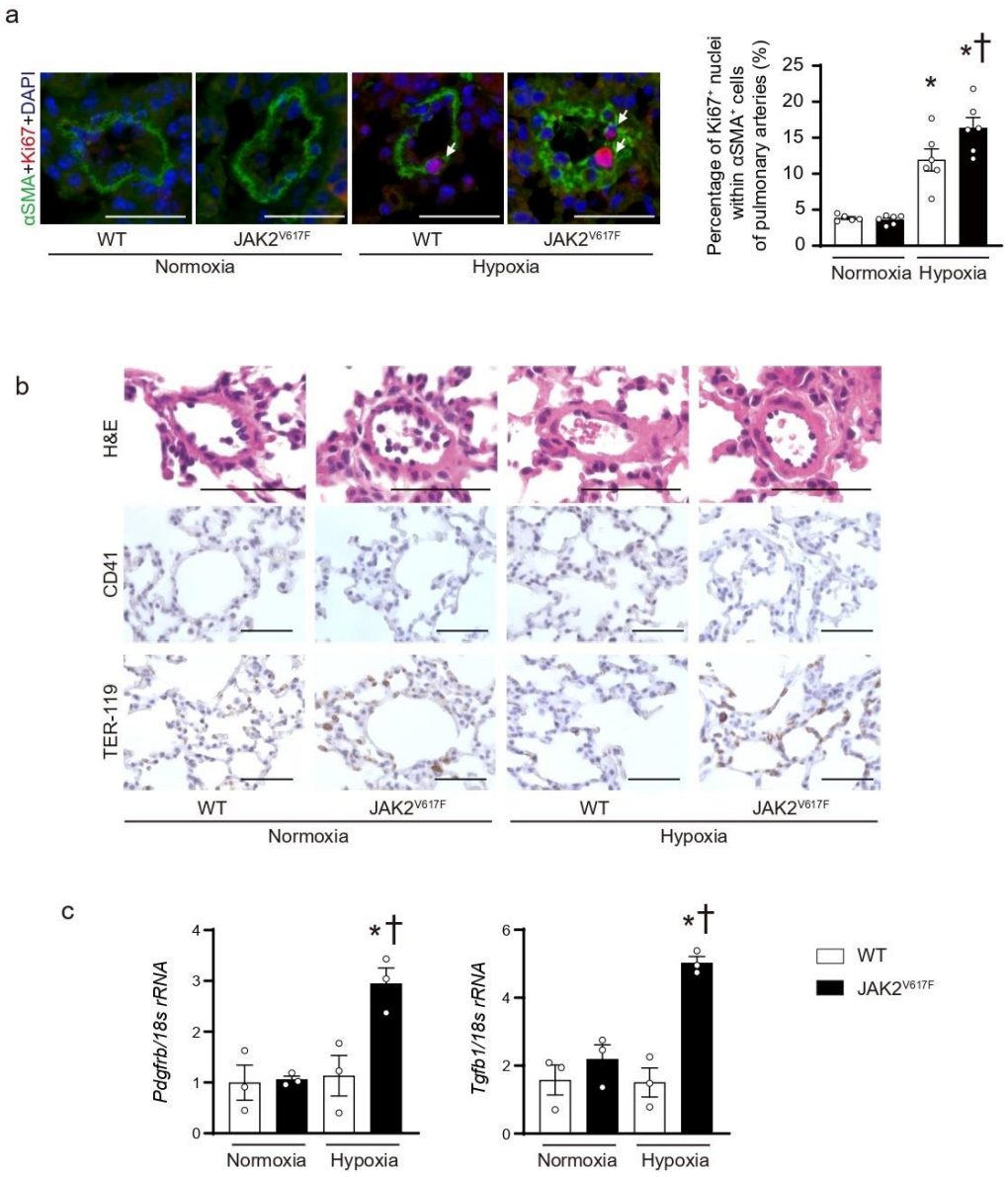

(a) Left, triple-labeled immunofluorescent staining (αSMA, green; Ki67, red; DAPI, blue) of the lung sections. Right, quantitative analyses of the percentage of Ki67-positive nuclei within αSMA+ cells of distal pulmonary arteries with a diameter of 50-100 μm (n = 5, 6, 6, 6, *P = 0.0005 [left], < 0.0001 [right], †P = 0.0448). More than 80 αSMA+ cells were counted. White arrows indicate Ki67-positive nuclei within αSMA+ cells. Scale bars, 50 μm. (b) Representative images of the lung sections of H&E staining and immunostaining

for CD41 and TER-119 from WT mice and JAK2V617F mice after normoxia and chronic hypoxia. Scale bars, 50 μm. (c) mRNA levels of Pdgfrb andTgfb1 in the lungs. The 18s rRNA was used for the normalization. Data are presented as mean ± SEM. The average value for the normoxia-WT mice was set to 1 (n = 3 in each group, *P = 0.0105, †P = 0.0132 for Pdgfrb, *P = 0.0036, †P = 0.0009 for Tgfb1). All data are presented as mean ± SEM. *P < 0.05 versus the corresponding normoxia-exposed group and †P < 0.05 versus the corresponding WT mice by the one-way ANOVA with Tukey post-hoc analysis. WT, wild-type mice; JAK2V617F, JAK2V617F-expressing transgenic mice.

Supplementary Figure 6.

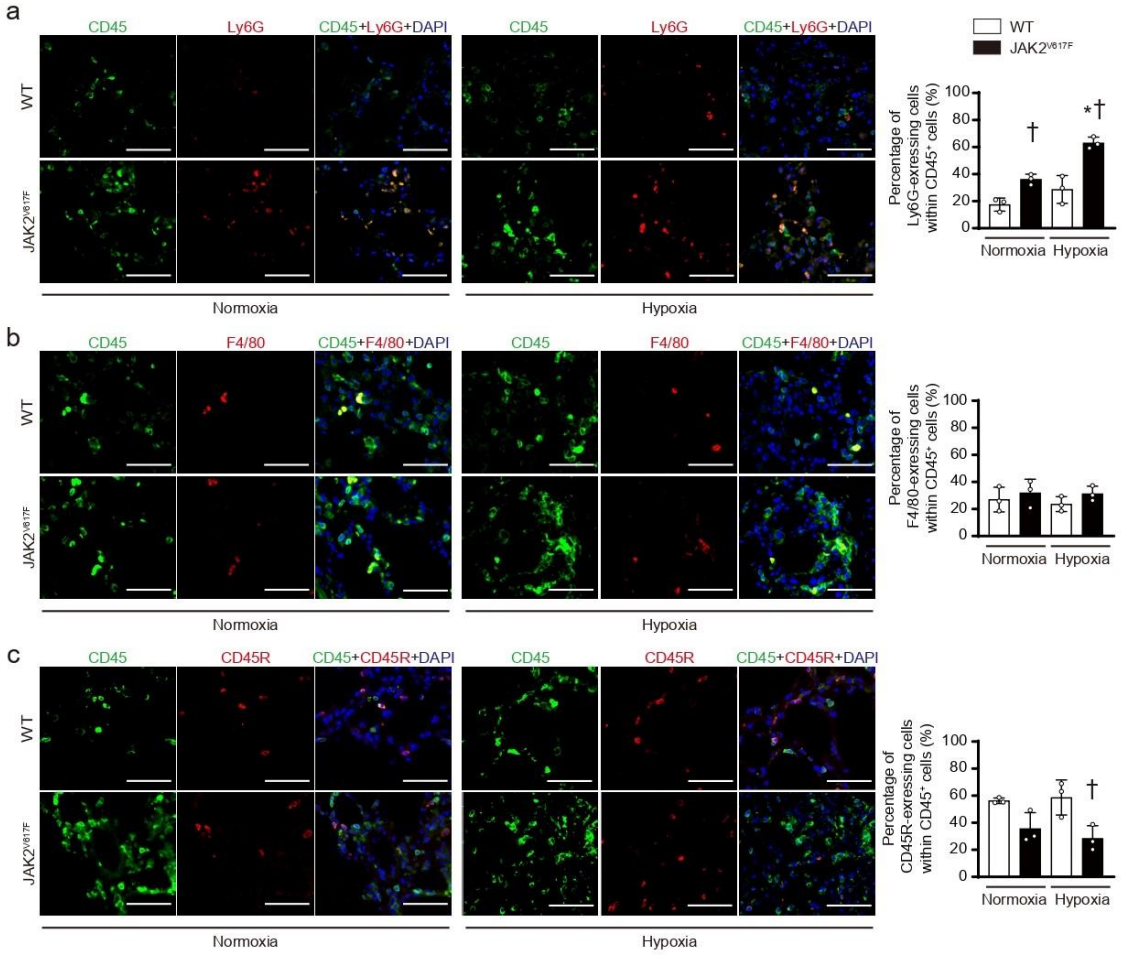

(a) Left, triple-labeled immunofluorescent staining (CD45, green; Ly6G, red; DAPI, blue) of the lung sections from WT mice and JAK2V617F mice after normoxia or chronic hypoxia. Right, quantitative analyses of the Ly6G-expressing cells within CD45+ cells (n = 3 in each group, *P = 0.0038, †P = 0.0297 [left], 0.0008 [right]). (b) Left, triple-labeled immunofluorescent staining (CD45, green; F4/80, red; DAPI, blue). Right, quantitative analyses of the F4/80-expressing cells within CD45+ cells (n = 3 in each group). (c) Left, triple-labeled immunofluorescent staining (CD45, green; CD45R, red; DAPI, blue). Right, quantitative analyses of the CD45R-expressing cells within CD45+ cells (n = 3 in each group, †P = 0.0250). At least 100 CD45+ cells were counted in each. Data are presented as mean ± SEM. *P < 0.05 versus the corresponding normoxia-exposed group and †P < 0.05 versus the corresponding WT mice by the one-way ANOVA with Tukey post-hoc analysis. Scale bars, 50 μm. WT, wild-type mice; JAK2V617F, JAK2V617F-expressing transgenic mice.

Supplementary Figure 7.

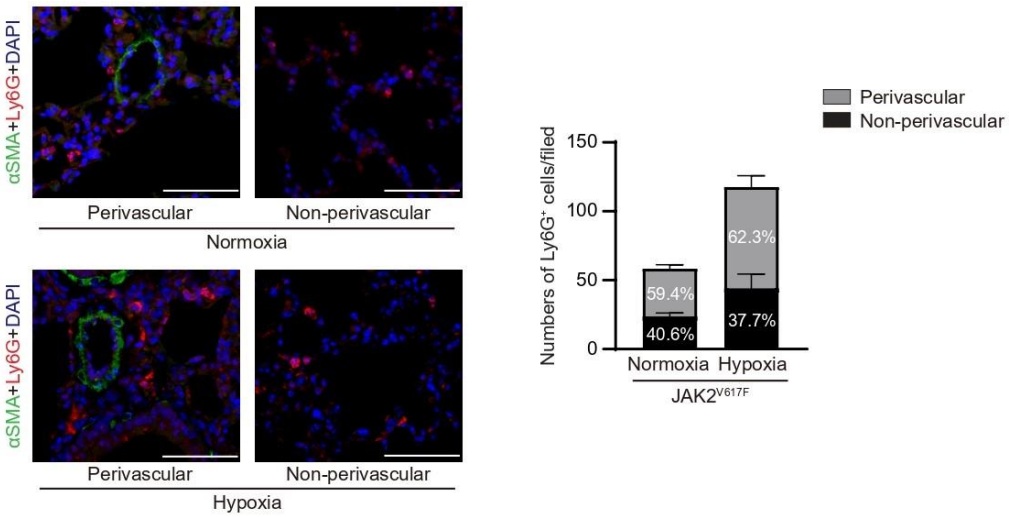

Left, triple-labeled immunofluorescent staining (αSMA, green; Ly6G, red; DAPI, blue) of the lung sections in JAK2V617F mice. Perivascular regions were determined as the area within 100 μm from distal pulmonary arteries with diameters of 50 μm. Scale bars, 50 μm. Right, quantitative analyses of the numbers of Ly6G+ cells in perivascular regions as well as non-perivascular regions (n = 3). More than 10 fields were analyzed in each group. One field was defined as 200 μm x 200 μm. The percentages of the Ly6G+ cells in perivascular regions and non-perivascular regions in each group are shown. All data are presented as mean ± SEM.

Supplementary Figure 8.

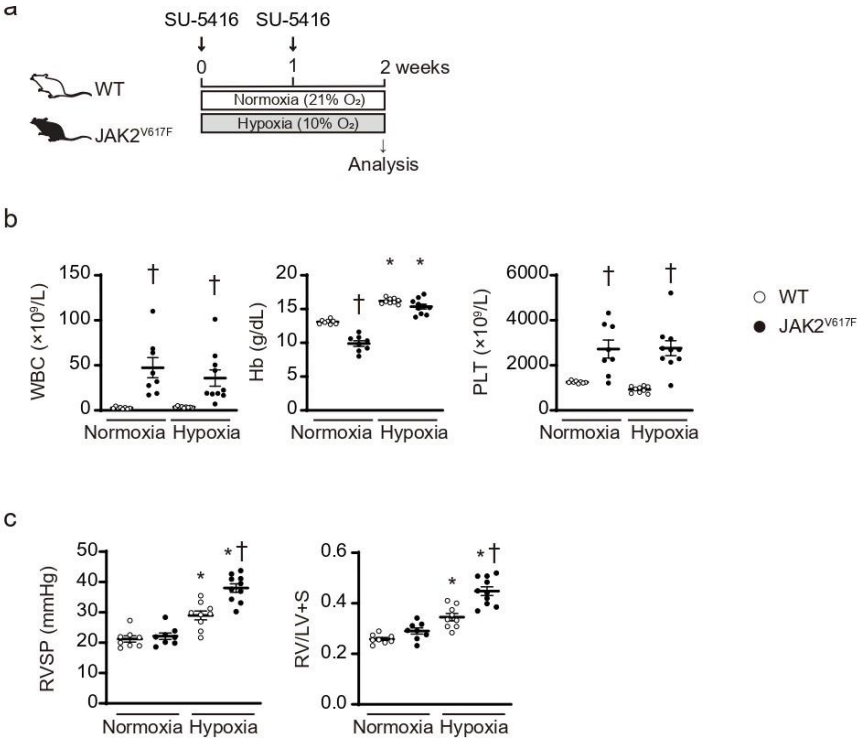

(a) Experimental design. Single weekly injection of a VEGF inhibitor, SU-5416, at 20 mg/kg followed by 2 weeks of normoxia (21% O2) or hypoxia (10% O2) in WT mice and JAK2V617F mice. (b) Peripheral blood cell counts (n = 8, 8, 9, 10, †P = 0.0014 [left],

0.0142 [right] for WBC, n = 8, 8, 9, 10, *P < 0.0001 [left], < 0.0001 [right], †P< 0.0001 for Hb, n = 8, 8, 9, 10, †P = 0.0040 [left], < 0.0001 [right] for PLT). (c) Right ventricular systolic pressure (RVSP) and right ventricular hypertrophy determined by the ratio of right ventricle (RV) weight to left ventricle weight plus septum weight (RV/LV+S) (n = 8, 8, 9, 10, *P = 0.0012 [left], < 0.0001 [right], †P < 0.0001 for RVSP, n = 8, 8, 9, 10, *P = 0.0007 [left], < 0.0001 [right], †P < 0.0001 for RV/LV+S). All data are presented as mean ± SEM. *P < 0.05 versus the corresponding normoxia-exposed group and †P < 0.05 versus the corresponding WT mice by the one-way ANOVA with Tukey post-hoc analysis. WBC, white blood cell count; Hb, hemoglobin concentration; PLT, platelet count. WT, wild-type mice; JAK2V617F, JAK2V617F-expressing transgenic mice.

Supplementary Figure 9.

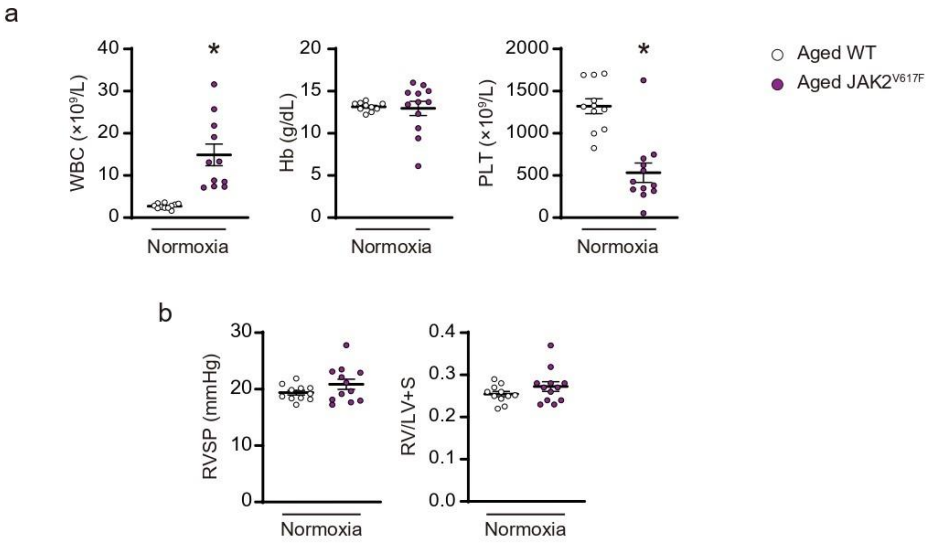

(a) Peripheral blood cell counts in WT and JAK2V617F female mice aged 8- to 9-month-old under normoxia (n = 12 in each group, *P = 0.0001 for WBC, n = 10, 12 for Hb, n = 11, 12, *P < 0.0001 for PLT). (b) Right ventricular systolic pressure (RVSP) and right ventricular hypertrophy determined by the ratio of right ventricle (RV) weight to left

ventricle weight plus septum weight (RV/LV+S) (n = 11, 12 in each). All data are presented as mean ± SEM. *P < 0.05 versus WT mice by the unpaired Student's t-test (two-sided). WBC, white blood cell count; Hb, hemoglobin concentration; PLT, platelet count. WT, wild-type mice; JAK2V617F, JAK2V617F-expressing transgenic mice.

Supplementary Figure 10.

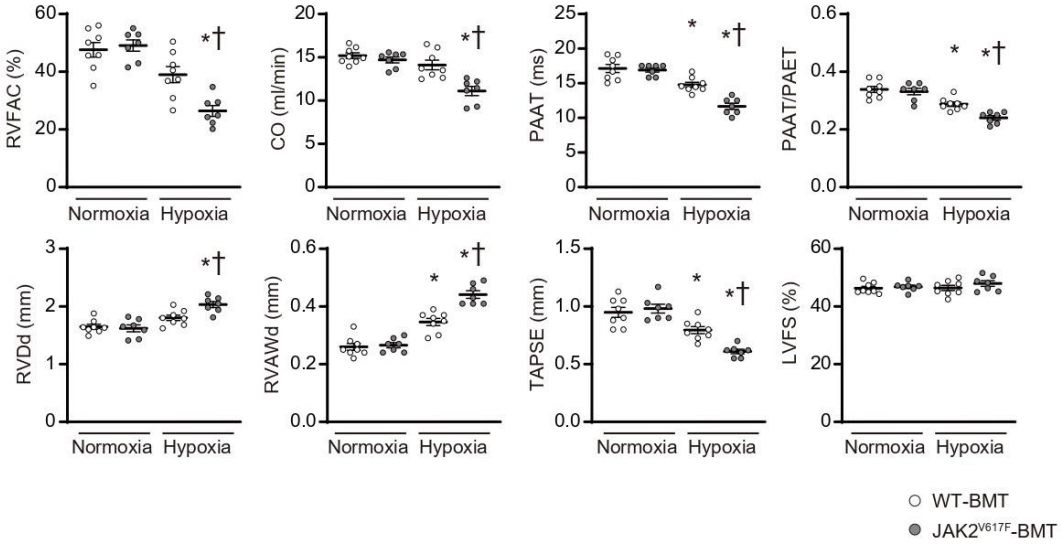

Echocardiography was performed to evaluate pulmonary hemodynamics and cardiac function 3 weeks after normoxia or chronic hypoxia (n = 8, 7, 8, 7, *P < 0.0001, †P = 0.0047 for RVFAC, *P < 0.0001, †P = 0.0004 for CO, *P = 0.0036 [left], < 0.0001 [right], †P = 0.0002 for PAAT, *P = 0.0027 [left], <0.0001 [right], †P = 0.0075 for PAAT/PAET, *P < 0.0001, †P = 0.0144 for RVDd, *P < 0.0001 [left], < 0.0001 [right], †P < 0.0001 for RVAWd, *P = 0.0168 [left], < 0.0001 [right], †P = 0.0041 for TAPSE). All data are presented as mean ± SEM. *P < 0.05 versus the corresponding normoxia-exposed group and †P < 0.05 versus the corresponding WT mice by one-way ANOVA with Tukey post-hoc analysis. RVFAC, right ventricular fractional area change; CO, cardiac output; PAAT, pulmonary artery acceleration time; PAET, pulmonary artery ejection time;

RVDd, right ventricular diastolic diameter, RVAWd, right ventricular anterior wall diameter; TAPSE, tricuspid annular plane systolic excursion; LVFS, left ventricular fractional shortening; WT-BMT, recipient WT mice transplanted with WT bone marrow cells; JAK2V617F-BMT, recipient WT mice transplanted with JAK2V617F bone marrow cells.

Supplementary Figure 11.

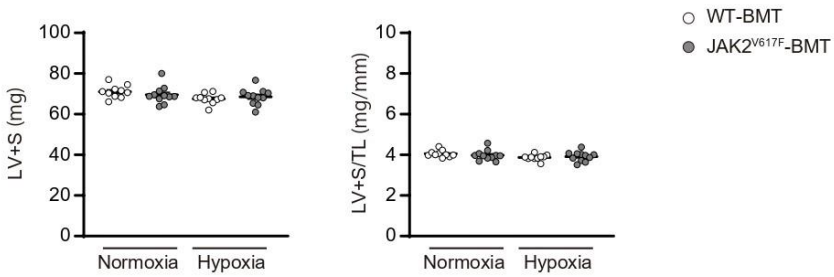

Left ventricular (LV) weight including septum (S) was measured after exposure to normoxia (21% O2) or chronic hypoxia (10% O2) for 3 weeks (n = 10, 11, 10, 11 in each). LV+S was normalized by tibia length (TL). All data are presented as mean ± SEM. The statistical comparison was performed by the one-way ANOVA. WT-BMT, recipient WT mice transplanted with WT bone marrow cells; JAK2V617F-BMT, recipient WT mice transplanted with JAK2V617F bone marrow cells.

Supplementary Figure 12.

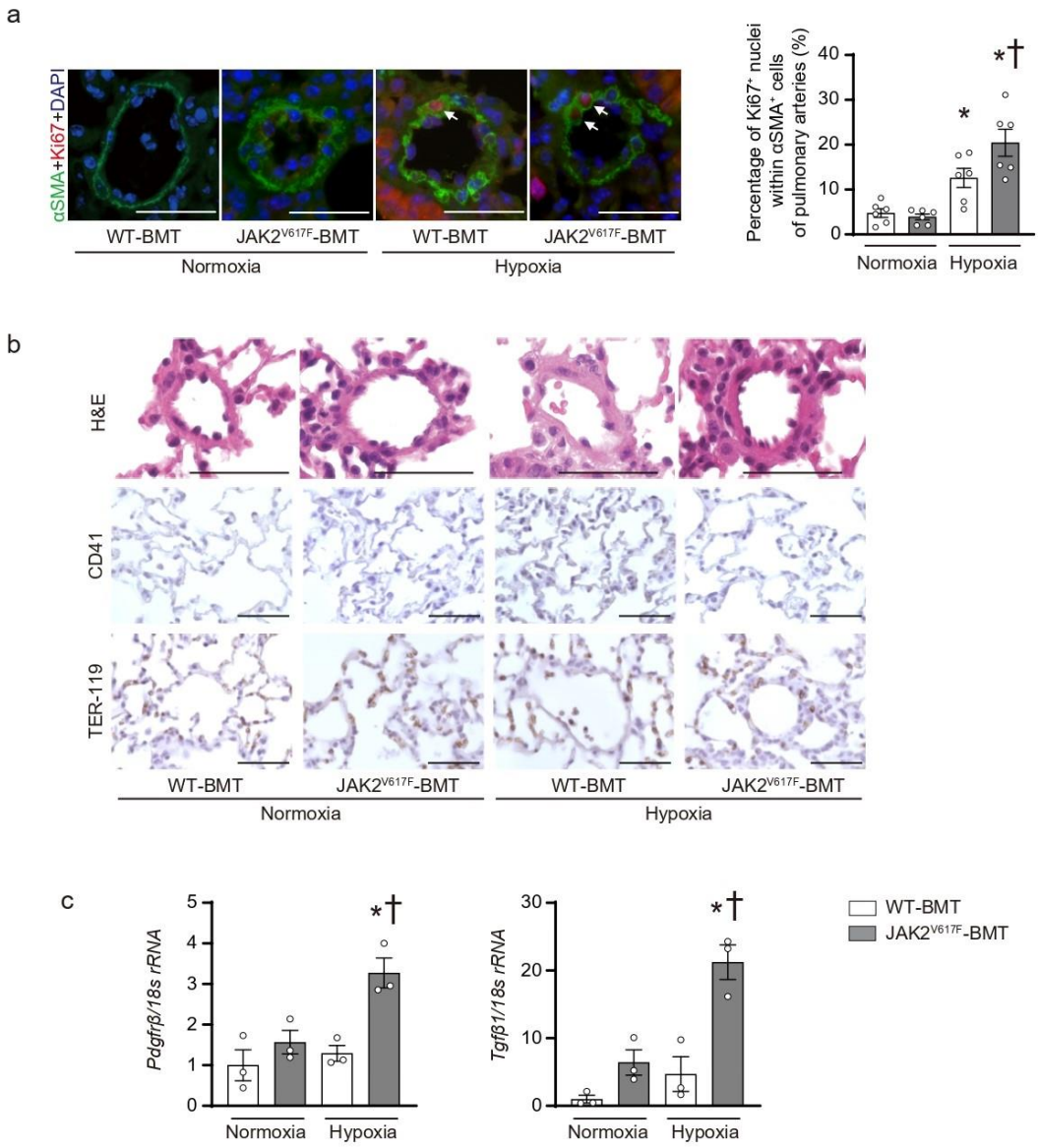

(a) Left, triple-labeled immunofluorescent staining (αSMA, green; Ki67, red; DAPI, blue) of the lung sections. Right, quantitative analyses of the percentage of Ki67-positive nuclei within αSMA+ cells of distal pulmonary arteries with a diameter of 50-100 μm (n = 6 in each group, *P = 0.0430 [left], < 0.0001 [right], †P = 0.0425). More than 80 αSMA+ cells were counted in each section. White arrows indicate Ki67-positive nuclei within αSMA+ cells. Scale bars, 50 μm. (b) Representative images of the lung sections of H&E staining and immunostaining for CD41 and TER-119 from WT-BMT mice and JAK2V617F-BMT

mice after normoxia and chronic hypoxia. Scale bars, 50 μm. (c) mRNA levels of Pdgfrb and Tgfb1 in the lungs. The 18s rRNA was used for the normalization. Data are presented as mean ± SEM. The average value for the normoxia-WT-BMT mice was set to 1 (n = 3 in each group, *P = 0.0214, †P = 0.0095 for Pdgfrb, *P = 0.0041, †P = 0.0021 for Tgfb1). All data are presented as mean ± SEM. *P < 0.05 versus the corresponding normoxia-exposed group and †P < 0.05 versus the corresponding WT-BMT mice by one-way ANOVA with Tukey post-hoc analysis. WT-BMT, recipient WT mice transplanted with WT bone marrow cells; JAK2V617F-BMT, recipient WT mice transplanted with JAK2V617F bone marrow cells.

Supplementary Figure 13.

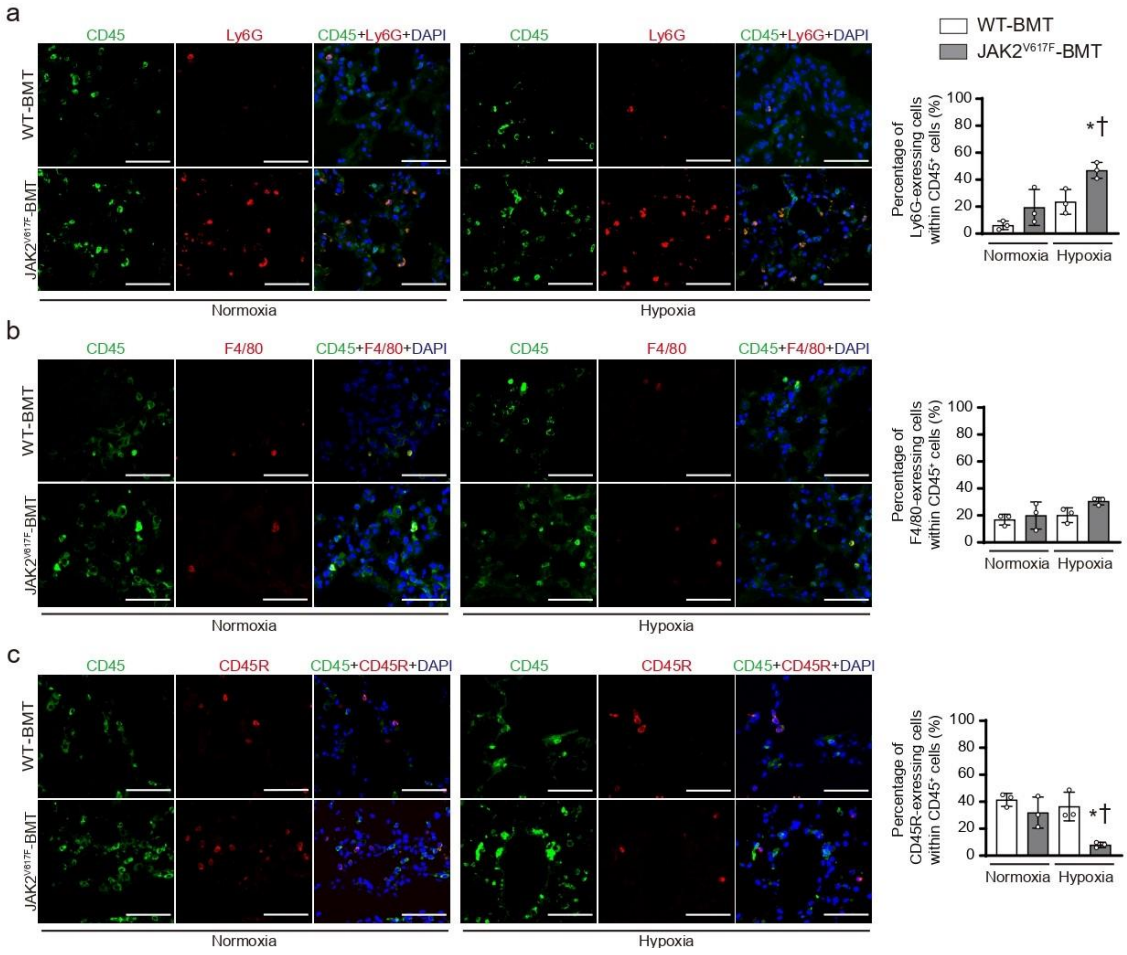

(a) Left, triple-labeled immunofluorescent staining (CD45, green; Ly6G, red; DAPI, blue) of the lung sections from WT mice and JAK2V617F mice after normoxia or chronic hypoxia. Right, quantitative analyses of the Ly6G-expressing cells within CD45+ cells (n = 3 in each group, *P = 0.0205, †P = 0.0459). (b) Left, triple-labeled immunofluorescent staining (CD45, green; F4/80, red; DAPI, blue). Right, quantitative analyses of the F4/80-expressing cells within CD45+ cells (n = 3 in each group). (c) Left, triple-labeled immunofluorescent staining (CD45, green; CD45R, red; DAPI, blue). Right, quantitative analyses of the CD45R-expressing cells within CD45+ cells (n = 3 in each group, *P = 0.0309, †P = 0.0125). At least 100 CD45+ cells were counted in each. All data are presented as mean ± SEM. *P < 0.05 versus the corresponding normoxia-exposed group and †P < 0.05 versus the corresponding WT-BMT mice by one-way ANOVA with Tukey post-hoc analysis. Scale bars, 50 μm. WT-BMT, recipient WT mice transplanted with WT bone marrow cells; JAK2V617F-BMT, recipient WT mice transplanted with JAK2V617F bone marrow cells.

Supplementary Figure 14.

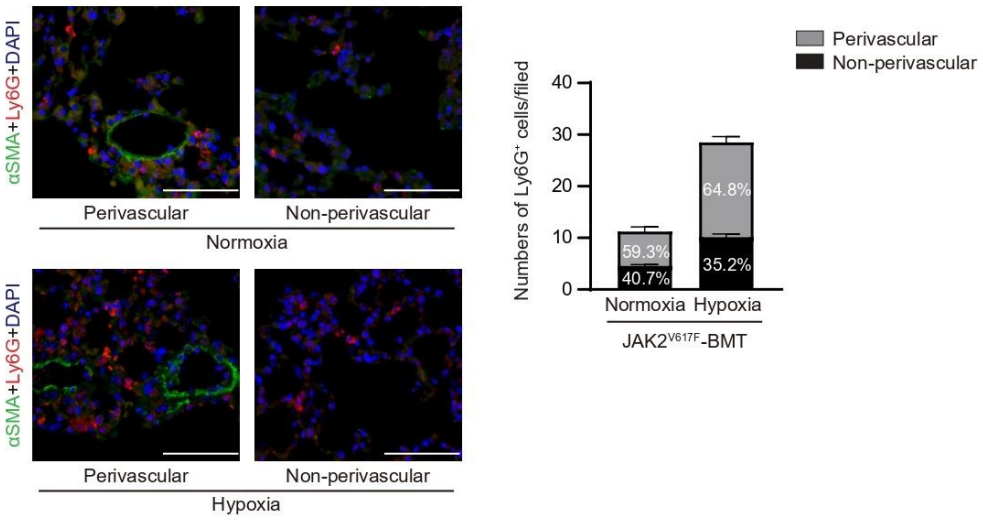

Left. triple-labeled immunofluorescent staining (αSMA, green; Ly6G, red; DAPI, blue) of the lung sections in JAK2V617F-BMT mice. Perivascular regions were determined as the area within 100 μm from distal pulmonary arteries with diameters of 50 μm. Scale bars, 50 μm. Right, quantitative analyses of the numbers of Ly6G+ cells in perivascular regions as well as non-perivascular regions (n = 3). More than 10 fields were analyzed in each group. One field was defined as 200 μm x 200 μm. The percentages of the Ly6G+ cells in perivascular regions and non-perivascular regions in each group are shown. JAK2V617F-BMT, recipient WT mice transplanted with JAK2V617F bone marrow cells. All data are presented as mean ± SEM.

Supplementary Figure 15.

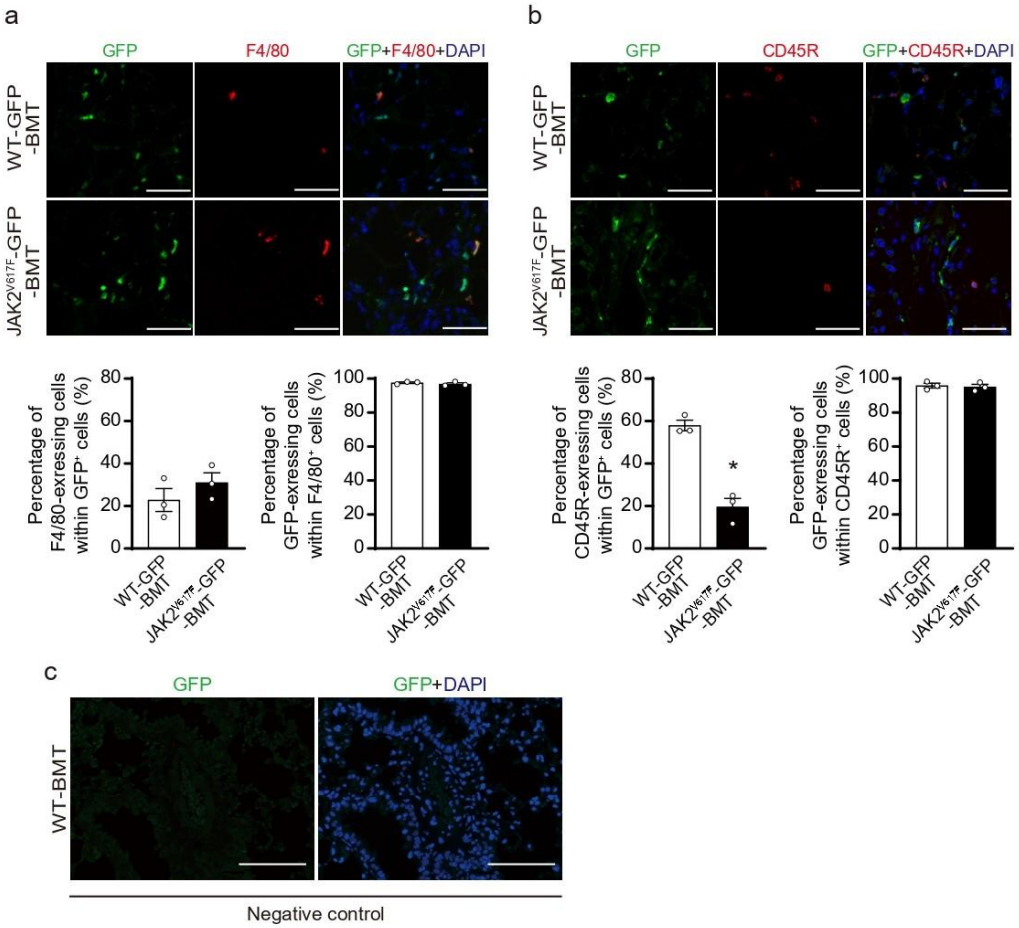

(a) Lethally irradiated WT mice were transplanted with bone marrow (BM) cells from control WT/CAG-EGFP (WT-GFP) or JAK2V617F/CAG-EGFP (JAK2V617F-GFP) double transgenic mice. Five weeks after BM transplantation (BMT), recipients were subjected to chronic hypoxia for 3 weeks, and then the lungs were fixed and stained with the indicated antibodies. Representative immunofluorescence images of lung sections stained with anti-GFP (green) and anti-F4/80 (red) antibodies and DAPI (blue) in WT-GFP-BMT or JAK2V617F-GFP-BMT mice are shown in top panels. Scale bars, 50 μm. Quantitative analyses of F4/80-expressing cells within GFP+ cells and GFP-expressing cells within F4/80+ cells are shown in the graphs (n = 3 in each group). (b) Representative immunofluorescence images of lung sections stained with anti-GFP (green) and anti-CD45R (red) antibodies and DAPI (blue) in WT-GFP-BMT or JAK2V617F-GFP-BMT mice. Scale bars, 50 μm. Quantitative analyses of CD45R-expressing cells within GFP+ cells and GFP-expressing cells within CD45R+ cells are shown in the graphs (n = 3 in each group). More than 100 cells were counted in each. *P = 0.0012 versus WT-GFP-BMT mice by the unpaired t-test (two-sided). All data are presented as mean ± SEM. (c) The lung sections from WT recipient mice transplanted with WT BM cells without GFP as a negative control. The sections were stained with an anti-GFP (green) antibody and DAPI (blue). Representative images of three independent experiments are shown. Scale bars, 100 μm. WT-GFP-BMT, recipient WT mice transplanted with WT-GFP BM cells; JAK2V617F-GFP-BMT, recipient WT mice transplanted with JAK2V617F-GFP BM cells.

Supplementary Figure 16.

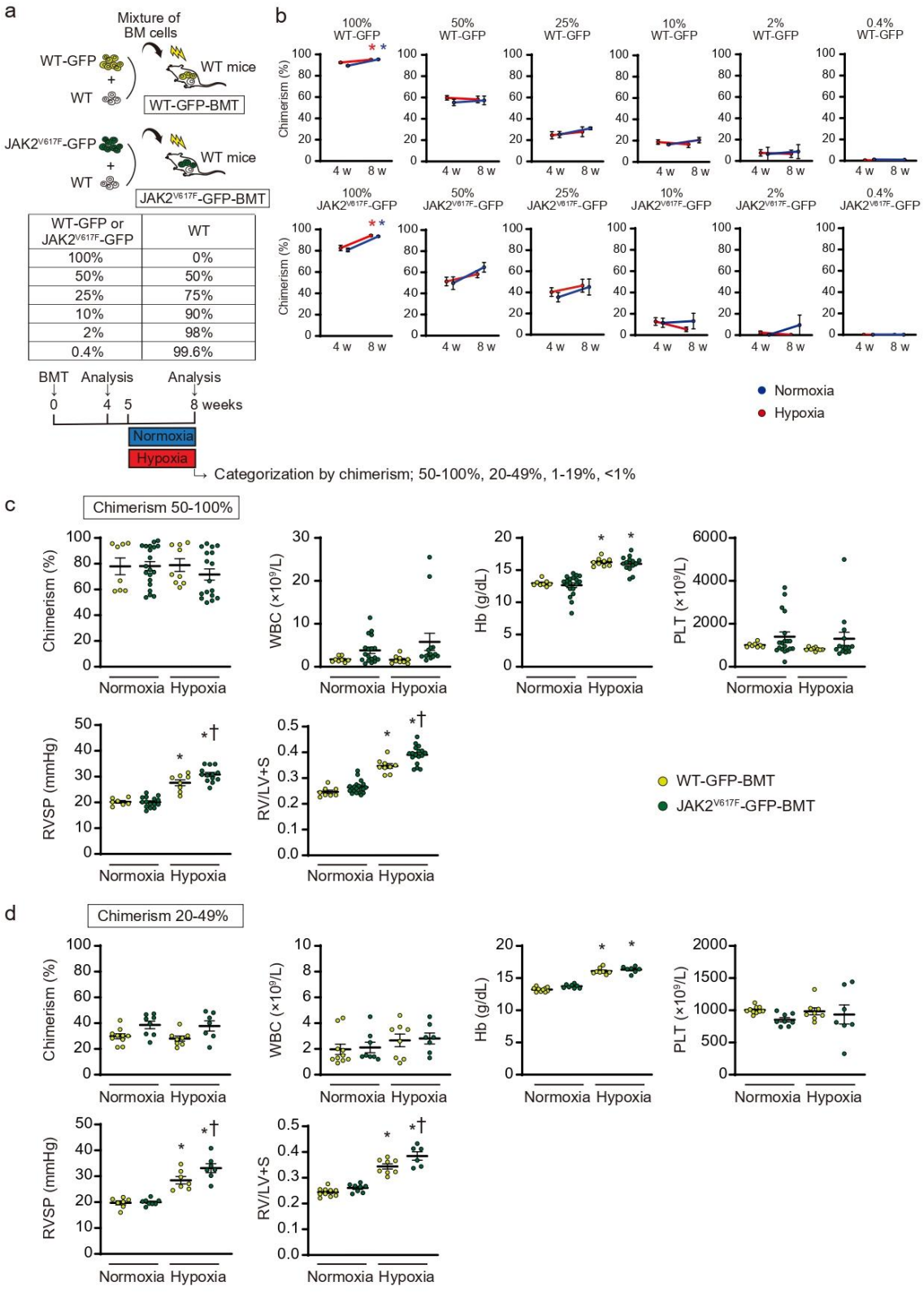

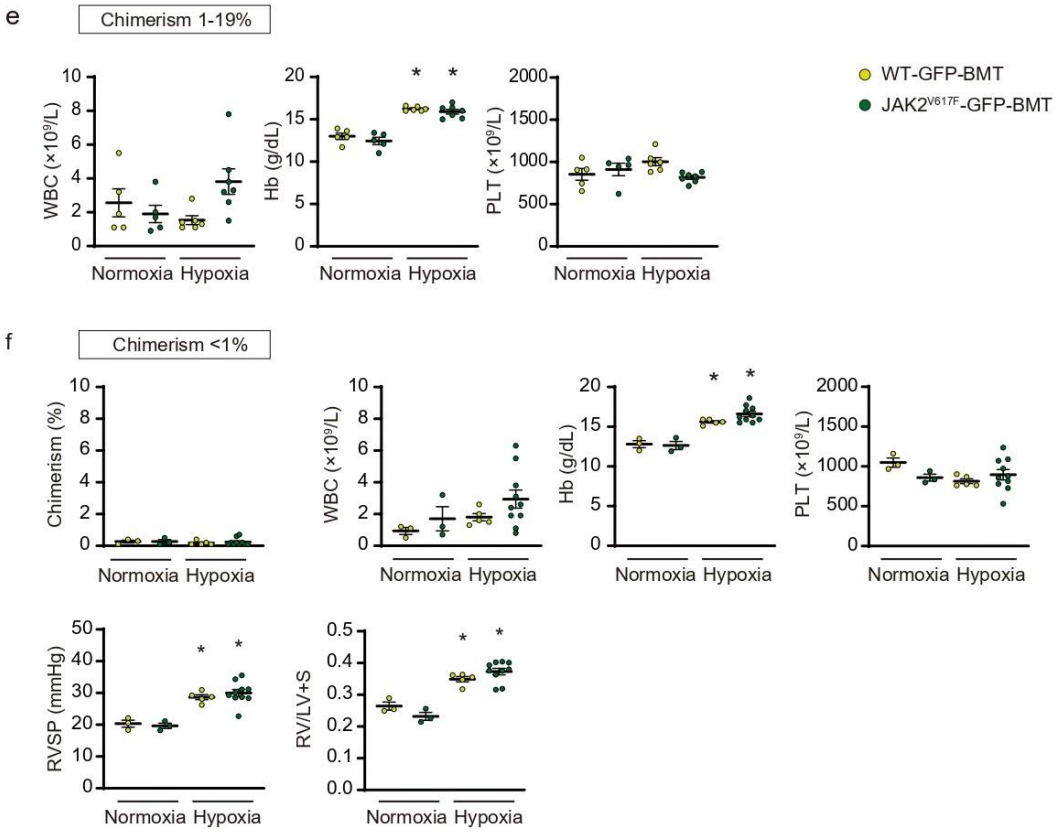

(a) Schematic depiction of the competitive bone marrow transplantation (BMT). The different ratio of WT-GFP or JAK2V617F-GFP and WT without GFP competitor was transplanted into the lethally irradiated recipient WT mice. The BMT mice at 8 weeks were categorized according to the chimerism; 50-100%, 20-49%, 1-19%, <1%. (b) The donor chimerism in the blood after BMT. The percentage of GFP+ cells within CD45+ cells was determined by flow cytometry at 4 and 8 weeks after BMT after normoxia or chronic hypoxia exposure (n= 9, 9, *P = 0.0001 [normoxia], 0.0211 [hypoxia] for 100% WT-GFP, n = 5, 5 for 50% WT-GFP, n = 5, 5 for 25% WT-GFP, n = 5, 5 for 10% WT-GFP; n = 5, 6 for 2% WT-GFP, n = 5, 5 for 0.4% WT-GFP, n = 11, 9, *P < 0.0001 [normoxia], 0.0025 [hypoxia] for 100% JAK2V617F-GFP, n = 10, 6 for 50% JAK2V617F-GFP, n = 8, 14 for 25% JAK2V617F-GFP, n = 5, 4 for 10% JAK2V617F-GFP, n = 5, 8 for 2% JAK2V617F-GFP, n = 5, 7 for 0.4% JAK2V617F-GFP). *P < 0.05

versus the corresponding 4-week group by the two-sided paired Student's t-test (blue, normoxia group; red, hypoxia group). (c, d) The recipients with donor chimerism of 50-100% (c, n = 8, 20, 9, 17) and 20-49% (d, n = 10, 8, 8, 7) at 8 weeks after BMT were enrolled for statistical comparison. Peripheral blood cell counts, RVSP, and RV/LV+S are shown (c, n = 8, 18, 9, 14 for WBC, n = 8, 19, 9, 14, *P < 0.0001 [left], < 0.0001 [right] for Hb, n = 8, 19, 9, 14 for PLT, n = 7, 15, 8, 13, *P < 0.0001 [left], < 0.0001 [right], †P = 0.0339 for RVSP, n = 8, 20, 9, 17, *P < 0.0001 [left], < 0.0001 [right], †P < 0.0021 for RV/LV+S; d, n = 10, 8, 8, 7 for WBC, n = 10, 8, 8, 7, *P < 0.0001 [left], < 0.0001 [right] for Hb, n = 10, 8, 8, 7 for PLT, n = 7, 8, 7, 7, *P = 0.0001 [left], < 0.0001 [right], †P = 0.0445 for RVSP, n = 10, 8, 8, 6, *P < 0.0001 [left], < 0.0001 [right], †P = 0.0291 for RV/LV+S). (e) Peripheral blood cell counts in the BMT mice with donor chimerism of 1-19% at 8 weeks after BMT (n = 5, 5, 6, 7 for WBC, n = 5, 5, 6, 7, *P < 0.0001 [left], < 0.0001 [right] for Hb, n = 5, 5, 6, 7 for PLT). The data of chimerism, RVSP, and RV/LV+S are shown in main Fig. 4. (f) The donor chimerism, peripheral blood cell counts, RVSP and RV/LV+S in the BMT mice with donor chimerism with <1% (n = 3, 3, 5, 10 for chimerism, n = 3, 3, 5, 10 for WBC, n = 3, 3, 5, 10, *P = 0.0014 [left], < 0.0001 [right] for Hb, n = 3, 3, 5, 10 for PLT, n = 3, 3, 5, 10, *P = 0.0043 [left], 0.0002 [right] for RVSP, n = 3, 3, 5, 10, *P = 0.0027 [left], < 0.0001 [right] for RV/LV+S). All data are presented as mean ± SEM. *P < 0.05 versus the corresponding normoxia-exposed group and †P < 0.05 versus the corresponding WT-GFP-BMT mice by the one-way ANOVA with Tukey post-hoc analysis. WBC, white blood cell count; Hb, hemoglobin concentration; PLT, platelet count; WT-GFP-BMT, recipient WT mice transplanted with WT-GFP BM cells; JAK2V617F-GFP-BMT, recipient WT mice transplanted with JAK2V617F-GFP BM cells.

Supplementary Figure 17.

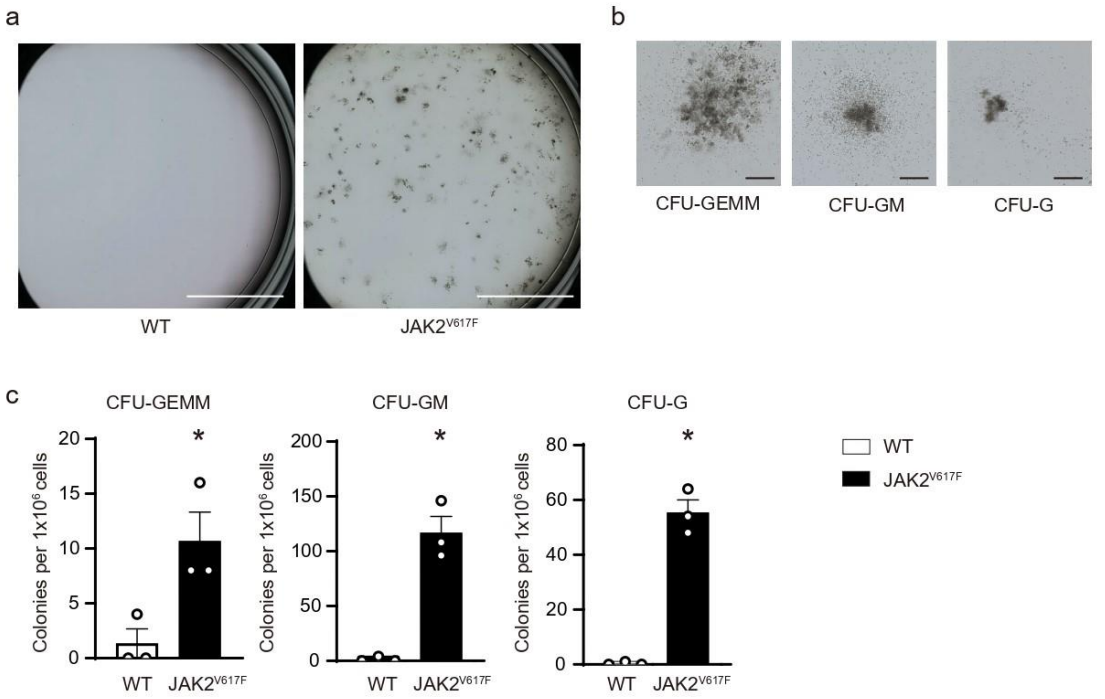

CD117 (c-kit)+ cells were sorted from the mouse lung tissue in WT and JAK2V617F mice using a magnetic bead method. On a 35-mm plate, 5x105 were grown in Methocult GF M3434. After 7 days, the colonies derived from colony-forming unit (CFU)-granulocyte, -erythroid, -macrophage, -megakaryocyte (CFU-GEMM), CFU-granulocyte, -monocyte (CFU-GM), CFU-granulocyte (CFU-G) were counted according to the morphology. (a, b) Representative images of the plates and colonies. Scale bars, 10 mm (a) and 300 μm (b). (c) Quantification of numbers of the colonies (n = 3 in each grooup, *P = 0.0352 for CFU-GEMM, *P = 0.0016 for CFU-GM, *P = 0.0003 for CFU-G). All data are presented as mean ± SEM. *P < 0.05 versus WT by the unpaired t-test (two-sided). WT, wild-type mice; JAK2V617F, JAK2V617F-expressing transgenic mice.

Supplementary Figure 18.

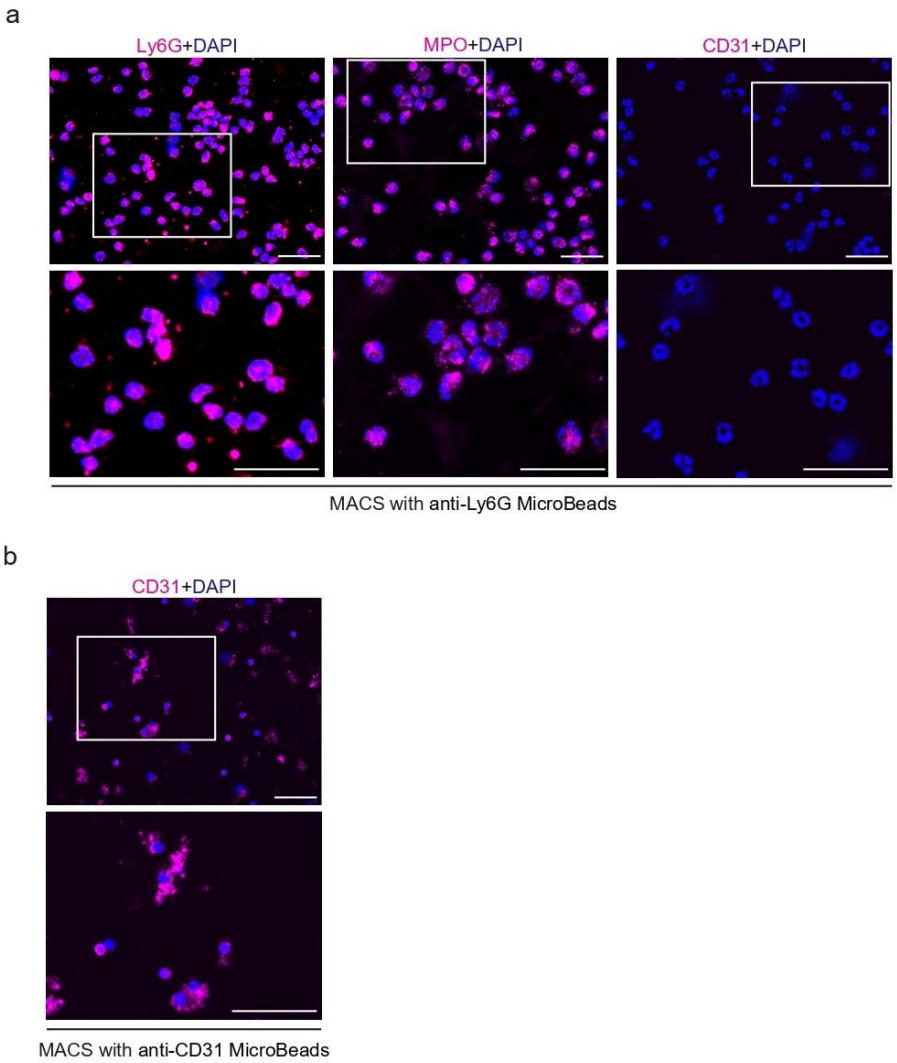

The cell suspensions from the lungs in wild-type mice were subjected to MACS with anti-Ly6G MicroBeads (a) or anti-CD31 MicroBeads (b). The sorted cells were fixed and stained with indicated antibodies (magenta) with DAPI (blue). Images in boxed areas at higher magnification are shown in bottom panels. Scale bars, 50 um. Nearly 100% of the MACS-isolated Ly6G+ cells were stained with anti-Ly6G and anti-myeloperoxidase (MPO) antibodies, a specific marker for neutrophils, while these cells were not stained with an anti-CD31 antibody, a specific marker for endothelial cells. Representative

images of three independent experiments are shown. MACS, Magnetic-activated cell sorting.

Supplementary Figure 19.

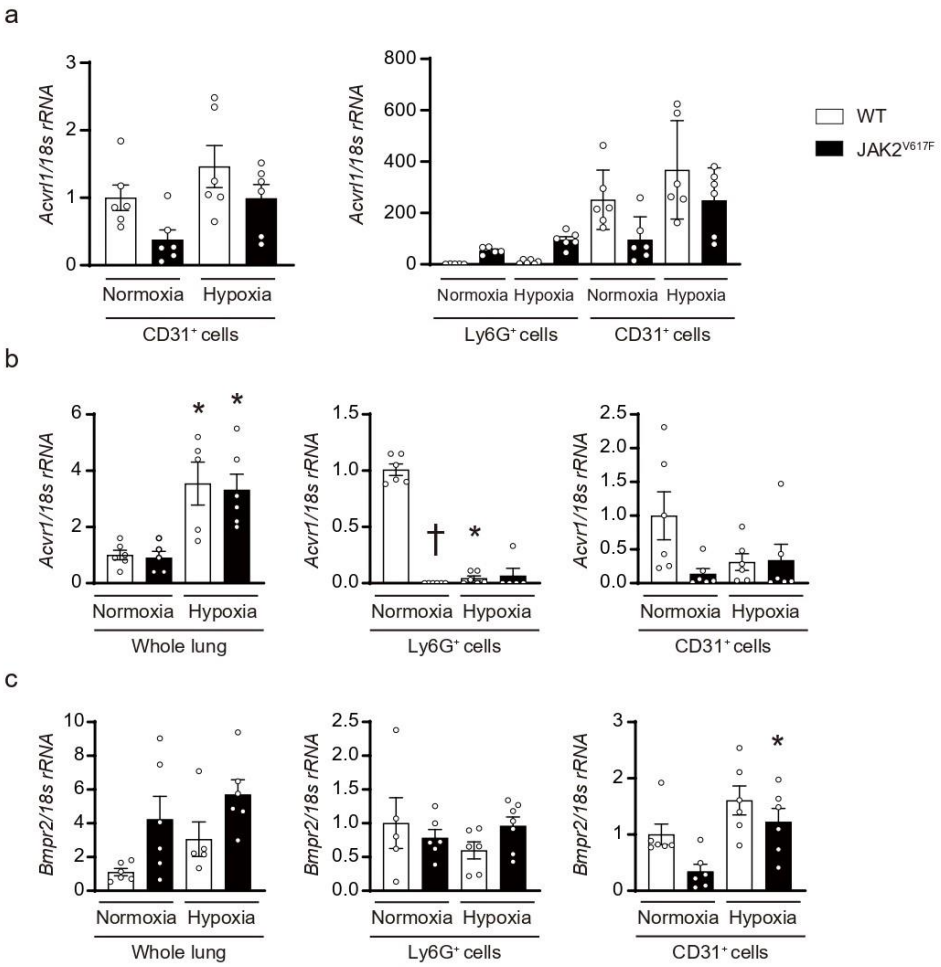

(a) Left, mRNA expression of Acvrl1 in the sorted cells by MACS with anti-CD31 MicroBeads from the lungs of WT mice and JAK2V617F mice after normoxia or hypoxia (n = 6 in each group). Right, The comparison of Acvrl1 mRNA expression levels between Ly6G+ and CD31+ cells from the lungs (n = 5, 5, 6, 6, 6, 6, 6, 6). The data of Ly6G+ cells are from main Figure 6. (b) mRNA expression of Acvr1 in the whole lung extracts (left graph, n = 6, 5, 5, 6, *P = 0.0079 [left], 0.0116 [right]), Ly6G+ cells from the lungs

(middle graph, n = 6, 6, 6, 5, †P < 0.0001), CD31+ cells from the lungs (right graph, n = 6 in each group). (c) mRNA levels of Bmpr2 in the whole lung extracts (left graph, n = 6, 6, 5, 6), Ly6G+ cells from the lungs (middle graph, n = 5, 5, 6, 7), CD31+ cells from the lungs (right graph, n = 6 in each group, *P = 0.0338). The 18s rRNA was used for the normalization. Data are presented as mean ± SEM. The average value for the normoxia-WT mice was set to 1. *P < 0.05 versus the corresponding normoxia-exposed group and †P < 0.05 versus the corresponding WT mice by the one-way ANOVA with Tukey post-hoc analysis. WT, wild-type mice; JAK2V617F, JAK2V617F-expressing transgenic mice.

Supplementary Figure 20.

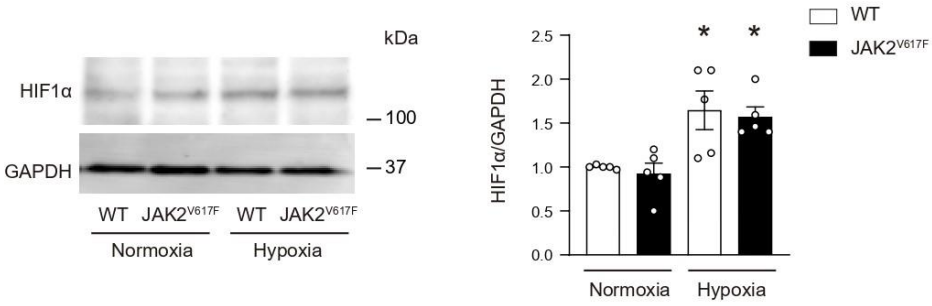

Immunoblotting of HIF1α in WT mice and JAK2V617F mice after normoxia and chronic hypoxia. Left panels show representative blots. Densitometric analysis is shown in the right graph (n = 5 in each group, *P = 0.0200 [left], 0.0200 [right]). GAPDH was used as the loading control. The average value for the normoxia-WT mice was set to 1. Data are presented as mean ± SEM. *P < 0.05 versus the corresponding normoxia-exposed group by the one-way ANOVA with Tukey post-hoc analysis. WT, wild-type mice; JAK2V617F, JAK2V617F-expressing transgenic mice.

Supplementary Figure 21.

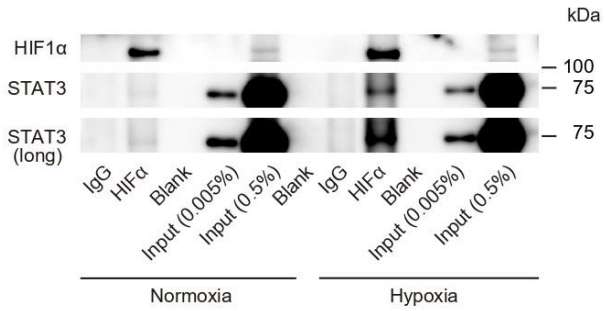

Co-immunoprecipitation of STAT3 and HIF1α in the lung tissue of JAK2V617F mice after exposure to normoxia and chronic hypoxia for 2 weeks. The lung homogenates were immunoprecipitated with Rabbit IgG or an anti-HIF1α antibody and subjected to immunoblotting with anti-HIF1α and anti-STAT3 antibodies. The two blots from the bottom were originated from the same membrane, and the longer exposure time was used in the bottom blot for clarity (long). Representative images of two independent experiments are shown.

Supplementary Figure 22.

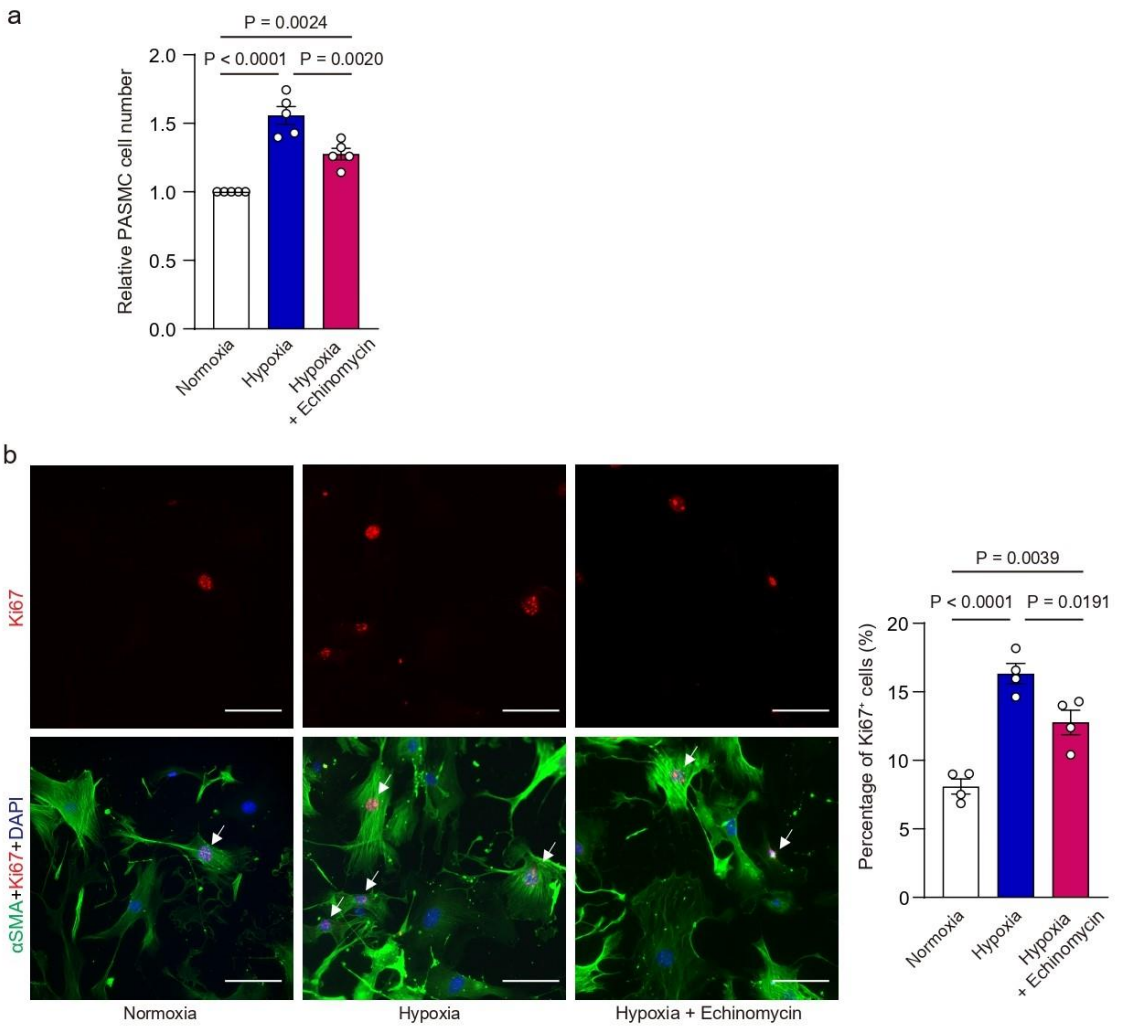

(a) The neutrophils were collected from peripheral blood of JAK2V617F mice by MACS with Ly6G+ MicroBeads. Cells were starved and then incubated in a hypoxia incubator chamber (10% O2) for 3 h. The neutrophils were pretreated with Echinomycin (1 nM), an anti-HIF1α inhibitor, prior to hypoxia for 1 h, and then the medium was freshly changed just before hypoxia stimulation. Control neutrophils were cultured in normoxic conditions for 3 h. The conditioned medium was collected and centrifuged to remove the cell debris. PASMC were incubated with the neutrophil-derived conditioned medium for 48 h. Cell numbers were determined by cell proliferation assay and expressed as a relative

ratio over the group of PASMC incubated with conditioned medium from normoxic conditions from 5 independent experiments. (b) Left, representative immunofluorescent images of Ki67 staining and triple staining (αSMA, green; Ki67, red; DAPI, blue) of PASMC 48 h after neutrophil-derived conditioned medium stimulation. White arrows indicate Ki67-positive nuclei. Right, quantitative analyses of the Ki67-positive cells. More than 100 cells were counted (n = 4 independent experiments). Scale bars, 100 μm. Data are presented as mean ± SEM. Statistical significance was determined by the one-way ANOVA with Tukey post-hoc analysis.

Supplementary Figure 23.

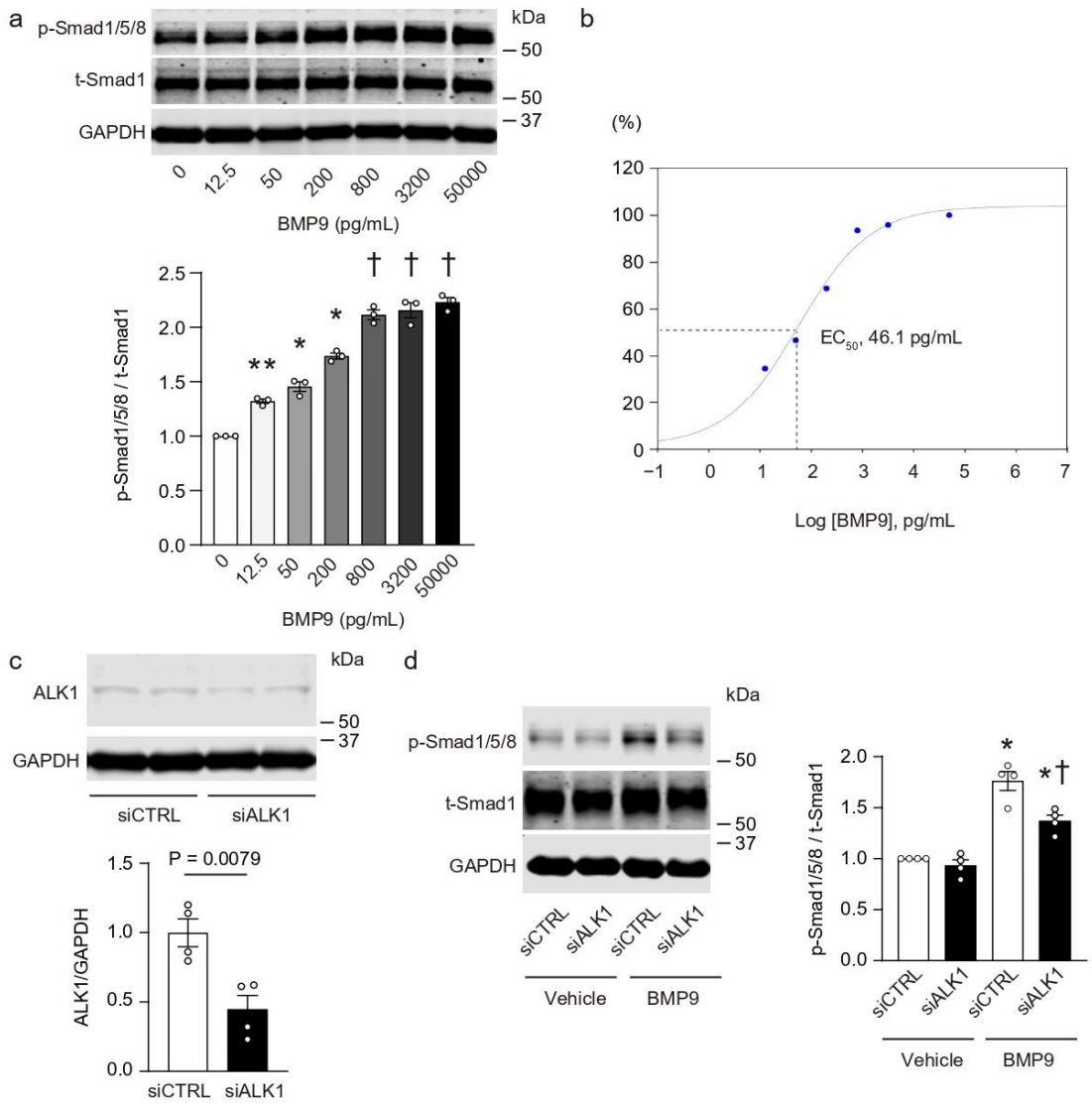

(a) Immnoblots of Smad1/5/8 phosphorylation in HCT116 cells. HCT116 cells were incubated with BMP9, a high-affinity ALK1 ligand, at the indicated concentration for 3 h, and then the cell lysates were subjected to immunoblotting. p-Smad1/5/8 and t-Smad1 indicate phosphorylated Smad1/5/8 and total Smad1, respectively. Data are presented as mean ± SEM (n = 3 independent experiments). *P < 0.05 versus all other groups, **P < 0.05 versus all other groups except 50 pg/mL of BMP9 and †P < 0.05 versus all other groups except 800, 3200, 5000 pg/mL of BMP9 by the one-way ANOVA with Tukey

post-hoc analysis. P = 0.0011 (0 vs. 12.5), < 0.0001 (0 vs. 50), < 0.0001 (0 vs. 200), < 0.0001 (0 vs. 800), < 0.0001 (0 vs. 3200), < 0.0001 (0 vs. 50000), 0.2984 (12.5 vs. 50), < 0.0001 (12.5 vs. 200), < 0.0001 (12.5 vs. 800), < 0.0001 (12.5 vs. 3200), < 0.0001 (12.5 vs. 50000), 0.0038 (50 vs. 200), < 0.0001 (50 vs. 800), < 0.0001 (50. vs. 3200), < 0.0001 (50 vs. 50000), 0.0002 (200 vs. 800), < 0.0001 (200 vs. 3200), < 0.0001 (200 vs. 50000), 0.9902 (800 vs. 3200), 0.4820 (800 vs. 50000), 0.8638 (3200 vs. 50000). (b) Concentration responses of BMP9 were calculated from (a). The BMP9 EC50 value was estimated to be 46.1 pg/mL (AAT Bioquest, Inc. Quest Graph™ EC50 Calculator). (c) HCT116 cells were transfected with ALK1-specific siRNA (siALK1) or non-targeting control siRNA (siCTRL) with 40 nM for 48 h. Data are presented as the mean ± SEM (n = 4). Statistical comparisons were performed by the unpaired Student's t test (two-sided). (d) Transfected cells were incubated with BMP9 of 200 pg/mL or vehicle for 3 h, and then Smad1/5/8 phosphorylation was determined by immunoblotting. Data are presented as mean ± SEM (n = 4, *P < 0.0001 [left], 0.0015 [right], †P = 0.0033). *P < 0.05 versus the corresponding vehicle groups and †P < 0.05 versus BMP9-stimulated siCTRL by the one-way ANOVA with Tukey post-hoc analysis.

Supplementary Figure 24.

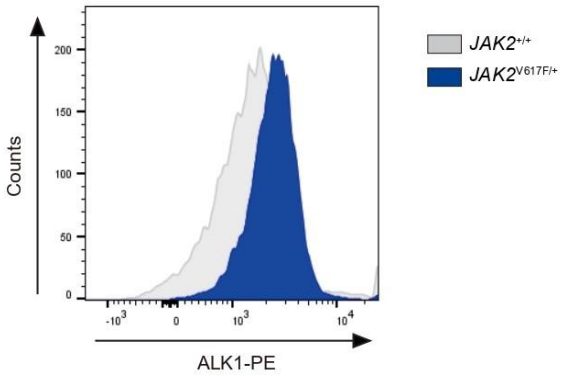

Flow cytometry analysis for ALK1 expression in JAK2+/+ and JAK2V617F/+ HCT116 cells. The cells were trypsinized and collected as a single cell suspension, and then stained with an anti-ALK1 antibody followed by a secondary anti-rabbit PE antibody and subjected to the flow cytometry. The representative histogram is shown.

Supplementary Figure 25.

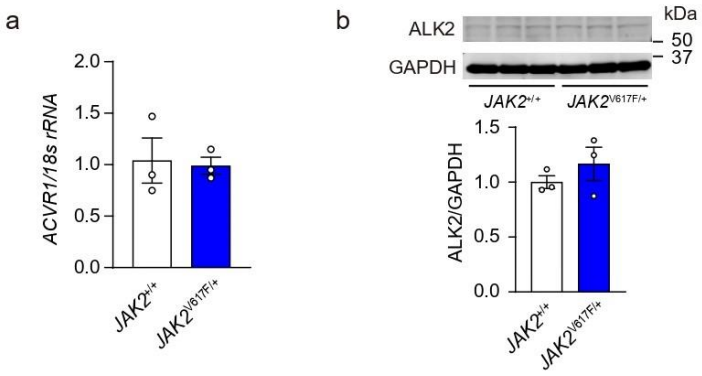

(a) mRNA expression of ACVR1 in JAK2V617F/+ knock-in HCT116 cells. The data were normalized to 18s rRNA and the average value of JAK2+/+ cells was set to 1 (n = 3). (b) ALK2 protein expression in JAK2V617F/+ HCT116 cells by Western blot analysis. GAPDH was used for the normalization and the average value of JAK2+/+ cells was set to 1 (n = 3). The data are presented as mean ± SEM (n = 3). Statistical comparisons were performed by the unpaired Student's t test (two-sided).

Supplementary Figure 26.

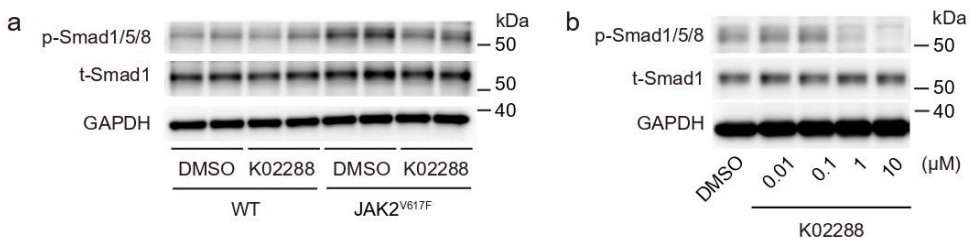

(a) Lung homogenates from the DMSO- or K02288-treated WT mice and JAK2V617F mice 2 weeks after chronic hypoxia (10% O2) were analyzed by immunoblotting with p-Smad1/5/8 and t-Smad1 antibodies. Representative images of two independent experiments are shown. (b) JAK2V617/+ HCT116 cells were incubated with K02288 at the indicated concentrations for 6 h. The cell lysates were subjected to immunoblotting on p-Smad1/5/8 and t-Smad1. p-Smad1/5/8 and t-Smad1 indicate phosphorylated Smad1/5/8 and total Smad1, respectively. Representative images of two independent experiments are shown. GAPDH was used as the loading control. WT, wild-type mice; JAK2V617F, JAK2V617F-expressing transgenic mice.

Supplementary Figure 27.

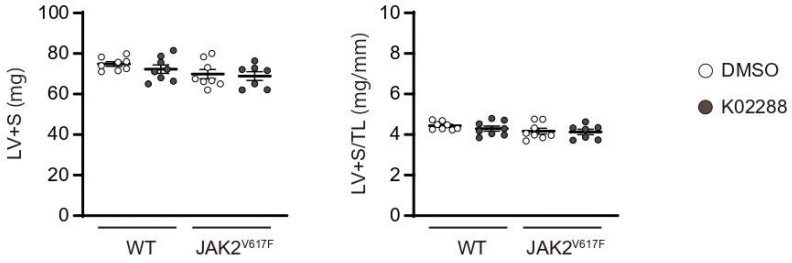

Left ventricular (LV) weight including septum (S) was measured after exposure to normoxia (21% O2) or chronic hypoxia (10% O2) for 2 weeks (n = 8, 8, 8, 7 in each). LV+S was normalized by tibia length (TL). All data are presented as mean ± SEM. The statistical comparison was performed by the one-way ANOVA.

Supplementary Figure 28.

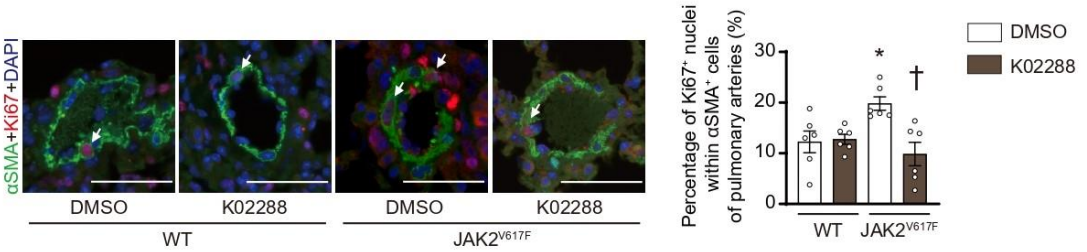

Left, triple-labeled immunofluorescent staining (αSMA, green; Ki67, red; DAPI, blue) of the lung sections in DMSO- or K02288-treated WT mice and JAK2V617F mice 2 weeks after chronic hypoxia. White arrows indicate Ki67-positive nuclei within αSMA+ cells. Scale bars, 50 μm. Right, quantitative analyses of the percentage of Ki67-positive nuclei within αSMA+ cells of distal pulmonary arteries with a diameter of 50-100 μm (n = 6). More than 80 αSMA+ cells were counted in each section. Data are presented as mean ± SEM. *P = 0.0330 versus the corresponding WT mice and †P = 0.0040 versus DMSO-treated JAK2V617F mice by the one-way ANOVA with Tukey post-hoc analysis.

Supplementary Figure 29.

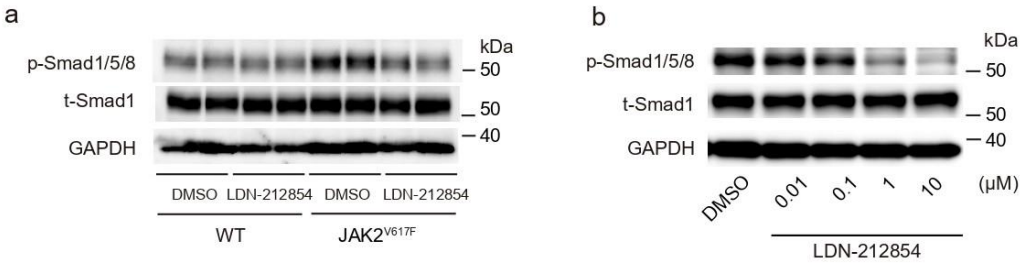

(a) Lung homogenates from the DMSO- or LDN-212854-treated WT mice and JAK2V617F mice after chronic hypoxia (10% O2) for 2 weeks were analyzed by immunoblotting with p-Smad1/5/8 and t-Smad1 antibodies. Representative images of two independent experiments are shown. (b) JAK2V617/+ HCT116 cells were incubated with LDN-212854 at the indicated concentrations for 6 h. The cell lysates were subjected to

immunoblotting on p-Smad1/5/8 and t-Smad1. p-Smad1/5/8 and t-Smad1 indicate phosphorylated Smad1/5/8 and total Smad1, respectively. Representative images of two independent experiments are shown. GAPDH was used as the loading control. WT, wild-type mice; JAK2V617F, JAK2V617F-expressing transgenic mice.

Supplementary Figure 30.

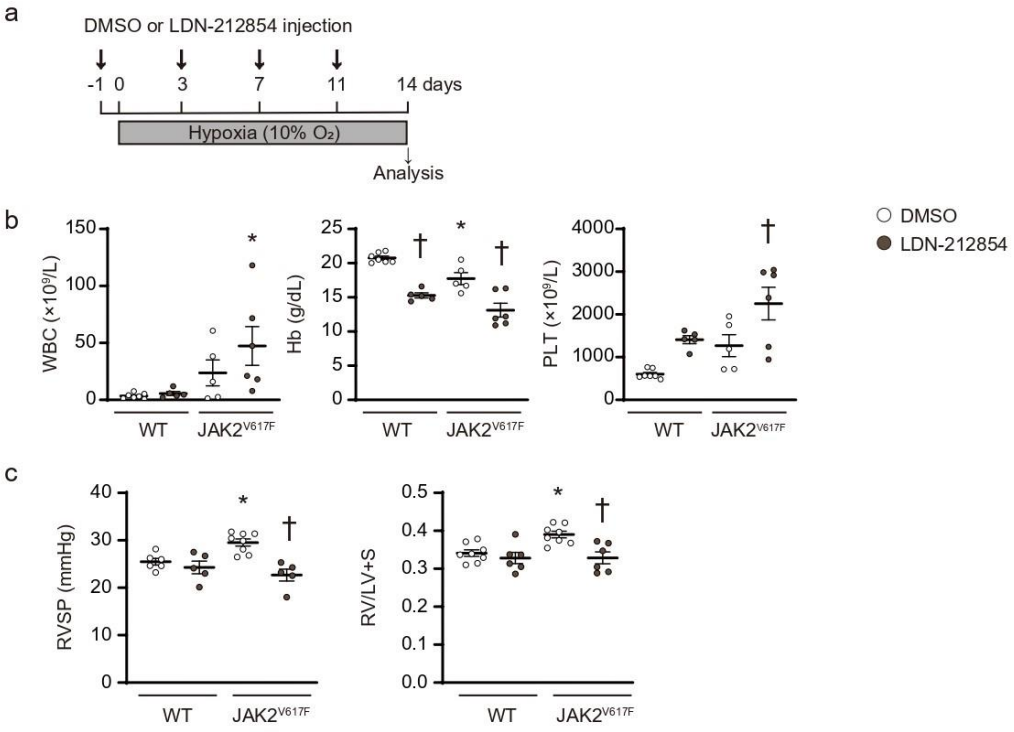

(a) Schematic protocol. Vehicle (DMSO) or LDN-212854 was administered via an intraperitoneal injection of 9 mg/kg body weight during 2-week chronic hypoxia-exposure as indicated. (b) Peripheral blood cell counts in DMSO- or LDN-212854-treated WT mice and JAK2V617F mice after exposure to chronic hypoxia for 2 weeks (n = 7, 5, 5, 6, *P = 0.0496 for WBC, n = 7, 5, 5, 6, *P < 0.0001, †P = 0.0261 [left], 0.0010 [right] for Hb, n = 7, 5, 5, 6, †P = 0.0403 for PLT). (c) RVSP and RV hypertrophy determined by RV/LV+S in DMSO- or LDN-212854-treated WT mice and JAK2V617F mice (n = 6, 5,

8, 5, *P = 0.0249, †P = 0.0003 for RVSP, n =8, 6, 8, 6, *P = 0.0197, †P = 0.0054 for RV/LV+S). Data are presented as mean ± SEM. *P < 0.05 versus the corresponding WT mice and †P < 0.05 versus DMSO-treated JAK2V617F mice by the one-way ANOVA with Tukey post-hoc analysis.

Supplementary Figure 31.

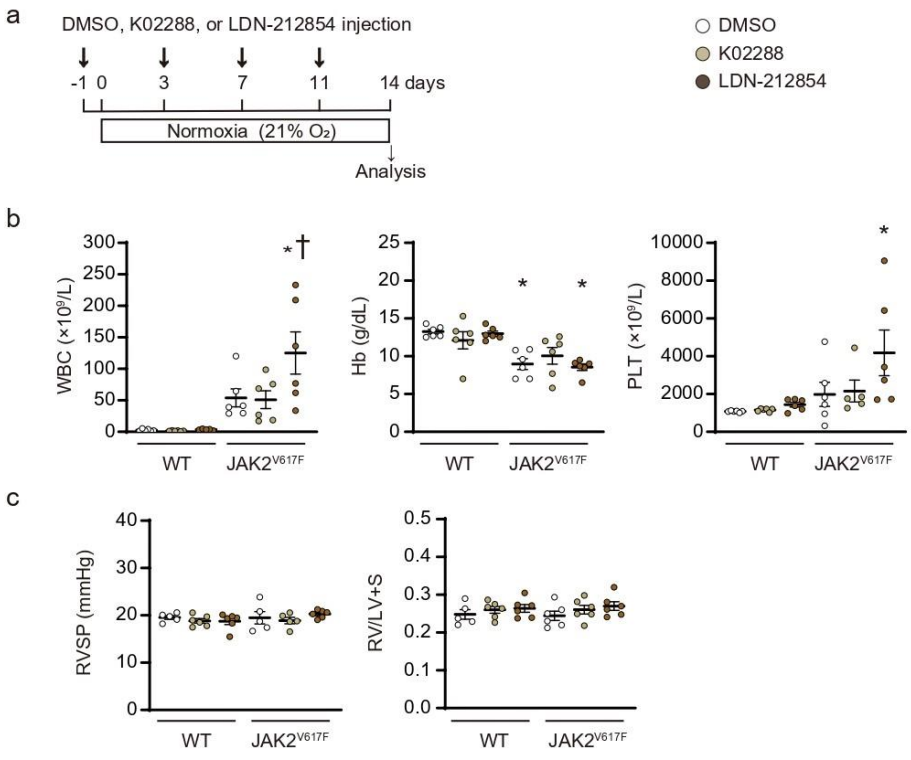

(a) Schematic protocol. Vehicle (DMSO, 12 mg/kg), K02288 (12 mg/kg), or LDN-212854 (9 mg/kg) was administered via an intraperitoneal injection during 2-week normoxia-exposure as indicated. (b) Peripheral blood cell counts in DMSO-, K02288-, or LDN-212854-treated WT mice and JAK2V617F mice after exposure to normoxia for 2 weeks (n = 6, 6, 5, 6, 6, 6, *P = 0.0003, †P = 0.0440 for WBC, n =6 in each group, *P = 0.0045 [left], 0.0031 [right] for Hb, n = 6, 6, 6, 6, 5, 6, *P = 0.0340 for PLT). (c) RVSP and RV hypertrophy determined by RV/LV+S in DMSO-, K02288-, or LDN-212854-

treated WT mice and JAK2V617F mice (n = 5, 6, 6, 5, 5, 6 for RVSP, n = 5, 6, 6, 6, 6, 6 for RV/LV+S). Data are presented as mean ± SEM. *P < 0.05 versus the corresponding WT mice and †P < 0.05 versus DMSO-treated JAK2V617F mice by the one-way ANOVA with Tukey post-hoc analysis. WT, wild-type mice; JAK2V617F, JAK2V617F-expressing transgenic mice.

Supplementary Figure 32.

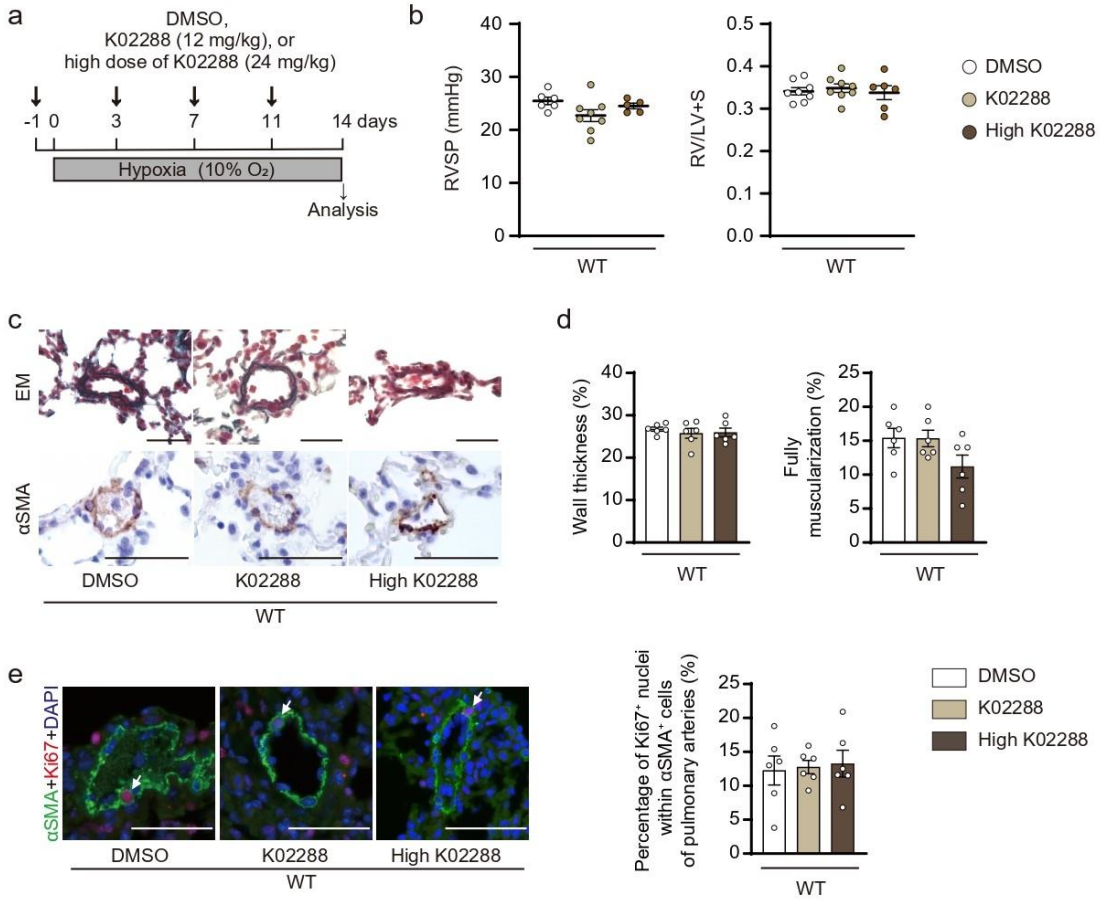

(a) Schematic representation. Vehicle (DMSO, 12 mg/kg), K02288 (12 mg/kg), or high dose of K02288 (24 mg/kg) was administered via an intraperitoneal injection during 2-week chronic hypoxia-exposure as indicated. The data of DMSO- and K02288 (12 mg/kg)-treated WT mice are from the main Fig. 8 for comparison. (b) RVSP (n = 6, 8, 5)

and RV hypertrophy determined by RV/LV+S (n = 8, 8, 6). (c) Representative images of EM-stained sections and sections immunostained with an anti-αSMA antibody. Scale bar, 25 μm. (d) Quantitative analysis of medial wall thickness in EM-stained sections (left, n = 6 in each group) and the percentage of muscularized distal pulmonary arteries in αSMA-immunostained sections (right, n = 6 in each group). (e) Left, representative images of triple-labeled immunofluorescent staining (αSMA, green; Ki67, red; DAPI, blue). White arrows indicate Ki67-positive nuclei within αSMA+ cells. Scale bars, 50 μm. Right, quantitative analyses of the percentage of Ki67-positive nuclei within αSMA+ cells of distal pulmonary arteries with a diameter of 50-100 μm (n = 6 in each group). More than 80 αSMA+ cells were counted in each section. All data are presented as mean ± SEM. The statistical comparison was performed by the one-way ANOVA.

Supplementary Figure 33.

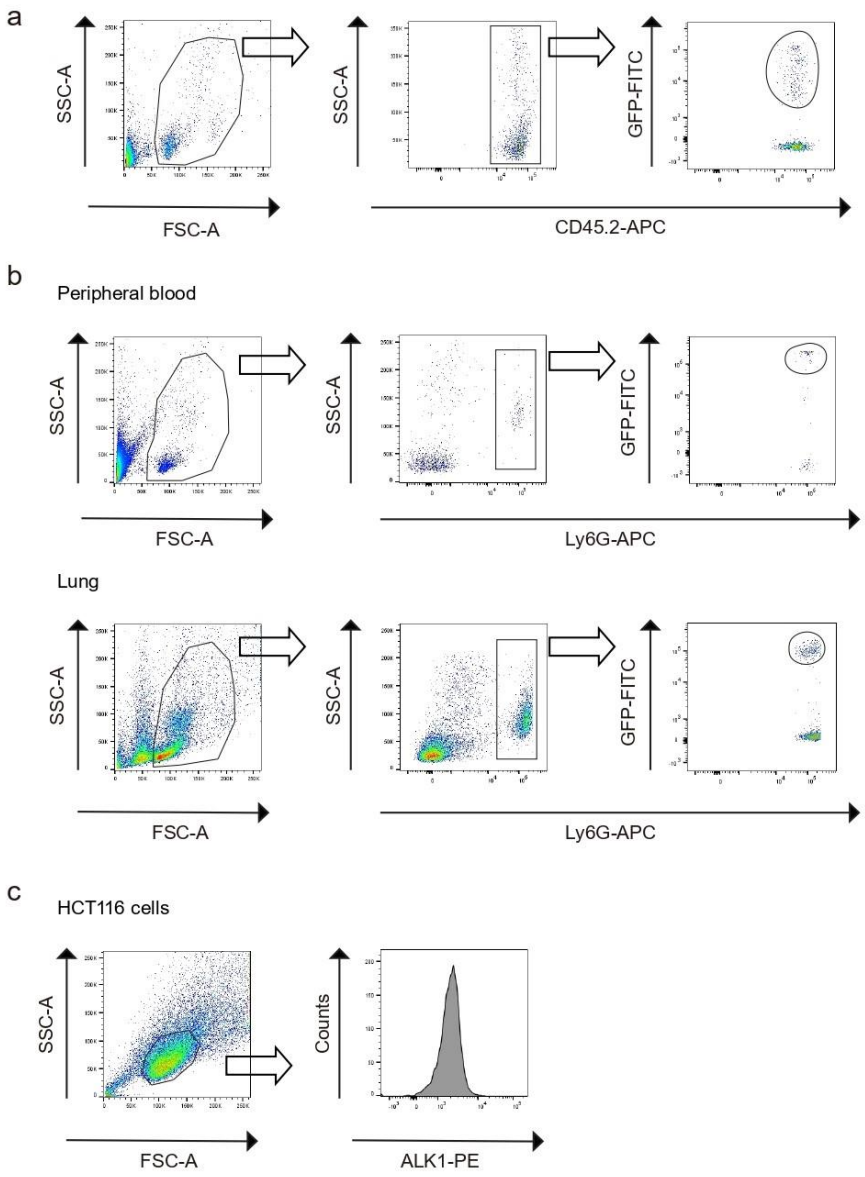

(a) Gating strategy used to analyze the chimerism in the peripheral blood. The percentages of GFP+ cells in the circulating CD45.2+ cells are shown in Figure 4b and Supplementary Figure 16. (b) Gating strategy used to analyze the percentages of GFP+ cells in Ly6G+ cells in comparison to the peripheral blood and lungs. Data are shown in Figure 4c and 4d. (c) Gating strategy used to analyze ALK1 expressions in HCT116 cells. Data are shown in Supplementary Figure 24.

Supplementary Table 1. Comparisons of the presence of *JAK2*V617F between control subjects and patients with PH.

	Control subjects (n = 83)	Patients with PH (n = 70)	P value
Age, years	59 ± 17	59 ± 15	0.904
Female, n (%)	45 (54)	47 (67)	0.104
Presence of *JAK2*V617F, n (%)	0	5 (7.1)	0.019

Values are mean ± SD or number (%). PH, pulmonary hypertension. Comparisons of means between the two groups were performed by the unpaired Student's t-test (two-sided). Categorical variables were compared using Chi-square test (two-sided) or Fisher's exact test (two-sided).

Supplementary Table 2. The cases of PH patients with *JAK2*V617F-positive clonal hematopoiesis.

Case	Age (years)	Gender (M/F)	Group of PH	*JAK2*V617F allele frequency (%)	WBC ($\times 10^9$/L)	Hb (g/dL)	PLT ($\times 10^9$/L)	Mean PAP (mmHg)	PVR (wood, unit)
1	60s	F	IV	14.90	8.1	12.7	360	25	3.6
2	50s	F	I	0.54	5.6	12.9	212	58	8.1
3	30s	F	I	0.06	7.8	12.8	236	64	21.1
4	60s	F	IV	16.08	7.2	13.6	339	57	14.9
5	70s	M	IV	70.96	8.7	11.4	206	41	4.2

Group category is defined by the WHO classification of PH; Group I, pulmonary arterial hypertension; Group IV, chronic thromboembolic pulmonary hypertension. WBC, white blood cell count; Hb, hemoglobin concentration; PLT, platelet count; PAP, pulmonary arterial pressure; PVR, pulmonary vascular resistance.

Supplementary Table 3. Comparison of the PH patients with and without *JAK2*V617F.

	*JAK2*V617F positive (n = 5)	*JAK2*V617F negative (n = 65)	P value
Age, years	58 ± 15	59 ± 15	0.902
Female, n (%)	4 (80)	43 (66)	1.000
Group of PH, I/II/III/VI/V, n (%)	2 (40) / 0 (0) / 0 (0) / 3 (60) / 0 (0)	30 (46) / 0 (0) / 9 (14) / 24 (37) / 2 (3)	NA
NYHA functional class, I/II/III/VI, n (%)	0 (0) / 3 (60) / 2 (40) / 0 (0)	9 (14) / 29 (45) / 23 (35) / 4 (6)	NA
Laboratory data			
WBC, $\times 10^9$/L	7.4 ± 1.1	6.4 ± 2.2	0.287
Hb, g/dL	12.6 ± 0.7	13.6 ± 2.2	0.331
Hematocrit, %	38.7 ± 7.9	41.4 ± 6.4	0.384
PLT, $\times 10^9$/L	270 ± 73	221 ± 78	0.118
Total bilirubin, mg/dL	0.88 ± 0.43	0.97 ± 0.62	0.767
Aspartate aminotransferase, IU/L	25.8 ± 11.7	27.6 ± 13.6	0.779
Lactate dehydrogenase, IU/L	262 ± 82	246 ± 91	0.697
Creatinine	0.83 ± 0.27	0.82 ± 0.29	0.917
Estimated GFR, mL/min/1.73 m^2	67.0 ± 26.7	70.7 ± 26.6	0.763
Serum iron, μg/dL	57 ± 29	85 ± 57	0.276
Ferritin, ng/mL	64 ± 64	117 ± 180	0.518
Uric acid, mg/dL	6.3 ± 2.5	6.1 ± 1.8	0.785
C-reactive protein, mg/dL	1.2 ± 1.8	0.7 ± 1.4	0.484
B-type natriuretic peptide, pg/mL	44.9 (33.1 – 542.7)	135 (40.8 – 291.6)	0.511
Echocardiography			
Left ventricular ejection fraction, %	68.2 ± 5.4	63.1 ± 12.0	0.348
RV end-diastolic area, cm^2	25.6 ± 10.3	25.1 ± 12.0	0.931
RV fractional area change, %	27.2 ± 9.1	32.4 ± 14.2	0.429
TR-PG, mmHg	66.4 ± 16.0	64.3 ± 25.6	0.864
Hemodynamics			
Mean PAP, mmHg	49 ± 15	44 ± 13	0.422
Mean PAWP, mmHg	16 ± 8	11 ± 5	0.261
Cardiac index, L/min/m^2	2.7 ± 0.4	2.6 ± 0.8	0.839
PVR, wood unit	10.3 ± 7.4	9.4 ± 5.3	0.688

Data are presented as mean ± SD, number (%) or median (inter-quartile range). The

patients were classified into 5 groups according to the WHO clinical classification of PH; Group I, pulmonary arterial hypertension; Group II, pulmonary hypertension due to left heart disease; Group III, pulmonary hypertension due to lung diseases and/or hypoxia; Group IV, chronic thromboembolic pulmonary hypertension; Group V, pulmonary hypertension with unclear multifactorial mechanisms. NA, not applicable; NYHA, New York Heart Association; WBC, white blood cell count; Hb, hemoglobin concentration; PLT, platelet count; GFR, glomerular filtration rate; RV, right ventricular; TR-PG, tricuspid regurgitation pressure gradient; PAP, pulmonary arterial pressure; PAWP, pulmonary arterial wedge pressure; PVR, pulmonary vascular resistance. Comparisons of values between the two groups were performed by the unpaired Student's t-test (two-sided) or Mann-Whitney U-test (two-sided). Categorical variables were compared using Fisher's exact test (two-sided).

Supplementary Table 4. Primers used for RT-qPCR.

Gene			Sequences		
Mouse	*Ccl2*	Forward	5'-	GGCTCAGCCAGATGCAGTTAAC	-3'
		Reverse	5'-	GCCTACTCATTGGGATCATCTTG	-3'
	Cxcl1	Forward	5'-	ACTCAAGAATGGTCGCGAGG	-3'
		Reverse	5'-	ACTTGGGGACACCTTTTAGCA	-3'
	Ccr1	Forward	5'-	TTAGCTTCCATGCCTGCCTTATA	-3'
		Reverse	5'-	TCCACTGCTTCAGGCTCTTGT	-3'
	Cxcr2	Forward	5'-	TCGTAGAACTACTGCAGGATTAAG	-3'
		Reverse	5'-	GGGACAGCATCTGGCAGAATA	-3'
	Pdgfrb	Forward	5'-	ACTACATCTCCAAAGGCAGCACCT	-3'
		Reverse	5'-	TGTAGAACTGGTCGTTCATGGGCA	-3'
	Tgfb1	Forward	5'-	AGCTGCGCTTGCAGAGATTA	-3'
		Reverse	5'-	AGCCCTGTATTCCGTCTCCT	-3'
	Acvrl1	Forward	5'-	GGCCTTTGGCCTAGTGCTAT	-3'
		Reverse	5'-	GGAGAGGACCGGATCTGC	-3'
	Acvr1	Forward	5'-	CGCTTCAGACATGACCTCCA	-3'
		Reverse	5'-	CCGAAGGCAGCTAACCGTAT	-3'
	Bmpr2	Forward	5'-	GGATGGCAGCAGTATACAGATAGG	-3'
		Reverse	5'-	CGCCACCGCTTAAGAGAGTAT	-3'
	18s rRNA	Forward	5'-	GTCTGTGATGCCCTTAGATG	-3'
		Reverse	5'-	AGCTTATGACCCGCACTTAC	-3'
Human	*ACVRL1*	Forward	5'-	CCATCGTGAATGGCATCGTG	-3'
		Reverse	5'-	GAGGGGTTTGGGTACCAGCA	-3'
	ACVR1	Forward	5'-	GAAGGGCTCATCACCACCAA	-3'
		Reverse	5'-	CCATACCTGCCTTTCCCGAC	-3'
	18s rRNA	Forward	5'-	GTAACCCGTTGAACCCCATT	-3'
		Reverse	5'-	CCATCCAATCGGTAGTAGCG	-3'

Supplementary Table 5. Primers used for ChIP-qPCR.

Gene			Sequences	
ACVRL1 TSS-875bp	Forward	5'-	CCTGCCGGTATGAAGCCATT	-3'
	Reverse	5'-	ACAGTCAGGATGGAGGGACA	-3'
ACVRL1 TSS-1660bp	Forward	5'-	TTGGGTGTGTCAGGGTTCTG	-3'
	Reverse	5'-	AGGAATAGAGGCTGGGGGAG	-3'

Supplementary Table 6. Primers and probes used for allele-specific qPCR.

Primers and probes			Sequences	
JAK2	Forward	5'-	CTTTCTTTGAAGCAGCAAGTATGA	-3'
*JAK2*wild-type	Reverse	5'-	GTAGTTTTACTTACTCTCGTCTCCACATAC	-3'
*JAK2*V617F	Reverse	5'-	GTAGTTTTACTTACTCTCGTCTCCACATAA	-3'
JAK2	Probe	5'-	FAM-TGAGCAAGCTTTCTCACAAGCATTTGGTTT-TAMRA	-3'